17th INTERNATIONAL CONGRESS of the Geological Society of Greece

BULLETIN OF THE GEOLOGICAL SOCIETY OF GREECE, SP. PUBL.

EXTENDED ABSTRACT 041

The Greek Database of Seismogenic Sources (GreDaSS) version 3.0. A compilation of potential seismogenic sources (Mw> 5.5) in the Aegean Region

Caputo R.[1], Koukouvelas I.[2], Papathanassiou G.[3], Russo D.[1], Taftsoglou M.[1,2], Tarabusi G.[4], Valkaniotis S.[3]

(1) University of Ferrara, Department of Earth Sciences, 44122 Ferrara, Italy
(2) University of Patras, School of Geology, Patras, Greece
(3) Aristotle University of Thessaloniki, Department of Geology, Thessaloniki, Greece
(4) Istituto Nazionale di Geofisica e Vulcanologia, Rome, Italy

The broader Aegean Region, including the Southern Balkans, is among the most tectonically active areas of the Mediterranean realm and has the highest seismicity both in terms of frequency of events and magnitudes. The principal aim of this note is to present the new release of the Greek Database of Seismogenic Sources (GreDaSS) corresponding to version 3.0 systematically revised in terms of sources and seismotectonic parameters and largely improved both qualitatively and quantitatively (Figure 1).

Background

The importance of a complete repository for active faults in the Aegean Region became clear since the late 1990's; however, the first efforts were primarily focused on tectonic structures associated to pre-instrumental and instrumental seismicity (e.g. Ambraseys and Jackson, 1998; Papazachos et al., 1999) and thus based almost entirely on historical and seismological data. This approach can be successful in studying recently activated seismogenic sources, but becomes inappropriate for sources without any seismological record (neither pre-instrumental nor instrumental) and characterized by a long recurrence period. The 13 May 1995 Kozani earthquake (Ms = 6.5; e.g. Pavlides et al., 1995; Meyer et al., 1996; 1998a; 1998b; Chiarabba and Selvaggi, 1997; Clarke et al., 1997, 1998; Hatzfeld et al., 1997; 1998) and the 7 September 1999 Athens earthquake (Mw = 6.0; e.g. Kontoes et al., 2000; Voulgaris et al., 2001; Ganas et al., 2004; Atzori et al., 2008; Foumelis et al., 2009) are emblematic examples of ruptures occurred in areas considered till that moment as aseismic or associated with low seismic activity. Although the subsequent works managed to include the geological records in the source identification process, most of them resulted to be too much descriptive, lacking in quantitative parameters information (e.g. Mountrakis et al., 2006; Pavlides et al., 2007; Karakaisis et al., 2010).

For these reasons, in the late '90ies on the track of the European FAUST Project and the Italian DISS, the GreDaSS Project was thus launched initially at the University of Basilicata and then permanently developed at the University of Ferrara (copyright owner) with an international working group. The financial support of this initiative was primarily provided by the Italian Ministry of University and the University of Ferrara.

The principal aim of the GreDaSS Project was indeed i) to overcome the above described critical issues , ii) to provide a complete and accurate repository of fully parametrized seismogenic sources and not simply, for example, a 2D map of (active) fault traces (Papazachos et al., 2001; Pavlides et al., 2008) and iii) to contribute to better and more realistic Seismic Hazard Assessment (SHA) analyses.

Since its beginning, GreDaSS was obviously populated by seismicity-related sources, but the preferred approach was intrinsically multidisciplinary (e.g. Caputo and Helly, 2008; Caputo et al., 2015) giving emphasis and exploiting as many as possible different sources of information digging any geological, structural, morphotectonic, geodetic, palaeoseismological, historical, archaeoseismological, geophysical, etc. data available in the literature or specifically collecting new data by the research group.

During the years and becoming a reference database for SHA analyses, the products of GreDaSS were included in several European projects, like the European Seismic Hazard Model (ESHM13; Woessner et al., 2015) and more recently the European Fault-Source Model 2020 (EFSM20; Basili et al., 2024).

Since its almost 30 years of research activity, the working group of the GreDaSS Project evolved in time and saw the collaboration and contribution of several PhD students, like Valkaniotis (2009), Sboras (2012), Maggini (2020) and Russo (2025) and colleagues. The authorship of this note is limited to the contributors of the new entirely revised and updated version 3.0 of GreDaSS, which is the object of the present note.

Method

For our purposes we used the well tested, time-proof, worldwide acknowledged database structure and method proposed by the Istituto Nazionale di Geofisica e Volcanologia (INGV) for the Italian Database of Individual Seismogenic Sources (DISS), which represents the result of almost twenty years research experience of its Working Group (Valensise and Pantosti, 2001). The DISS uses many basic levels of data that can be either independent or directly related. Among the most important ones are the Individual Seismogenic Sources (ISS), the Composite Seismogenic Sources (CSS) and the Subduction Sources (SDS); see also Basili et al. (2008) for a more detailed description of the informatic framework.

- "Individual Seismogenic Sources" (ISS) are obtained from geological and geophysical data and are characterized by a full set of geometric (strike, dip, length, width and depth), kinematic (rake) and seismological-palaeoseismological parameters (average displacement per event, magnitude, slip rate, return period) and by a rating of the associated uncertainties. ISSs are assumed to exhibit "characteristic" behaviour with respect to rupture length/width and expected mean and maximum magnitude. They are tested against worldwide databases for internal consistency in terms of length, width, average displacement and magnitude. This category of sources favours accuracy of the information supplied over completeness of the sources themselves. As such, they can be used for deterministic assessment of seismic hazard, for calculating earthquake and tsunami scenarios, and for tectonic and geodynamic investigations.

- "Composite Seismogenic Sources" (CSS) are still obtained from geological and geophysical data and characterized by geometric (strike, dip, width, depth) and kinematic (rake) parameters, but their length is more loosely defined and spans two or more Individual Sources. They are not assumed to be capable of a specific earthquake, but their potential can be derived from existing earthquake catalogues. A CSS is essentially inferred on the basis of regional surface and subsurface geological data, that are exploited well beyond the simple identification of active faults or youthful tectonic features. Opposite to the previous case, this category of sources favours completeness of the record of potential earthquake sources over accuracy of source description. In conjunction with seismicity and modern strain data, CSSs can thus be used for regional probabilistic seismic hazard assessment and for investigating large-scale geodynamic processes.

- "Subduction Sources" (SDS) are designed to include a simplified model of this complex tectonic environment. They represent the dipping slab at mantle depth, the interface between the two plates at crustal depth, and the detachment at the base of the accretionary wedge. In map view, a set of depth contour lines depicts the geometry of the subducted slab. At the upper end of the slab, a fault trace marks the boundary of the two plates. A set of basic parameters relative to the tectonic behavior, the possible segmentation of the Wadati-Benioff surface and the net convergence direction and rate are also added in the corresponding layers of information. This type of reconstruction is typically performed using data from geology, exploration geophysics, seismicity distribution, and seismic tomography.
The details about how faults are graphically represented in the database and what are the attributes of every information field can be found in the paper of Basili et al. (2008).

Informatic platform

Different from version 2.0 that is available as a Google Maps version or a downloadable KMZ version, Gredass 3.0 is hosted on "SEISMOFAULTS.EU" IT infrastructure (Basili et al, 2022) that provides access through standard web services protocols such as the Web Map Service (WMS), Web Feature Service (WFS), or Web Coverage Service (WCS), developed by the Open Geospatial Consortium (OGC; https://ogc.org). Through the OGC web services, data can also be downloaded as CSV (Comma-Separated Values), SHP (Esri shapefile), KML (Keyhole Markup Language), GeoJson, and many others.
The last release of GreDaSS (version 3.0) is also publicly available through a web GIS interface (Figure 1). Since the database structure remains consistent, we have chosen to adopt the same web interface designed and developed by DISS Working Group of INGV for the most recent version of Italian Database of Individual Seismogenic Sources (DISS Working Group, 2021). This interface is developed in JavaScript language, using the open-source library OpenLayers for mapping data directly querying the web services made available by the "SEISMOFAULTS.EU" infrastructure.

Results

Within the investigated area, we have already recognized, characterized and parametrized numerous CSSs and

ISSs. All ISSs show evidence of Late Pleistocene-Holocene activity and sometimes also the occurrence of past 'linear morphogenic earthquakes' (sensu Caputo, 2005) as inferred, for example, from palaeoseismological trenches, archaeoseismological investigations or detailed morphotectonic mapping. In some cases, a moderate to strong earthquake has occurred in the last few decades, therefore allowing us to investigate the re-activated fault with a great detail, based on a modern scientific approach, and especially exploiting a rich seismological information associated with the mainshock. In particular, available instrumental data commonly provide crucial constraints about focal depth, magnitude, focal mechanism (i.e. strike, dip and rake) and aftershock distribution. This additional 'co-seismic' information is obviously not available for all the other geologically-derived seismogenic sources (ISSs) where no historical or instrumental earthquakes have been recorded. Accordingly, these faults represent a crucial test for the database and especially for its possible applications in seismic hazard assessment analyses. They have been independently investigated according to the two approaches, in one case the available 'co-seismic' constraints of the principal seismotectonic parameters have been ignored and mainly the cumulative effects of Late Quaternary morphogenic events have been considered; in the other case this additional co-seismic information has been included (Caputo et al., 2015).

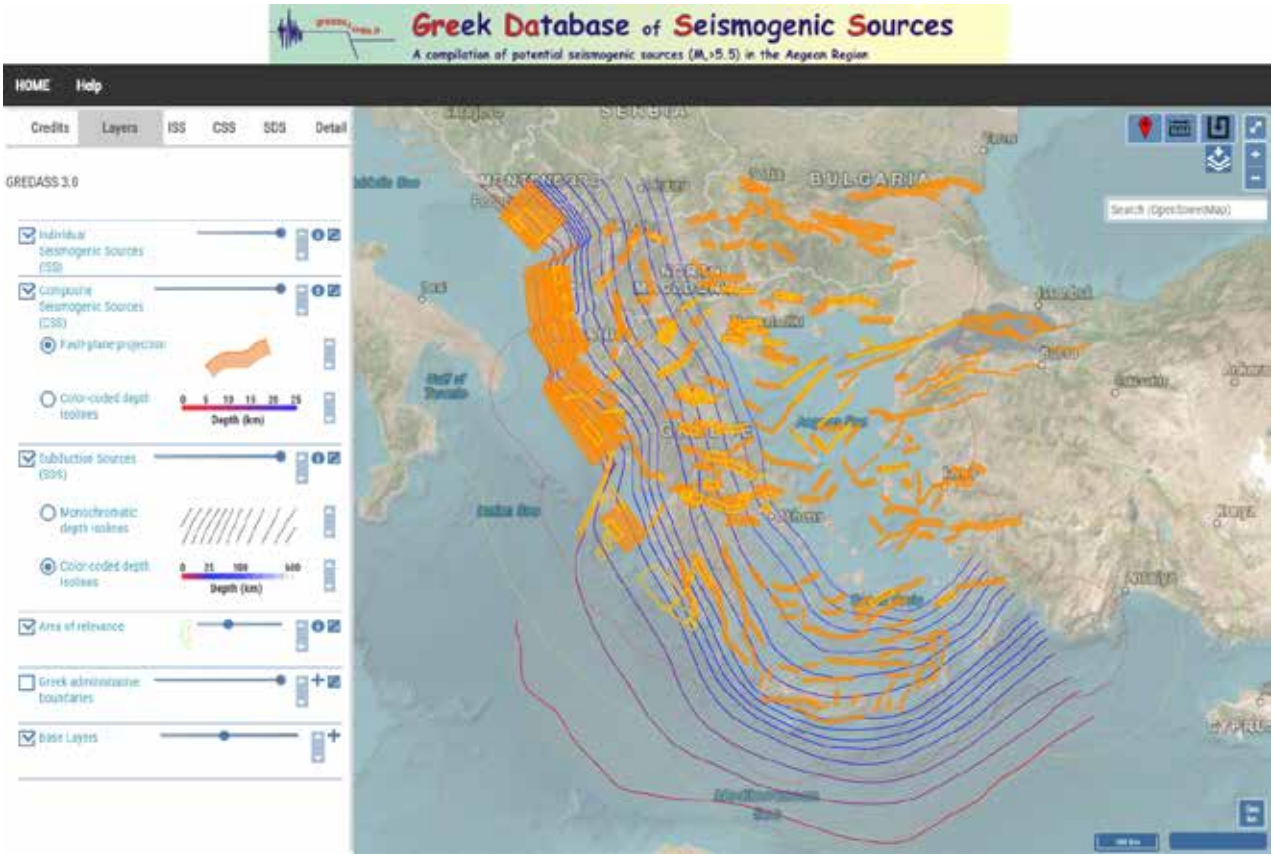

Figure 1. Screen capture of the last release of GreDaSS (version 3.0) available through the new web GIS interface.

It is worth noting that relative to the previous one (release 2.0; Caputo and Pavlides, 2013) the new version of GreDaSS (release 3.0) has been largely improved both qualitatively and quantitatively. In particular, all seismotectonic parameters have been systematically revised and most of the numerical fields have been completed and/or compiled where missing. This work produced an overall rough increase in the order of +70% of the information contained. It is worth noting the significant improvement that was achieved in better constraining the seismogenic layer all over the investigated area by applying the results of the 3D thermo-rheological model recently produced for the broader Aegean Region (Maggini, 2020; Maggini and Caputo, 2020; 2021; Maggini et al., 2023). Based on this model, a set of crucial seismotectonic parameters, like maximum depth, width, dip-angle and maximum credible magnitude of the seismogenic sources, have been systematically revised and/or better quantified.

Crustal faults (i.e. CSSs and ISSs) included in the database are at present 277 (instead of 267) and 117 (108), respectively. As concerns the other two informative layers (the graphical one and the relevant literature), the number

of figures associated with the sources are now 1667 (916) and references 853 (679), showing in both cases an important step forward the completeness and improvement of the database especially if compared to version 2.0.
When a seismogenic source is associated with secondary effects, especially liquefaction features, because of a recent or historical event, this information taken from DALO (Papathanassiou et al., 2010) has been systematically included in the descriptive layer of the new GreDaSS release.
A further major difference of the last release is represented by the reconstructed and modelled Wadati-Benioff zones that were not included in the previous version of GreDaSS. In version 3.0, they are actually two, the Hellenic Subduction Zone and the Adriatic Continental Collision (Figure 1), therefore better defining the seismotectonics of the active accretionary wedges surrounding the southern Balkan peninsula.
As a final comment, we want to stress the fundamental and intrinsic difference of GreDaSS with respect to other apparently similar catalogues and/or databases available or under construction for the broader Aegean Region. Indeed, GreDaSS with its philosophical approach, its informatic structure and especially the choice of including some crucial parameters is the only one that could be directly exported and easily used for performing seismic hazard assessment analyses, like for example, in the Seismic Hazard Harmonization in Europe Project (SHARE; http://www.share-eu.org/) or the TAP Project between the Greece-Turkey border and southern Italy (Slejko et al., 2021; Moratto et al., 2021).

Acknowledgements
We acknowledge the financial contribution provided by INGV and the EPOS Italia Project and the multi-decennial support of the University of Ferrara. We also thank R. Basili for the continuous discussions and exchanges of ideas and the contributors to the previous release of the database.

References

Ambraseys, N.N., Jackson J.A., 1998. Faulting associated with historical and recent earthquakes in the Eastern Mediterranean region. Geophys. J. Int., 133, 390-406.
Atzori, S., Manunta, M., Fornaro, G., Ganas, A., Salvi, S., 2008. Postseismic displacement of the 1999 Athens earthquake retrieved by the Differential Interferometry by Synthetic Aperture Radar time series. J. Geophys. Res., 113, B09309.
Basili, R., Valensise, G., Vannoli, P., Burrato, P., Fracassi, U., Mariano, S., Tiberti, M.M., Boschi, E., 2008. The database of individual seismogenic sources (DISS), version 3: summarizing 20 years of research on Italy's Earthquake Geology. Tectonophys., 453(1-4), 20-43.
Basili R., Danciu L., Beauval C., Sesetyan K., Vilanova S., Adamia S., Arroucau P., Atanackov J., Baize S., Canora C., Caputo R., Carafa M., Cushing M., Custódio S., Demircioglu Tumsa M., Duarte J., Ganas A., García-Mayordomo J., Gómez de la Peña L., Gràcia E., Jamšek Rupnik P., Jomard H., Kastelic V., Maesano F. E., Martín-Banda R., Martínez-Loriente S., Neres M., Perea H., Sket-Motnikar B., Tiberti M. M., Tsereteli N., Tsironi V., Vallone R., Vanneste K., Zupančič P. (2022). European Fault-Source Model 2020 (EFSM20): online data on fault geometry and activity parameters [Data set]. Istituto Nazionale di Geofisica e Vulcanologia (INGV), https://doi.org/10.13127/efsm20.
Basili R., Danciu L., Beauval C., Sesetyan K., Vilanova S.P., Adamia S., Arroucau P., Atanackov J., Baize S., Canora C., Caputo R., Carafa M.M.C., Cushing E.M., Custódio S., Demircioglu Tumsa M.B., Duarte J.C., Ganas A., García-Mayordomo J., Gómez de la Peña L., Gràcia E., Jamšek Rupnik P., Jomard H., Kastelic V., Maesano F.E., Martín-Banda R., Martínez-Loriente, S., Neres M., Perea H., Šket Motnikar B., Tiberti M.M., Tsereteli N., Tsironi V., Vallone R., Vanneste K., Zupančič P. and Giardini D., 2024. The European Fault-Source Model 2020 (EFSM20): geologic input data for the European Seismic Hazard Model 2020. Nat. Haz. Earth Syst. Sci. 24., 3945-3976, doi: 10.5194/nhess-24-3945-2024.
Caputo, R., 2005. Ground effects of large morphogenic earthquakes. J. Geodyn., 40(2-3), 113-118.
Caputo R. and Helly B., 2008. The use of distinct disciplines to investigate past earthquakes. Tectonophys., 453(1-4), 7-19, doi: 10.1016/j.tecto.2007.05.00.
Caputo, R., Pavlides, S., 2013. The Greek Database of Seismogenic Sources (GreDaSS), version 2.0.0: A compilation of potential seismogenic sources (Mw > 5.5) in the Aegean Region. https://gredass.unife.it/, doi: 10.15160/unife/gredass/0200.
Caputo, R., Sboras, S., Pavlides, S., Chatzipetros, A., 2015. Comparison between *single-event effects* and *cumulative effects* for the purpose of seismic hazard assessment. A review from Greece. Earth-Science Reviews 148, 94-120.
Chiarabba, C., Selvaggi, G., 1997. Structural central on fault geometry: example of the Grevena Ms 6.6, normal

faulting earthquake. J. Geophys. Res., 102, 22445-22457.
Clarke, P., Paradisis, D., Briole, P., England, P., Parson, B., Billiris, H., Veis, G., Ruegg, J-C., 1997. Geodetic investigation of the 13 May 1995 Kozani-Grevena (Greece) earthquake. Geophysical J Int., 135, 195-214.
Clarke, P.J., Paradisis, D., Briole, P., England, P.C., Parson, B.E., Billiris, H., Veis, G., Ruegg, J-C., 1998. Geodetic investigation of the 13 May 1995 Kozani-Grevena (Greece) earthquake. Geophys. Res. Letts., 24(6), 707-710.
DISS Working Group, 2021. Database of Individual Seismogenic Sources (DISS), Version 3.3.0: A compilation of potential sources for earthquakes larger than M 5.5 in Italy and surrounding areas. Istituto Nazionale di Geofisica e Vulcanologia (INGV), https://doi.org/10.13127/diss3.3.0.
Foumelis, M., Parcharidis, Is., Lagios, E., Voulgaris, N., 2009. Evolution of post-seismic ground deformation of the Athens 1999 earthquake observed by SAR interferometry. Journal of Applied Geophysics, 69(1), 16-23.
Ganas, A., Pavlides, S.B., Sboras, S., Valkaniotis, S., Papaioannou, S., Alexandris, G.A., Plessa, A., Papadopoulos, G.A., 2004. Active fault geometry and kinematics in Parnitha Mountain, Attica, Greece. J. Struct. Geol., 26, 2103-2118.
Hatzfeld, D., Karakostas, V., Ziazia, M., Selvaggi, G., Lebogne, S., Berge, C., Makropoulos K., 1998. The Kozani-Grevena (Greece) earthquake of May 13, 1995, a seismological study. J. Geodyn., 26(2-4), 245-254.
Hatzfeld, D., Karakostas, V., Ziazia, M., Selvaggi, G., Leborgne, S., Berge, C., Guiguet, R., Paul, A., Voidomatis, P., Diagourtas, D., Kassaras, I., Koutsikos, I., Makroulos, K., Azzara, R.., Di Bona, M., Baccheschi, S., Bernard, P., Papaioannou, C., 1997. The Kozani-Grevena (Greece) earthquake of 13 May 1995 revisited from a detailed seismological study. Bull. Seism. Soc. Am., 87(2), 463-473.
Karakaisis, G.F., Papazachos, C.B., Scordilis, E.M., 2010. Seismic sources and main seismic faults in the Aegean and surrounding area. Bull. Geol. Soc. Greece, 43(4), 2026-2042.
Kontoes, C., Elias, P., Sykioti, O., Briole, P., Remy, D., Sachpazi, M., Veis, G., Kotsis, I., 2000. Displacement field and fault modelling for the September 7, 1999 Athens Earthquake inferred from Ers-2 Satellite Radar Interferometry. Geophys. Res. Lett., 27(24), 3989-3992.
Maggini M., 2020. 3D rheological modelling in the Aegean Region and its importance for the seismotectonics of the area. PhD Thesis, University of Ferrara, Italy, 268 pp.
Maggini M. and Caputo R., 2020. Sensitivity analysis for crustal rheological profiles: examples from the Aegean Region. Ann. Geophys., 63(3), SE334, doi: 10.4401/ag-8244.
Maggini M. and Caputo R., 2021. Seismological data versus rheological modelling: comparisons across the Aegean Region for improving the seismic hazard assessment. J. Struct. Geol., 145, 104312, doi: 10.1016/j.jsg.2021.104312.
Maggini M., Russo D. and Caputo R., 2023. A 3D rheological model for the Aegean Region: mechanical layering and seismotectonic implications. J. Struct. Geol., 175, 104956, doi: 10.1016/j.jsg.2023.104956.
Meyer, B., Armijo, R., De Chabalier, J., Delacourt, C., Ruegg, J., Acache, J., Brioke, P., Papanastassiou, D., 1996. The 1995 Grevena (Northern Greece) earthquake: fault model constrained with tectonic observations and SAR interferometry. Geophys. Res. Lett., 23(19), 2,677-2,680.
Meyer, B., Armijo, R., Massonnet, D., de Chabalier, J.B., Delacourt, C., Ruegg, J.C., Achache, J., Papanastassiou, D., 1998. Results from combining tectonic observations and SAR interferometry for the 1995 Grevena earthquake: a summary. J. Geodyn., 26(2-4), 255-259.
Meyer, B., Armijo, R., Massonnet, D., de Chabalier, J.B., Delacourt, C., Ruegg, J.C., Achache, J., Papanastassiou, D., 1998. Comment on “Geodetic investigation of the 13 May Kozani-Grevena (Greece) earthquake” by Clarke et al., Geophys. Res. Lett., 25, 129-l30.
Moratto L., Vuan A., Saraò A., Slejko D., Papazachos C., Caputo R., Civile D., Volpi V., Ceramicola S., Chatzipetros A., Daja S., Fabris P., Garcia-Pelaez J., Geletti R., Karvelis P., Pavlides S., Rapti D., Rebez A., Rossi G., Sandron D., Santulin M., Sboras S., Tamaro A., Zecchin M., Zgur F. and Zuliani D., 2021. Seismic hazard for the Trans Adriatic Pipeline (TAP) (Part2): broadband scenarios at the Fier Compressor Station (Albania). Bull. Earthq. Eng., 19, 3389-3143, doi: 10.1007/s10518-021-01122-z.
Mountrakis, D., Tranos, M., Papazachos, C., Thomaidou, E., Karagianni, E., Vamvakaris, D., 2006. Neotectonic and seismological data concerning major active faults, and the stress regimes of Northern Greece. In: Robertson, A.H.F., Mountrakis D. (Eds.), Tectonic Development of the Eastern Mediterranean Region. Geol. Soc. London Spec. Publ., 260, 649-670.
Papathanassiou, G., Valkaniotis, S., Chaztipetros, A., Pavlides, S., 2010. Liquefaction susceptibility map of Greece. Bull. Geol. Soc. Greece, 43, 1383-1392.
Papazachos, B.C., Papaioannou, C.A., Papazachos, C.B., Savvaidis, A.S., 1999). Rupture zones in the Aegean region. Tectonophys., 308, 205-221.

Pavlides, S.B, Zouros, N.C, Chatzipetros, A.A., Kostopoulos, D.S., Mountrakis, D.M., 1995. The 13 May 1995 western Macedonia, Greece (Kozani Grevena) earthquake; preliminary results, Terra Nova, 7, 544-549.

Pavlides S.B., Valkaniotis S. and Chatzipetros A. (2007): Seismically capable faults in Greece and their use in seismic hazard assessment. 4th Int. Conf. Earthq. Geotech. Eng., Thessaloniki, Greece, p. 1609.

Pavlides, S., Chatzipetros, A., Valkaniotis, S., 2008. Active faults of Greece and surroundings. 33rd Int. Geol. Congr., August 6-14, 2008, Oslo, Norway.

Russo D., 2025. Seismotectonic characterization of the South-Western Balkans seismogenic sources and 3D modelling of the uppermost part of the Hellenic Subduction Zone. PhD Thesis, University of Ferrara, Italy, 214 pp.

Sboras S., 2012. The Greek Database of Seismogenic Sources: seismotectonic implications for North Greece. PhD Thesis, University of Ferrara, Italy, 252 pp.

Slejko D., Rebez A., Santulin M., Garcia-Pelaez J., Sandron D., Tamaro A., Civile D., Volpi V., Caputo R., Ceramicola S., Chatzipetros A., Daja S., Fabris P., Geletti R., Karvelis P., Moratto L., Papazachos C., Pavlides S., Rapti D., Rossi G., Saraò A., Sboras S., Vuan A., Zecchin M., Zgur F. and Zuliani D., 2021. Seismic hazard for the Trans Adriatic Pipeline (TAP). Part 1: probabilistic seismic hazard analysis along the pipeline. Bull. Earthq. Eng., 19, 3349-3388, doi: 10.1007/s10518-021-01111-2.

Valensise, G., Pantosti, D. (Eds), 2001. Database of potential sources for earthquakes larger than M 5.5 in Italy. Ann. Geofisica, 44(4), 797-807.

Valkaniotis S., 2009. Συσχέτιση Νεοτεκτονικών ομών και Σεισμικότητας στην Ευρύτερη Περιοχή του Κορινθιακού Κόλπου (Κεντρική Ελλάδα). PhD Thesis, Aristotle University of Thessaloniki, 240 pp.

Vallone R., Basili R., 2023. Technical documentation of SEISMOFAULTS.EU: the IT infrastructure employed by the European Databases of Seismogenic Faults (EDSF) installation. Rapp. Tec. INGV, 474: 134, doi: 10.13127/rpt/474.

Voulgaris, N., Pirli, M., Papadimitriou, P., Kassaras, J., Makropoulos K., 2001. Seismotectonic characteristics of the area of western Attica derived from the study of the September 7, 1999 Athens earthquake aftershock sequence. Bull. Geol. Soc. Greece, 34(4), 1645-1651.

Woessner, J., Danciu, L., Giardini, D., Crowley, H., Cotton, F., Grünthal, G., Valensise, G., Arvidsson, R., Basili, R., Demircioglu, M. B., Hiemer, S., Meletti, C., Musson, R. W., Rovida, A. N., Sesetyan, K., Stucchi, M., and the SHARE Consortium: The 2013 European Seismic Hazard Model: key components and results, Bull. Earthq. Eng., 13, 3553–3596, doi: 10.1007/s10518-015-9795-1, 2015.

17th INTERNATIONAL CONGRESS of the Geological Society of Greece

BULLETIN OF THE GEOLOGICAL SOCIETY OF GREECE, SP. PUBL.

EXTENDED ABSTRACT 042

Sousa Dinosaur Valley, Brazil: The largest record of Lower Cretaceous dinosaur footprints in South America and its influence in local communities

Carvalho I.S.[1,2], Henriques M.H.[2], Leonardi G.[3]

(1) Department of Geology, Federal University of Rio de Janeiro, Cidade Universitária - Ilha do Fundão, CCMN/ IGEO 21.949-900, Rio de Janeiro, Brazil, ismar@geologia.ufrj.br, Geosciences Centre, (2) Department of Earth Sciences, Faculty of Sciences and Technology, University of Coimbra (Polo II), Rua Sílvio Lima 3030-790, Coimbra, Portugal, (3) Istituto Cavanis, Venice, Italy

Introduction

The "Rio do Peixe Dinosaur Valley" comprises four sedimentary basins: Sousa, Triunfo (also called the Uiraúna-Brejo das Freiras basin), Pombal, and Vertentes. Located in the western part of the Brazilian Paraíba State, these areas are intracratonic basins that developed along preexisting structural trends of the basement during the origin of the South Atlantic Ocean. The age of these basins, based on microfossils, is characteristic of the Rio da Serra (Berriasian to Hauterivian) and Aratu (early Barremian) local stages (Lima and Coelho, 1987; Regali, 1990; Sousa *et al.*, 2019). Deposition is the result of tectonic activity, and it is represented by alluvial fans at the faulted borders, changing to an anastomosing fluvial system more distally, and by meandering fluvial system with a wide floodplain, where perennial and temporary lakes developed, in the central region of the basins (Carvalho, 2000; Fig. 1).

Especially in the Sousa Basin footprints and trackways, mainly of large theropods, sauropods, and ornithopods are common, as well as invertebrate ichnofossils, such as traces and burrows (Fernandes and Carvalho, 2001). Body fossils are represented by ostracods, conchostracans, plant fragments, palynomorphs, fish scales, and bones of crocodylomorph and dinosaurs. The abundance of dinosaurian ichnofaunas represents an extensive Lower Cretaceous megatracksite (Viana *et al.,* 1993; Carvalho, 2000; Leonardi and Carvalho, 2000, 2002) established during the early stages of the South Atlantic opening. In this area, 42 sites and approximately 96 individual stratigraphic levels preserve occurrences of more than 636 individual dinosaur trackways and isolated footprints, as well as rare tracks and traces of the vertebrate mesofauna (Leonardi and Carvalho, 2021). To date, the four basins of "Rio do Peixe Dinosaur Valley" show together the following dinosaur trackmakers for the corresponding trackways or isolated footprints: 38 graviportal ornithopods (Fig. 2A); one ankylosaur; one small quadrupedal thyreophoran; two small ornithopods (altogether, 42 ornithischians). Then, 447 individual theropods (Fig. 2B-C) and 90 sauropods (altogether, 537 saurischians) were identified. In total, the number of classifiable individual dinosaur tracks is 579; and the total number of dinosaur footprints and trackways, including the indeterminate tracks, is 636. This last number includes also four possible dinosaur tail impressions.

The meso-ichnofauna, very rare in these basins, is represented by just one set of batrachopodid prints, some crocodilian traces and tracks, one lacertoid footprint, perhaps a poor specimen of mammal tracks, and a very large number of small chelonian swimming tracks (Leonardi, 1989, 2021; Leonardi and Carvalho, 2021, 2024).

It is noteworthy that the large number of theropods represented is impressive, compared to the number of herbivores, which is quite common in the whole world. This phenomenon seems to be contrary to the biomass pyramid theory. It can be explained, however, considering that carnivores probably had a higher level of mobility and therefore printed more tracks and footprints daily. It is also quite remarkable that the ankylosaur hand-foot set (specimen SOES 7, from the Serrote do Pimenta, Sousa), discovered in 1979 (Leonardi, 1984, 1989, 1994), represents the first record of the presence of this clade of Thyreophora in the South American continent.

The diversity of dinosaur tracks: an insight into the Early Cretaceous ecosystems

The dinosaur footprints in the Sousa Basin occur in at least 42 localities, in clastic deposits within all the formations of the Rio do Peixe Group (Antenor Navarro, Sousa and Rio Piranhas formations). At least 636 individual trackmakers are recorded in the Rio do Peixe basins (Carvalho and Leonardi 1992; Leonardi, 1984, 1994; Leonardi and Carvalho, 2021, 2024), and many others in a widely distributed set of track localities named the Borborema Megatracksite (Viana *et al.*, 1993). This megatracksite expands to the neighboring basins of Icó, Iguatu, Malhada Vermelha, Lima Campos (Leonardi, 1989; Leonardi and Spezzamonte, 1994), Cedro (Carvalho *et al.*, 1993), Araripe (Carvalho *et al.*, 1994, 2019, 2024; Carvalho and Leonardi, 2021, 2024), and can also be extended to encompass the region of the Cameroon Basin (Africa) as suggested by Jacobs *et al.* (2024).

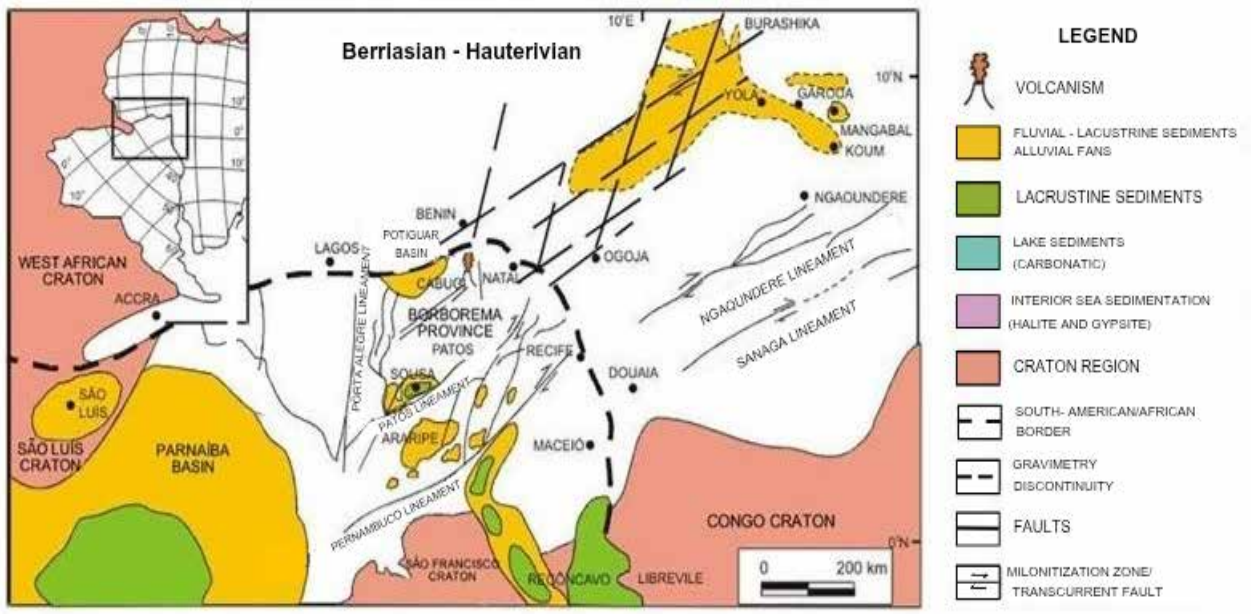

Figure 1. Geological context of Sousa Basin, northeastern Brazil during the Barremian-Hauterivian. The dinosaur footprints from the Sousa Basin were formed in the environments established during the first stages of South America – Africa drifting (modified from Popoff, 1988).

The set of footprints is indicative of the high diversity of dinosaurs in the terrestrial ecosystems, despite the few osteological remains. Footprints are rare in the Antenor Navarro and Rio Piranhas formations as they are preserved only in fine sediments that accumulated as subaerial sandy bars in alluvial fans and anastomosing rivers close to the basin margins. In the Sousa Formation, the sediments of finer grain sizes are more suitable for track preservation. This last unit is interpreted as deposited in lacustrine, swampy, and meandering braided fluvial environments (Leonardi and Carvalho, 2024; Fig. 2).

The Dinosaur Valley and its Influence in the Sousa Community

The town of Sousa is undeniably the "capital" of the "valley of the dinosaurs" of western Paraíba. The Sousa municipality has a territory of 842 km² located in the region of the Alto Sertão da Paraíba, in the semi-arid belt of Paraíba State. The municipality of Sousa has 67,259 inhabitants (IBGE, 2022).

The influence of the scientific studies concerning dinosaur tracks in the region allowed new economic perspectives. After one hundred years of research (beginning with Moraes, 1924), dinosaur footprints became a popular aspect of the local culture. The main occurrence and most accessible ichnosite is located at Passagem das Pedras (Ilha Farm) in the Sousa municipality. In December 1992 (Diário Oficial do Estado da Paraíba, Decree nº 14.833, December 20th, 1992), through a state act, the area was defined as a natural monument and named "Dinosaur Valley Natural Monument" (Monumento Natural Vale dos Dinossauros). Since then, the influence of the dinosaur theme on a variety of community activities has been incontestable, reflecting the improvement of science knowledge in the municipality.

Over the last fifty years, the region, previously known mainly for its cotton agriculture, acquired a new identity as a result of the regular presence of researchers, undergraduate and graduate students, and the media's diffusion about the dinosaur tracks in Sousa County. In the downtown area of Sousa city references to dinosaurs progressively invaded different aspects of community life, from sports to commercial and social activities, which shows the way that the people of Sousa connect to the dinosaur tracks recorded in their municipality, considered to be a heritage that deserves to be preserved (Fig. 3).

It is possible to preserve any geological heritage through public policies, but the main way to preserve it is the reconnaissance by the community about their importance and economic relevance. The tourism in the Sousa region, the local museum, a national identity based on the soccer team (Green Dinosaurs from Sertão, Sousa Futebol Clube), and the continuous support of scientific research allowed the engagement of the local population to the preservation of their ichnofossils. They are recognized as important objects to the economy and social development (Carvalho and Leonardi, 2007; Fernandes and Carvalho, 2007; Santos *et al.*, 2016, 2019), a fundamental condition for safeguarding their physical integrity.

But the ichnofossils of Sousa are exposed to risks of non-anthropic origin that call for new approaches to the issue of in-situ preservation of this type of heritage. Although the best way for educational and economic purposes is the preservation of the footprints in the natural outcrops, the environmental conditions to which they are currently subject can destroy them. Many of the

track-bearing surfaces will be worn out by natural erosion, especially where the tracks occur in surfaces nearside the temporary rivers. Besides the traditional methodology of documentation, it is also necessary to digitally reconstruct the ichnosites and their footprints (Falkingham *et al.*, 2014, 2018) as they are subject to destruction by erosion and in some rare cases to vandalism. In these cases, the removal and subsequent storage in museums, universities and research centers is the best solution to an ex-situ preservation of the paleontological heritage. Given the relevance of these ichnofossils to the population of Sousa, it would be necessary to consider replacing the original footprints with replicas, as happened within prehistoric cave paintings like Lascaux and Chauvet in France, or Altamira in Spain, a non-consensual management strategy but generally well accepted by tourists (Hughes *et al*., 2021). Other geoconservation issues of technical nature include expanding signage and improving accessibility to ichnosites, and enlargement of the Visitor Center with upgrade of the exhibition space on the theme of fossil footprints and dinosaurs of Sousa. Tormey (2019) refers to several ways of communicating geoheritage with people who are visiting protected areas or who are looking at a distance from the traditional to the most innovative social media platforms around the world which may inspire local authorities (Sousa municipality) and state authorities (Pernambuco State).

Figure 2. The great diversity of dinosaur tracks in the region of the Sousa Basin allows the reconstruction of terrestrial Cretaceous ecosystems. A. Iguanodontid footprints, the longest trackway (57 m) found in Sousa Basin, Passagem das Pedras ichnosite; B. Theropod footprints after excavation on mudstones with mudcracks, Passagem das Pedras ichnosite; C. Theropod footprint on coarse sandstones from Serrote do Letreiro ichnosite.

Figure 3. References to dinosaurs and their tracks in the emergence of a new identity for the region: A. Sousa Radio (Progresso AM); B. Sousa Sport Club, the main soccer game from the Sousa city, Paraíba State; C. A small inn located in the downtown; D. A market and bakery; E. A veterinary drugstore.

Geoconservation practitioners, researchers, and all the geoscience community need to enhance the engagement of the Sousa community with its geoheritage. This requires communication strategies targeted to different publics, such as local communities, local entrepreneurs and stakeholders, media, scientific community, tourists, politicians and policymakers around an ambitious geotourism plan to boost economic activity in the region and improve the social

conditions of the population, without jeopardizing the conservation of the paleontological heritage.
Future actions to promote the economy and social development of Sousa should include establishing guidelines by the State of Paraíba to stimulate private initiative aimed at tertiary sector activities geared towards employability around scientific tourism. At the same time, it is necessary to establish education programs that focus on the geoheritage value of Sousa ichnosites, which play a major role in raising people's awareness of their territory's paleontological heritage (Santos *et al*., 2019). On the part of the academic community, it will be important to maintain a continuous program of excavations and prospecting for new localities with fossil footprints, to guarantee a continuous flow of scientific publications and dissemination about Sousa's paleontological heritage.

Acknowledgements
The authors acknowledge the support from Conselho Nacional de Desenvolvimento Científico e Tecnológico (303596/2016-3) and Fundação Carlos Chagas Filho de Amparo à Pesquisa do Estado do Rio de Janeiro (E-26/200.998/2024). This study was supported by Portuguese funds of Fundação para a Ciência e a Tecnologia in the frame of the UIDB/00073/2025 (https://doi.org/10.54499/UIDB/00073/2020) and the UIDP/00073/2025 (https://doi.org/10.54499/UIDP/00073/2020) projects.

References

Carvalho, I.S., 2000. Geological Environments of Dinosaur Footprints in the Intracratonic Basins of Northeast Brazil during the Early Cretaceous Opening of the South Atlantic. Cretaceous Research 21, 255–267.

Carvalho, I.S., Leonardi, G., 1992. Geologia das bacias de Pombal, Sousa, Uiraúna-Brejo das Freiras e Vertentes (Nordeste do Brasil). Anais da Academia Brasileira de Ciências 64, 231–52.

Carvalho, I.S., Leonardi, G., 2007. The Dinosaur Valley Natural Monument: Dinosaur Tracks from Rio do Peixe Basins (Lower Cretaceous, Brazil). Reunión Argentina de Icnología, 5, Y Reunión de Icnología del Mercosur, 3. Ushuaia, Argentina, Marzo, Ushuaia, Argentina, p. 28–30.

Carvalho, I.S., Leonardi, G., 2021. Fossil footprints as biosedimentary structures for paleoenvironmental interpretation: Examples from Gondwana. Journal of South American Earth Sciences 106, 102936.

Carvalho, I.S., Leonardi, G. (Eds.), 2024. Dinosaur Tracks of Mesozoic Basins in Brazil Impact of Paleoenvironmental and Paleoclimatic Changes. 1st. ed. Switzerland: Springer Nature.

Carvalho, I.S., Viana, M.S.S., Lima Filho, M.F., 1993. Bacia de Cedro: a icnofauna cretácica de vertebrados. Anais da Academia Brasileira de Ciências 65, 459–460.

Carvalho, I.S., Viana, M.S.S., Lima Filho, M.F., 1994. Dinossauros do Siluriano: um anacronismo crono-geológico nas bacias interiores do Nordeste? 38º Congresso Brasileiro de Geologia, Camboriú. Boletim de Resumos Expandidos, Camboriú, Santa Catarina, Sociedade Brasileira de Geologia 3, 213-214.

Carvalho, I.S., Rios-Netto, A.M., Borghi, L., Freitas, A.P., Leonardi, G., Andrade, J.A., Freitas, F.I., 2019. Dinosaur Trampling from the Rio da Batateira Formation–Lower Cretaceous of Araripe Basin, Brazil, in: Fialho, P., Silva, R. (Eds.), Livro de Resumos. Paleo Fall Meeting 2019. Universidade de Évora, Portugal, p. 21.

Carvalho, I.S., Leonardi, G., Dias, J.J., 2024. The Cretaceous Araripe Basin Dinosaur Tracks and Their Paleoenvironmental Meaning. Dinosaur Tracks of Mesozoic Basins in Brazil, in: Carvalho, I.S., Leonardi, G. (Eds.), 1st. ed. Switzerland: Springer Nature Switzerland, 147-177.

Falkingham, P.L., Bates, K.T., Farlow, J.O., 2014. Historical Photogrammetry: Bird's Paluxy River Dinosaur Chase Sequence Digitally Reconstructed as It Was Prior to Excavation 70 Years Ago. Public Library of Science ONE 9(4): e93247. https://doi.org/10.1371/journal.pone.0093247.

Falkingham, P.L., Bates, K.T., Avanzini, M., Bennett, M., Bordy, E.M, Breithaupt, B.H., Castanera, D., Citton, P., Diaz-Martinez, I., Farlow, J.O. *et al.*, 2018. A Standard Protocol for Documenting Modern and Fossil Ichnological Data. Palaeontology, Frontiers In Palaeontology 61(4), 469-480.

Fernandes, A.C.S., Carvalho, I.S., 2001. Icnofósseis de invertebrados da Bacia de Sousa (Estado da Paraíba, Brasil): a localidade de Serrote do Letreiro. Simpósios Sobre a Bacia do Araripe e Bacias Interiores do Nordeste, 1 e 2. Novembro de 1997. Crato—Ceará. Comunicações 2001. Coleção Chapada do Araripe, Brazil, 1, p. 147–155.

Fernandes, A.C.S., Carvalho, I.S., 2007. As pegadas de dinossauros da Bacia do Rio do Peixe: elementos de transformação cultural em Sousa, Paraíba—Brasil, in: 5 Reunión Argentina de Icnologia, Y 3 Reunión de Icnología del Mercosur, Resúmenes, Laboratório de Geología Andina CADIC—CONICET, Argentina, p. 57.

Hughes, K., Mkono, M., Myers, D., Echentille, S., 2021. Are you for real?! Tourists' reactions to four replica cave sites in Europe. Tourism Management Perspectives 37, 100780.

IBGE (2022) Instituto Brasileiro de Geografia e Estatística. *censos.ibge.gov.br*. Access December 15th 2024.

Jacobs, L.L., Flynn, L.J., Scotese, C.R., Vineyard, D.P., Carvalho, I.S., 2024. The Early Cretaceous Borborema-Cameroon dinosaur dispersal corridor, in: Taylor, L.H., Raynolds, R.G., Lucas, S.G. (Eds.), Vertebrate

Paleoichnology: A Tribute to Martin Lockley. New Mexico Museum of Natural History and Science Bulletin 95, 199-212.

Leonardi, G., 1984. Le impronte fossili di dinosauri, in: Bonaparte, J. F., Colbert, E.H., Currie, P.J., Ricqlès, A.J de, Keilan-Jaworowska, Z., Leonardi, G., Morello, F., Taquet, P. (Eds.), Sulle orme dei dinosauri. Venezia-Mestre, Erizzo, 1984. (Esplorazioni e ricerche, IX) 335, 161–186.

Leonardi, G., 1989. Inventory and Statistics of the South American Dinosaurian Ichnofauna and its Paleobiological Interpretation, in: Gillette, D.D., Lockley, M.G. (Eds.), Dinosaur Tracks and Traces. Cambridge, Cambridge University Press, 165-178.

Leonardi, G., 1994. Annotated Atlas of South America Tetrapod Footprints (Devonian to Holocene) with an appendix on Mexico and Central America. Companhia de Pesquisa de Recursos Minerais, Brasília, Brasil. 248 p., 35 plates

Leonardi, G., 2021. Main results of 45 years of ichnological research on the dinosaur tracks of the Rio do Peixe basins (Paraíba, Brazil, Early Cretaceous). Annali del Museo Civico di Rovereto, Sez. Archeologia, Storia, Scienze Naturali 37, 159-182.

Leonardi, G., Carvalho, I.S., 2000. As pegadas de dinossauros das bacias Rio do Peixe, PB. [The Dinosaur Footprints from Rio do Peixe Basins, Paraíba State, Northeastern Brazil]; 15 pp., in: Schobbenhaus, C., Campos, D.A., Queiroz, E.T., Winge, M., Berbert-Born, M. (Eds.), Sítios Geológicos e Paleontológicos do Brasil. http://sigep.cprm.gov.br/sitio079/sitio079english.htm.

Leonardi, G., Carvalho, I.S., 2002. Icnofósseis da Bacia do Rio do Peixe, PB. O mais marcante registro de pegadas de dinossauros do Brasil, in: Schobbenhaus, C., Campos, D.A., Queiroz, E.T., Winge, M., Berbert-Born, M. (Eds.), Sítios geológicos e paleontológicos do Brasil. Brasília. Brasil, Departamento Nacional de Produção Mineral, 2002, Brazil, 101–111.

Leonardi, G., Carvalho, I.S., 2021. Dinosaur Tracks from Brazil: A Lost World of Gondwana. 1st. ed. Indiana: Indiana University Press.

Leonardi, G., Carvalho, I.S., 2024. Walking in the Gondwanic Floodplains of Rio do Peixe Basins, in: Carvalho, I.S., Leonardi, G. (Eds.), Dinosaur Tracks of Mesozoic Basins in Brazil. 1st. ed. Switzerland: Springer Nature Switzerland, 179-214.

Leonardi, G., Spezzamonte, M., 1994. New Tracksites (Dinosauria: Theropoda and Ornithopoda) from the Lower Cretaceous of the Ceará, Brasil. Studi Trentini di Scienze Naturali. Acta Geologica 69(1992), 61–70.

Lima, M.R., Coelho, M.P.C.A., 1987. Estudo palinológico da sondagem estratigráfica de Lagoa do Forno, Bacia do Rio do Peixe, Cretáceo do Nordeste do Brasil. Boletim do Instituto de Geociências–USP, Série Científica 18, 67–83.

Moraes, L.J., 1924. Serras e montanhas do Nordeste; pp. 43–58, in: Inspectoria de Obras Contra As Seccas. Geologia. Rio de Janeiro. Ministério da Viação e Obras Publicas. (Série I. D. Publ. 58). 2nd ed. Coleção Mossoroense 35(1). Fundação Guimarães Duque, Rio Grande do Norte, Brasil.

Popoff, M., 1988. Du Gondwana à l'Atlantique sud: les conexions du fossé de la Bénoué avec bassins du Nord-Est brésilien jusqu'à l'ouverture du golfe de Guinée au Crétacé inférieur. Journal of African Earth Sciences 7, 409–431.

Regali, M.S.P., 1990. Biocronoestratigrafia e paleoambiente do Eocretáceo das bacias do Araripe (CE) e Rio do Peixe (PB), NE-Brasil, in: Simpósio Sobre a Bacia do Araripe e Bacias Interiores do Nordeste, 1, Atas, Crato, Ceará, Brazil, p. 163–72.

Santos, W.F.S., Carvalho, I.S., Brilha, J.B., 2019. Public Understanding on Geoconservation Strategies at the Passagem das Pedras Geosite, Paraíba (Brazil): Contribution to the Rio do Peixe Geopark Proposal. Geoheritage 11, 2065–2077.

Santos, W.F.S., Carvalho, I.S., Brilha, J.B., Leonardi, G., 2016. Inventory and Assessment of Palaeontological Sites in the Sousa Basin (Paraíba, Brazil): Preliminary Study to Evaluate the Potential of the Area to Become a Geopark. Geoheritage 8(4), 315–32.

Sousa, A.J., Carvalho, I.S., Ferreira, E.P., 2019. Non-marine Ostracod Biostratigraphy of Cretaceous Rift Lake Deposits (Sousa Basin, Brazil): Paleogeographical Implications and Correlation with Gondwanic Basins. Journal of South American Earth Sciences 96, 102345.

Tormey, D., 2019. New approaches to communication and education through geoheritage. International Journal of Geoheritage and Parks 7, 192–198.

Viana, M.S.S., Lima Filho, M.F., Carvalho, I.S., 1993. Borborema Megatracksite: uma base para correlação dos "arenitos inferiores" das bacias intracontinentais do Nordeste do Brasil, in: Simpósio de Geologia do Nordeste, Sociedade Brasileira de Geologia/Núcleo Nordeste, Boletim 13, 23–25.

17th INTERNATIONAL CONGRESS
of the Geological Society of Greece

BULLETIN OF THE GEOLOGICAL SOCIETY OF GREECE, SP. PUBL.

EXTENDED ABSTRACT 043

A Preliminary 3D Gravity Model for the Pre-volcanic Basement of Lesvos Island, Greece

S. Chailas[1], A. Tzanis[1]
(1) Section of Geophysics – Geothermy, National and Kapodistrian University of Athens, Athens, Greece; schailas@geol.uoa.gr.

Introduction / Background

The present work focuses on mapping the relief of the pre-volcanic basement on the Island of Lesvos, by interpreting the Bouguer gravity anomalies map using a 3D inversion scheme. Although the resulting model is not yet optimal, it nevertheless reveals the magnitude of the volcanic activity experienced by the area, as well as its relationship with the observed tectonic grain.

Lesvos, along with the region of the north-central Aegean, is part of a wider area that extends to northwestern Turkey, which has exhibited shoshonitic-type volcanism as part of the volcanic arc that has operated since during the Upper Oligocene – Middle Miocene periods. The volcanic rocks occupy almost the entire central and western part of Lesvos. (Hecht, 1972-1976; Pe-Piper et *al*., 2019).

Outcrops of the pre-alpine and alpine basement through which the volcanic formations were emplaced are mainly seen in the southeast part of the island; only minor occurrences exist at the western extremity of the island. In terms of age, the lithological formations of the basement cover the period from the Carboniferous to the upper Triassic, while there are also post-alpine formations of the Oligocene epoch.

The volcanic activity on Lesvos lasted for almost 6.0 Ma. Volcanic rocks are mainly shoshonitic in composition. A few calcareous andesites are placed at the beginning (Eressos area, 21.5Ma) and the end (Mytilene area, 16.5Ma) of volcanic activity.

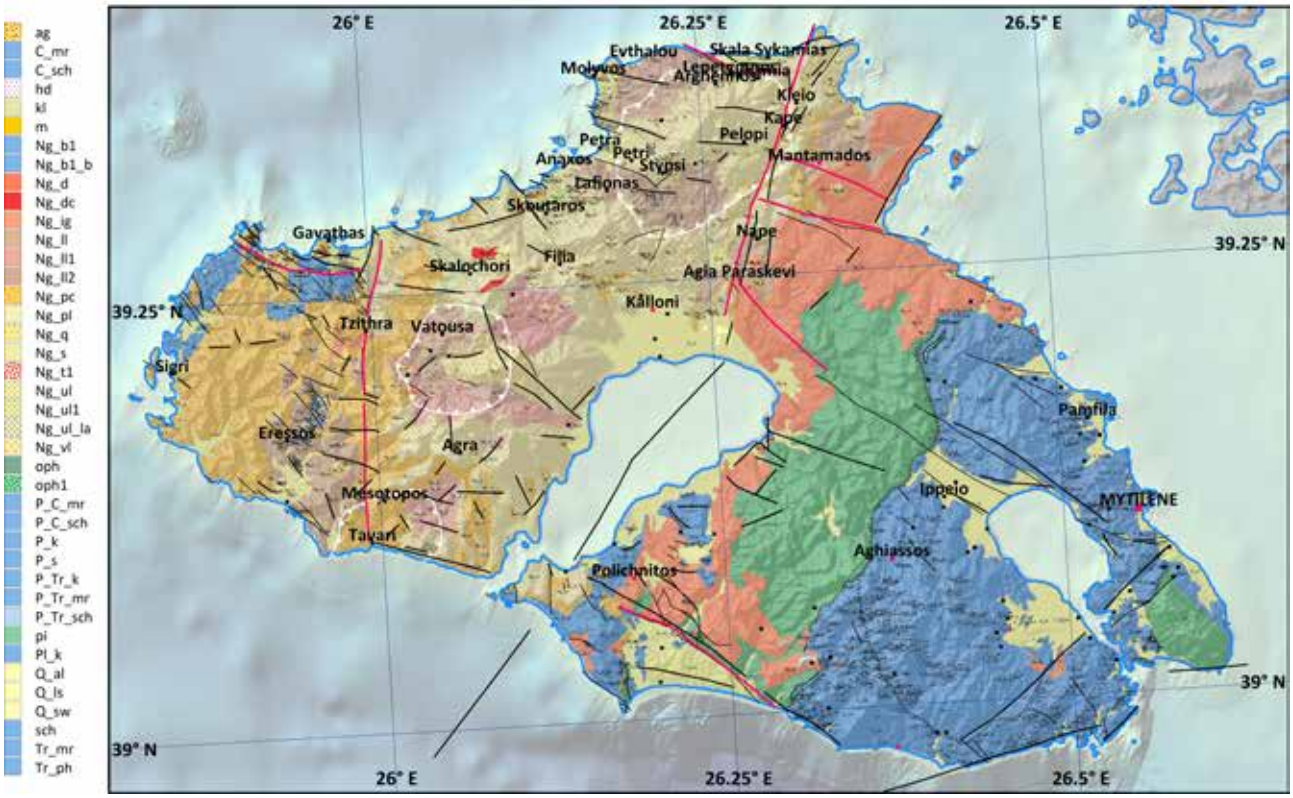

Figure 1. Geological map of Lesvos digitized from Hecht (1972-1976). The tectonic lines are from various sources

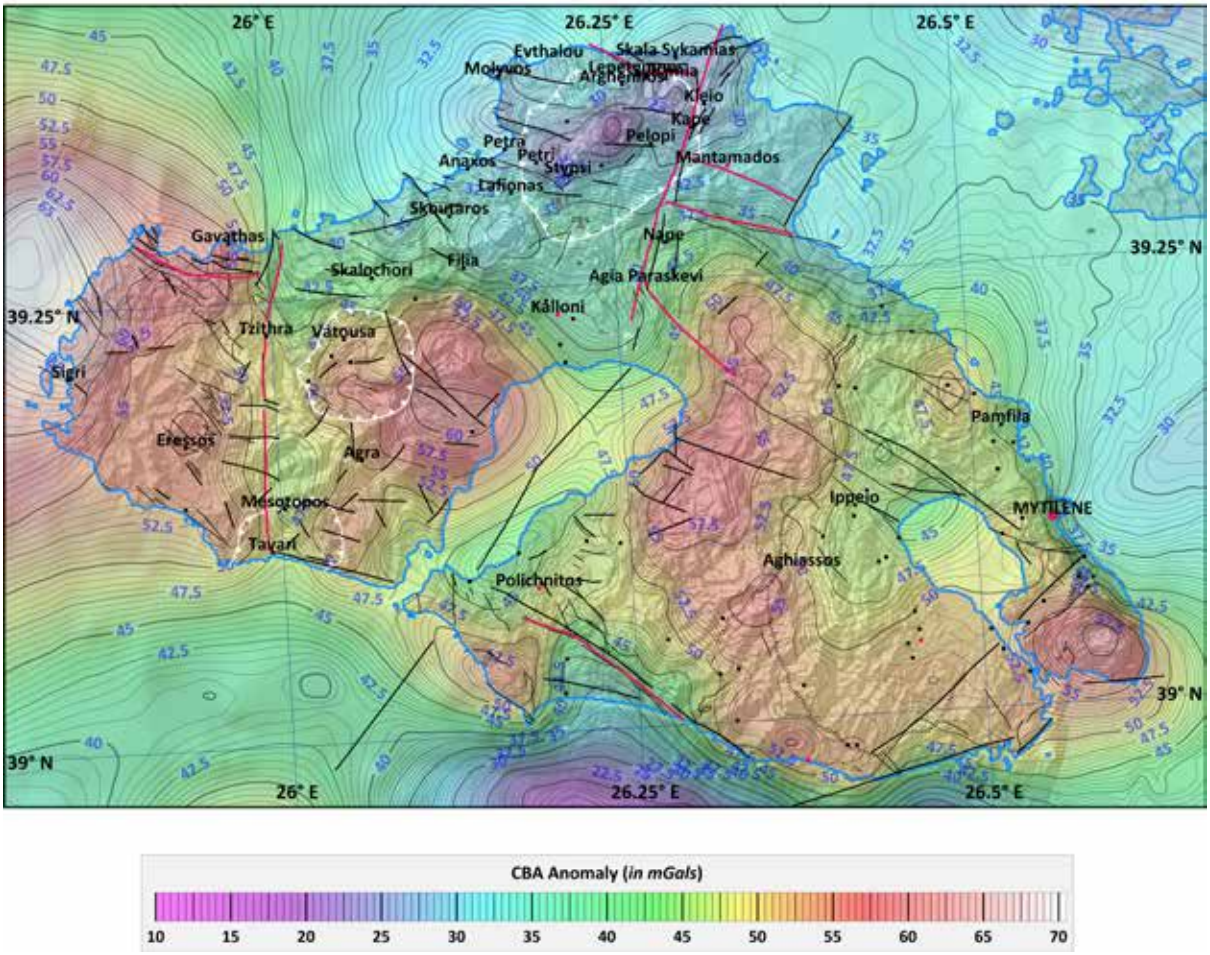

Figure 2. Bouguer Gravity Anomaly Map

The stratigraphy of the volcanic formations presented below is summarized from the work of Pe-Piper et *al*. (2019) and was based on the 1:50,000 geological maps of Hecht (1972–1976) and paleomagnetic and radiometric datings by Pe-Piper (1980) and Pe-Piper and Piper (1993). At 21.6 ± 0.5 Ma (new radiometric dating from Nissiopi Island is giving 23.3 ± 0.5 Ma) for the first andesitic-dacitic domes to break through and cover the basement at the Eressos area of western Lesbos (*Eressos Formation*). This, together with the Gavathas formation, was overlaid by the *Sigri Pyroclastic Formation* of several hundreds of meters thickness in western Lesbos and comprises principally tuffs. A prominent welded ignimbrite approx. 25 m thick is interbedded in the upper Sigri Pyroclastic Formation to the west of Antissa. In turn, the Sigri Pyroclastic Formation is covered by the *Skoutaros Formation* consisting of basaltic and andesitic flows. Some younger andesites and dacites are also included in the formation. The *Polychnitos Ignimbrite Formation* in eastern Lesbos comprises seven widespread welded ignimbrite units, each 30–50 m thick (Pe-Piper, 1980b). They appear to be contemporary with the upper part of the Skoutaros Formation. Pe-Piper (1977) suggests two different centers for its origin: a caldera near Lepetymnos for the older units and the caldera at Vatoussa for the younger (deposited in the southeast of the Gulf of Kalloni). The *Skalohorion* (eastern Lesvos) *and Sykaminea* (northern Lesvos) formations, consisting of younger andesitic and dacitic lavas, were paleomagnetically dated to between 17.0 – 17.6 Ma; these were followed by younger (16.8 Ma) minor basalts and andesites of the *Mytilene Formation* (Pe-Piper and Piper, 2002). Several sets of dykes run in different directions through the above formations. A significant stage of the geological evolution of the western Lesvos is the main volcanic phase, dated to around 17 Ma; in this, an increase in the tempo of volcanism is observed in the central volcanic chain, resulting apart from the eruption of the Polichnitos ignimbrites to the formation of the Lepetymnos and Vatoussa calderas.

As remnants of the volcanic activity, significant surface hydrothermal alterations have been mapped. These are distributed in two major groups, each collocated with one of the two calderas. The alteration ranges from argillic to pyritic and to silicic and is associated with veins whose length varies from several meters to a few kilometers and whose formation was controlled by the then active faulting.

The gravity anomaly map

The Bouguer Gravity Anomalies Map

A complete Bouguer Gravity (CBA) anomaly map of Lesvos was compiled on the basis of the Gravity Data Bank of the Department of Geophysics of NKUA (Lagios et *al.* 1995,1996). Gravity measurements (stations) are evenly distributed over the island, with a spatial density of approximately two stations per 5 km^2. The data has been referred to the IGSN71 datum and has been subject to complete Bouguer correction up to a radius of 166 km around each station. This allows the generation of gravity anomaly grids with 1km spacing. In the offshore area, the sparsity of gravity measurements, together with the absence of data from the gulfs of Kalloni, Gera and Edermit (Turkey), do not allow for any reliable representation of gravity anomalies in these areas; the contours shown in Fig. 2, 3 and 4 are only results of extrapolation.

The final CBA (Fig. 2) allows for the analysis of the gravitational signatures, not only of the volcanics as a whole, but also of individual volcanic formations with sizes comparable to the distances between stations, and of the main fault zones. Gravity anomaly amplitudes range between 10 and 70 mGal; they generally trend to the North with the highest values observed over areas of outcropping alpine and pre-alpine basement, while the lowest values are observed at the northernmost parts of the island.

Regional – Residual Anomalies Separation

To isolate gravity anomalies due to the geological structure of the area, we proceeded with the determination and reduction of the long wavelength anomalies from the Bouguer anomaly map. The resulting long wavelength (regional) anomaly map is presented in Fig. 3 and the residual Bouguer anomaly map, after subtracting it from the CBA, is presented in Fig. 4 (on top of the Geological map).

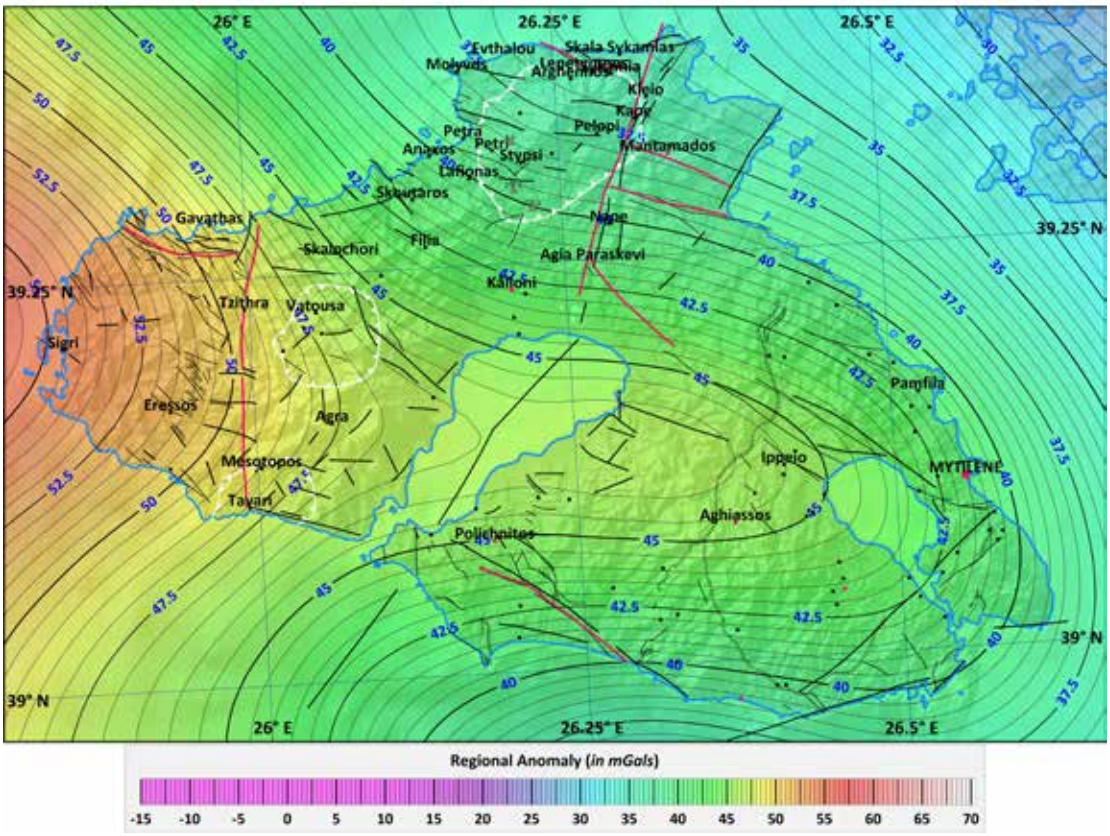

Figure 3. Regional Gravity Anomaly Map.

In the western part of Lesvos, the morphology of the residual anomalies correlates with the geology of the area. It displays a high over the area where the allochthonous basement is exposed on the surface, which is attributed to the high densities of the peridotitic rocks and the metamorphic sole. In the eastern and central parts of the Island, the presence of volcanics is evident in the comparatively lower anomaly amplitudes. Since the only extensive formations with unambiguously “low” density appearing in the area are the Sigri pyroclastics in the west, and the ignimbrites surrounding the ophiolites in the east, the low values in the rest of the area should probably be attributed to volcanic structures that extend in depth. A pronounced positive local anomaly between Vatoussa and Kalloni, not related to the exposure of an apparent high-density geological formation, requires further investigation. The presence of the

lower lavas in the area, east of Agra at an altitude of 500 meters (Fig. 1), in combination with the anomaly, points to the possibility of the generally small thickness of the volcanics in that area. Considering also the amplitude and width of this anomaly, we tentatively conclude that it could be attributed to the presence of the allochthonous basement.

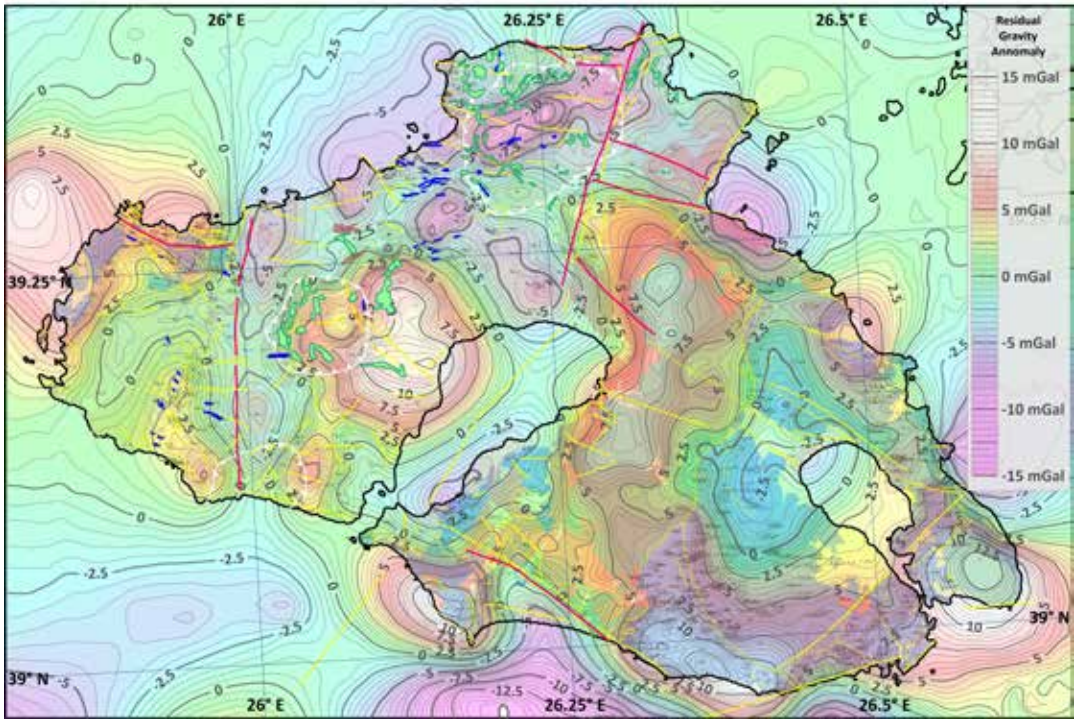

Figure 4. Residual Gravity Anomaly Map (overlaid on the geological map)

The gravity signals of Lepetymnos and Vatoussa calderas (expected to present low anomalies) seem to exist but neither of them is as clear as they were expected to be. The Lepetymnos caldera shows a significant elongate gravity low, delimited though in the area covered by the upper lavas (*Ng_ul* in the geological map). The gravity effect of the lower lavas (*Ng_ll2*) that are in contact with Ng_ll and extend to the north of the caldera, and to the south up to the trace of the caldera, seems to be unaffected by the formation of the caldera. The caldera of Vatoussa shows a more complicated figure. The caldera itself is located at the top of the topography. The gravity anomalies within the boundary of the caldera exhibit lower amplitudes with respect to the adjacent gravity high.

Inversion and Modeling

The modelling was performed with an unpublished algorithm developed by S. Chailas. In this approach, buried three-dimensional geological bodies are approximated by polyhedra of polygonal cross-section and their gravity effect is calculated by the method of Radhakrishna Murthy et *al*., (1989, 1990). Because any polyhedron can be defined by an upper and a lower boundary surface, the shape of any geological body can be determined by using prior information to fix one of the surfaces while adjusting the other. Surface topography, boreholes, other geophysical surveys and surface geology are some obvious sources of prior information.

The adjustment of the boundary surface(s) is automated by an iterative procedure derived from Bott (1960). Letting $\hat{\mathbf{g}}$ denote the matrix of observed gravity anomalies, $\mathbf{g}(k)$ the matrix of calculated gravity anomalies at the k^{th} iteration and $\Delta\mathbf{g}(k) = \hat{\mathbf{g}} - \mathbf{g}(k-1)$ the corresponding residual anomalies, the adjusted boundary surface $\mathbf{Z}(k)$ is modified according to the scheme

$$\mathbf{Z}(k) = \mathbf{Z}(k-1) - \frac{\Delta\mathbf{g}(k)}{2\pi G\Delta\rho} \circ \mathbf{W}_Z, \qquad k = 2,3,\ldots$$

where G is the universal gravitational constant, $D\rho$ is the density contrast across $\mathbf{Z}(k)$, $\mathbf{W}_z$ is a matrix of weights and ◦ denotes the Hadamard product. The iterative procedure aims at minimizing the objective function

$$\sum\sum\left(\hat{\mathbf{g}} - \mathbf{g}\right)^2 \circ \mathbf{W}_G ,$$

where $\mathbf{W}_G$ is a matrix of weights. The elements of $\mathbf{W}_z$ and $\mathbf{W}_G$ are either 0 or 1. Thus it is possible to keep $\mathbf{Z}(k)$ fixed wherever prior information exists and to isolate and study specific gravity anomalies.

In the present analysis and based on the data of Section 3.2.1 and Table 1, we have assumed that the volcanic rocks and Quaternary sediments on one hand, and the pre-alpine basement on the other, have a uniform density contrast of -0.25gr/cm^3. Accordingly, the analysis entailed the stripping of the gravity effect of the volcanic layer from the residual Bouguer anomaly. The upper boundary surface $\mathbf{Z}_U^{(1)}$ represents the actual topography and bathymetry (elevation) and was therefore fixed, while the lower boundary surface $\mathbf{Z}_L^{(1)}$ was allowed to vary. The thickness of the volcanic layer is $\mathbf{Z}_U^{(1)} - \mathbf{Z}_L^{(1)}$ and was kept fixed and equal to zero at the outcrops of the pre-volcanic basement. The final surface $\mathbf{Z}_L^{(2)}$ was taken to represent the topography of the pre-volcanic basement.

The adopted density contrast of -0.25 gr/cm^3 is plausible, as it represents the average value of lava densities. Note though that using a common average density for all the volcanic formations may introduce a degree of upward or downward bias to the thickness of the volcanics in localities where local densities deviate significantly from the average. For example, this may occur in areas where the cross-section of the low-density Sigri Pyroclastics is very thick. Nevertheless, it is expected that the resulting model of the volcanics layer is sufficiently representative of geological reality.

The elevation of the lower surface of the volcanic layer, i.e. the topography of the basement, is shown in Fig. 7 in both shaded relief and contour map forms. It exhibits an intricate pattern of structural features. An explanation of the more significant of these features is attempted below.

Discussion and Conclusions

The pre-volcanic basement exhibits a relief that appears to correlate with the older tectonism of the region and is only partly modulated by contemporary active tectonics. In western Lesvos, the basement is relatively shallow (-500 to –900 m) to the west of the currently active tectonic zone of Antissa, but plunges abruptly to the east, reaching elevations of -900 to -1250 m.

The Sigri formation, which extends to the orange dashed line, appears to have covered a preexisting basin (**B$_1$**) and an elongated morphological trough (**B$_2$**), possibly related to past tectonism. Along the orange line, which passes through the center of the Vatousa caldera, a sharp morphological change is observed in the basement, running from coast to coast subparallel to the Antissa fault and parallel to the active zone of Agia Paraskevi. On either side of the southern part of the Gulf of Kalloni, the morphology of the basement indicates the possible existence of an older basin (**B$_3$**). Further north, the area of Kalloni appears to be the southern end of basin **B$_4$**, which has a NW-SE oriented axis at the deepest point of which the Agia Paraskevi fault terminates.

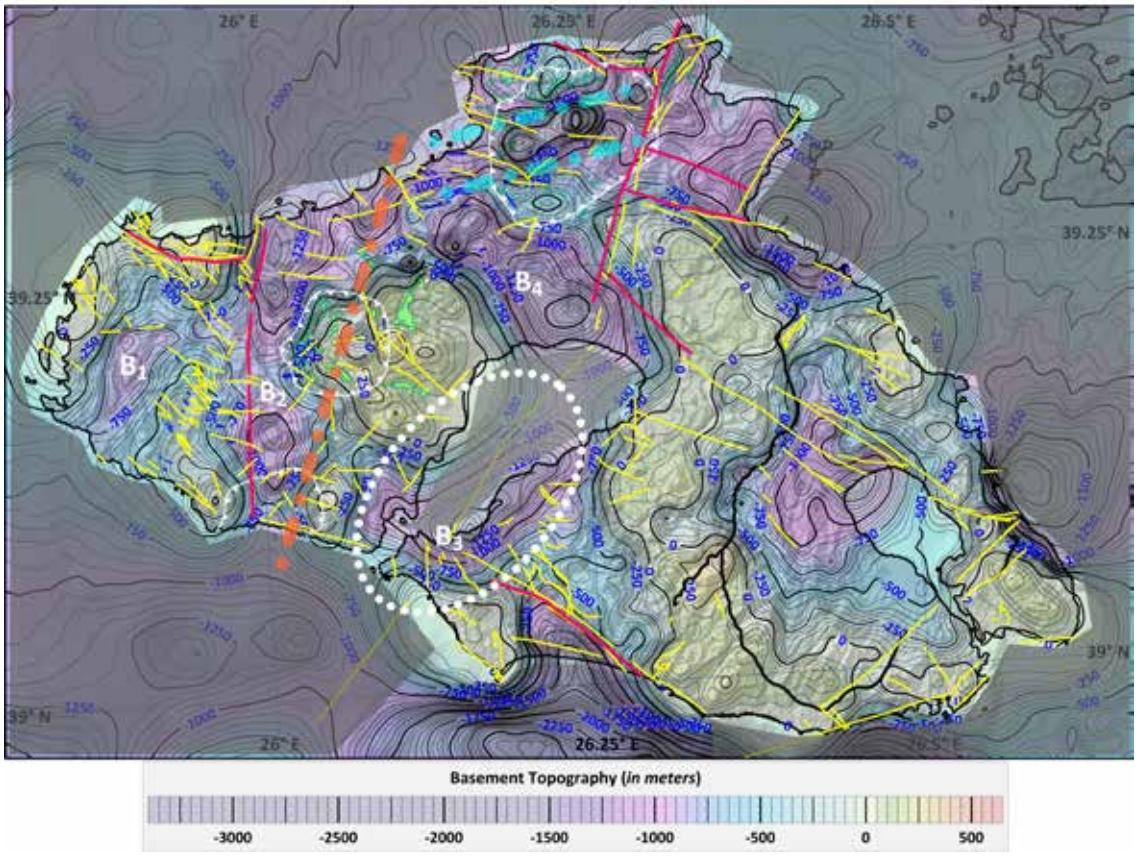

Figure 5. Model of the relief of the pre-volcanic basement

In the caldera of Lepetymnos, a significant NE-SW depression can be observed in the basement, which may be the result of density reduction through chemical alteration by hydrothermal activity facilitated by (past?) active faulting. Finally, in southern Lesvos, the model indicates a structural connection between the Vrissa – Vatera area and the submarine Lesvos basin, with the former feature appearing to fuse smoothly into the latter.

References

Bott, M.H.P., 1960. The use of rapid computing methods for direct interpretation of sedimentary basins, Geophys. J. Royal Astr. Soc., 3, (1), 63-67.

Hecht, J. (1972–1976). Geological map of Greece, Scale 1:50,000: Sheets of Plomari-Mytilene, Hagia Paraskevi, Mithymna, Polychnitos and Eresos. Institute of Geological and Mining Research (IGME), Athens, Greece.

Lagios E., Chailas, S. and Hipkin R., 2007. Gravity and topographic data banks of Greece. Geophysical Journal International. 126,

Pe-Piper, G., 1980. The Cenozoic volcanic sequence of Lesbos, Greece. Zeitschrift Der Deutschen Geologischen Gesellschaft, 131, 889–901.

Pe-Piper, G., & Piper, D. J. W., 1993. Revised stratigraphy of the Miocene volcanic rocks of Lesbos, Greece. Neues Jahrbuch Fur Geologie Und Palaeontologie Monatshefte, 2, 97–110.

Pe-Piper G., Piper D.J.W., Zouros N. and Anastasakis G., 2019. Age, stratigraphy, sedimentology and tectonic setting of the Sigri Pyroclastic Formation and its fossil forests, Early Miocene, Lesbos, Greece, Basin Res., **31,** 1178–1197, doi: 10.1111/bre.12365.

Radhakrishna Murthy, I.V., Rama Rao, P. and Ramakrishna, P., 1989. Gravity Anomalies of Three-dimensional Bodies with Variable Density Contrast., PAGEOPH, 130(4), 711-719.

Radhakrishna Murthy, I.V., Rama Rao, P. and Jagannardha Rao, S., 1990. The density difference and generalized programs for two and three-dimensional gravity modeling., Computers & Geosciences, 16(3), 277-287.

17th INTERNATIONAL CONGRESS
of the Geological Society of Greece

BULLETIN OF THE GEOLOGICAL SOCIETY OF GREECE, SP. PUBL.

EXTENDED ABSTRACT 044

Sediment dynamics in the Sperchios river basin and their influence on stevia cultivation

Chantzi P.[1], Doani, S.[1], Albanakis K.[1]
(1) Department of Physical and Environmental Geography, Aristotle University of Thessaloniki, Thessaloniki, Greece, pchantzi@geo.auth.gr

Introduction / Background

The purpose of this study was to conduct sedimentological analyses at selected stations within the Spercheios River basin, corresponding to specific sampling locations in stevia cultivation fields found in the area. The sediments, formed through rock weathering and erosion, transported downstream and deposited within the Spercheios basin, 2) the tectonic structures that determine the available space for sediment deposition, 3) the type of the Spercheios River, which defines the types and forms of deposited sediments, and 4) the lithological differentiation which influence the geochemical characteristics of the sediments, collectively define the cultivation environment. The simultaneous action of these mechanisms creates a unique geological identity for the sedimentary basin of the Spercheios River, framing the cultivation background. Consequently, this geological identity is reflected in the products grown in these specific fields. The focus of the study was to understand the variations between different agricultural areas in terms of their sedimentological identity and to explore the mechanisms driving any observed differences.

Methods

A sedimentological analysis was undertaken in the Laboratory of Sedimentology, Department of Physical and Environmental Geography A.U.Th. More specifically, grain size analysis was conducted on 12 samples from the first sampling period in 2023 (Figure 1). Particles larger than 2 mm were analyzed using the mechanical sieve method and a set of sieves at half-phi (ϕ) intervals. Following the removal of organic matter with a 10% H_2O_2 solution (Trautmann et al., 2000a, b), the finer fractions were analyzed through laser diffraction with a Malvern Master Sizer Hydro 3000.
The grain size statistical parameters were computed using Gradistat software (Blott & Pye, 2001), applying the Folk and Ward (1957) method. The granulometric indices, Mean grain diameter (M_z), Skewness (Sk_I), Sorting (σ_I), and Kurtosis ($K._I$), were also calculated, and the grain size distributions were visualized through cumulative and frequency curves.

Figure 1: First sampling period in 2023 in the cultivated areas in the Sperchios River basin

Results

The sedimentological analysis of 12 samples from the Spercheios River basin highlighted a variety of grain sizes, textural groups, and granulometric characteristics that reflect diverse sedimentary conditions within the stevia cultivation fields. The mean grain size ranged from coarse-grained material (e.g., gravel) to finer materials (e.g., mud). The samples were categorized into different textural groups, including “Muddy Gravel,” “Muddy Sandy Gravel,” “Gravelly Mud,” and “Sandy Mud,” indicating diverse depositional environments ranging from fluvial to mixed settings. Figures 2 and 3 show the varying percentages of gravel, sand, and mud in the samples. Samples such as Stev1, Stev2, Stev3, and Stev10 exhibit higher gravel percentages (above 40%), indicating coarse-grained sediment deposits. The highest gravel content is observed in Stev10, suggesting proximity to higher-energy conditions, such as active river channels or areas affected by strong fluvial transport. Conversely, Stev7 and Stev8 have significantly lower gravel percentages, indicating deposition in relatively lower-energy environments. Sand content varies moderately across the samples, generally falling within 10% to 30% in most cases. Samples like Stev5 and Stev6 show balanced amounts of sand, suggesting areas where medium-energy conditions persist during sediment deposition. Stev7 shows relatively higher sand content compared to others, but the dominance of mud remains significant in this sample. Stev7 and Stev8 are dominated by high mud content (~60% to 80%), indicating deposition of fine particles. Most other samples, particularly Stev1, Stev2, and Stev10, have lower mud percentages.

Table 1. Results of the grain size statistical parameters: Mean grain size, Sorting, Skewness, Kurtosis; in phi scale, Folk and Ward method (φ).

Sample	Mean (M)	Sorting (σ)	Skewness (Sk)	Kurtosis (Ku)	Textural Group
Stev1	1.515	3.847	-0.103	0.659	Muddy Gravel
Stev2	1.595	3.749	-0.143	0.675	Muddy Gravel
Stev3	1.265	3.880	0.179	0.697	Muddy Gravel
Stev4	0.507	3.130	0.894	0.471	Muddy Sandy Gravel
Stev5	1.858	3.370	0.158	0.718	Muddy Sandy Gravel
Stev6	1.610	3.683	-0.031	0.684	Muddy Sandy Gravel
Stev7	5.148	1.923	0.100	0.933	Sandy Mud
Stev8	2.579	4.141	-0.381	0.614	Muddy Gravel
Stev9	2.555	3.431	-0.255	1.004	Gravelly Mud
Stev10	2.880	3.603	-0.235	0.656	Gravelly Mud
Stev11	0.204	3.484	0.512	0.698	Muddy Sandy Gravel
Stev12	2.101	3.864	-0.273	0.655	Muddy Gravel

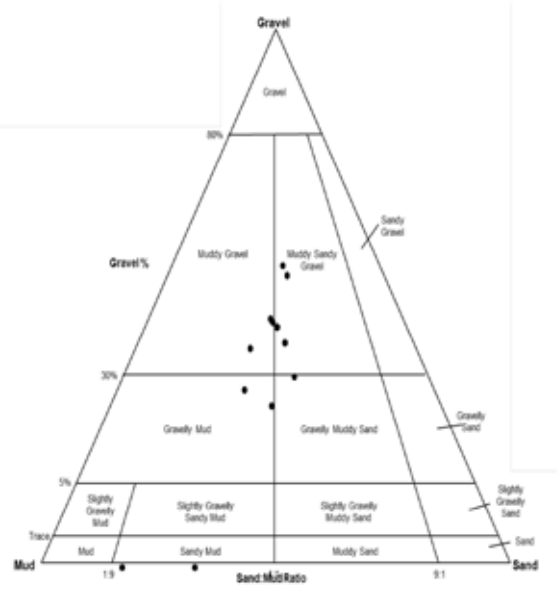

Figure 2. Gravel Sand Mud Diagram for all samples.

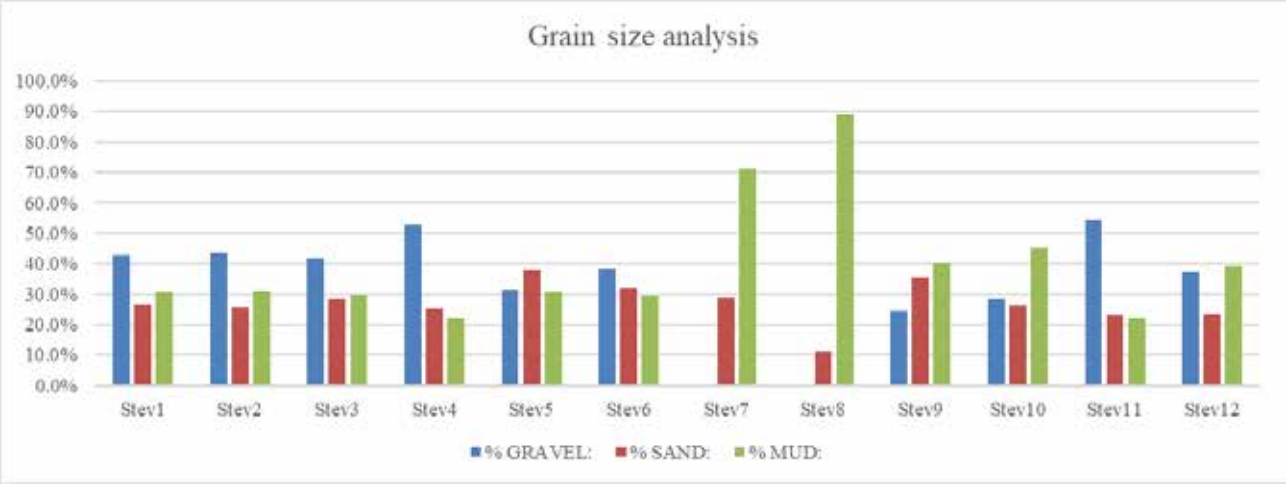

Figure 3. Gravel (%)"; the percentage of gravel fraction, "Sand (%)"; percentage of sand fraction, "Mud (%)"; percentage of silt and clay fraction, for all samples.

Conclusions

The Spercheios River basin exhibits considerable spatial variability in sedimentological characteristics, highlighting the complexity of sediment transport, deposition, and weathering processes within the region. The differences between samples can be attributed to local lithological variations and fluvial dynamics shaping sediment deposition patterns. Fields dominated by finer sediments (e.g., "Sandy Mud") offer higher water retention, potentially benefiting stevia growth, while coarser sediments (e.g., "Muddy Gravel") could enhance drainage but limit moisture availability. Poorly sorted and negatively skewed samples reflect dynamic depositional conditions, likely influenced by periodic floods or sediment influx from upstream erosion. These characteristics may lead to variable nutrient availability and soil fertility across the cultivation areas.

Acknowledgements

The work is funded by"Measure 16 'Cooperation" in the framework of National Rural Development Programme and it is co-financed by the European fund for rural development (EAFRD) and national budgets (GIstevSp: Project code M16SYN2-00237).

References

Blott, S.J., Pye, K., 2001. GRADISTAT: a grain size distribution and statistics package for the analysis of unconsolidated sediments. Earth Surf. Process. Landforms 26 (11), 1237–1248.

Folk, R., Ward, W., 1957. Brazos river bar: a study in the significance of grain size parameters. J. Sediment. Petrol. 27, 2–26.

Trautmann, T., Krbetschek, M.R., Dietrich, A., Stolz, W., 2000a. The basic principle of radioluminescence dating and a localized transition model. Radiat. Meas. vol. 32, 487–492.

Trautmann, T., Krbetschek, M.R., Stolz, W., 2000b. A systematic study of radioluminescence properties of single feldspar grains. Radiat. Meas. vol.32, 685–690.

17th INTERNATIONAL CONGRESS of the Geological Society of Greece

BULLETIN OF THE GEOLOGICAL SOCIETY OF GREECE, SP. PUBL.

EXTENDED ABSTRACT 045

Sustainable Practices for Resilient Hydrosystems at a Municipal Level: Insights from the Greek Island of Chios

Angelos Chasiotis[1], Elissavet Feloni[2], Panagiotis Nastos[1]

(1) Laboratory of Climatology and Atmospheric Environment, Department of Geology and Geoenvironment, National and Kapodistrian University of Athens, University Campus 15784, Athens, Greece; a.chasiotis@geol.uoa.gr

(2) Department of Surveying and Geoinformatics Engineering, University of West Attica, 28 Ag. Spiridonos, 12243 Egaleo, Athens, Greece

Abstract

Ensuring sustainable water resources management is crucial for the long-term resilience of municipal hydrosystems, particularly in Mediterranean island communities where water scarcity, aging infrastructure, and climate variability pose significant challenges. The island of Chios, located in NE Aegean, as many other areas in Greece faces high non-revenue water (NRW) losses, seasonal demand fluctuations, and over-reliance on groundwater abstraction, making it essential to implement innovative and sustainable interventions. This study explores smart water monitoring technologies, nature-based solutions (NBS), and modernized wastewater management to enhance the system's water efficiency, quality, and security. By integrating IoT-enabled leak detection, digital twin modeling, and automated pressure regulation, the island can reduce NRW losses by up to 40%, improving network performance and cost efficiency. Additionally, infrastructure modernization, including pipeline replacements and wastewater treatment upgrades, will enhance water reuse potential and minimize environmental impacts. Finally, studies have demonstrated that digital twin models can optimize network efficiency and reduce NRW losses significantly. The proposed interventions align with EU water management directives and climate adaptation strategies, ensuring resilience to future water challenges. With technological innovation, policy support, and community engagement, Chios has the potential to become a leading example of sustainable island water management, ensuring secure and equitable access to water resources for future generations. These findings align with broader EU climate adaptation policies, reinforcing Chios' commitment to a sustainable water management strategy that remains resilient and adaptable to future challenges.

Keyword: Sustainable water management; Mediterranean islands; Non-revenue water (NRW) losses; Smart water monitoring; Digital twin modeling; IoT-enabled leak detection; Climate adaptation strategies

Introduction

Water scarcity, exacerbated by climate change and increasing population pressures, presents a significant challenge for Mediterranean islands. The Greek island of Chios, like many coastal and insular regions, experiences high non-revenue water (NRW) losses, seasonal demand fluctuations, and heavy reliance on groundwater abstraction, raising concerns over long-term sustainability. Effective water resource management in these environments requires a combination of technological innovation, policy interventions, and nature-based solutions (NBS) to ensure resilience against hydrological variability and climate-induced risks.

Recent studies highlight the effectiveness of GIS-based water management strategies and hydrological modeling techniques in mitigating water resource vulnerabilities in Mediterranean regions. Additionally, nature-based solutions, such as rainwater harvesting, aquifer recharge, and wetland restoration, have been identified as promising approaches to enhance water sustainability while reducing reliance on energy-intensive desalination systems (Monokrousou et al., 2024). However, limited infrastructure investments and governance challenges continue to hinder the adoption of such measures.

Chios offers a unique case study for implementing smart water technologies and decentralized management strategies. By integrating IoT-enabled leak detection, digital twin modeling, and automated water distribution systems, municipalities can significantly reduce NRW, enhance operational efficiency, and ensure equitable access to water resources. Moreover, coastal aquifer conservation and groundwater quality monitoring are critical for protecting the island's freshwater supply from saline intrusion, a growing threat due to over-extraction and rising sea levels.

This study aims to explore sustainable water management interventions tailored to Mediterranean island hydrosystems, with a focus on Chios. The proposed framework leverages smart water governance, digital water technologies, and community-driven conservation strategies to enhance efficiency, resilience, and long-term sustainability. The findings will contribute to EU climate adaptation policies and regional water management frameworks, supporting efforts to

build climate-resilient hydrosystems for future generations.

Proposed Interventions for Sustainable and Resilient Hydrosystems

Water sustainability in municipal hydrosystems requires a multifaceted approach that integrates smart water technologies, nature-based solutions (NBS), and data-driven governance models. This section outlines a series of proposed interventions aimed at enhancing water efficiency, mitigating non-revenue water (NRW), and strengthening climate resilience in the municipal water infrastructure of Chios, a Greek island facing significant water challenges. Recent studies highlight the crucial role of digital water management and decentralized hydrological governance in addressing water scarcity and quality issues (Wendling et al., 2019). By adopting these innovations, Chios can transition toward a more resilient and sustainable water management framework.

One of the primary challenges for municipal hydrosystems is the high level of NRW, which results from leakage, inaccurate metering, and unauthorized water consumption. Implementing IoT-based smart leak detection systems and digital twin models can significantly enhance real-time monitoring and predictive maintenance (Kumar et al., 2023). The deployment of IoT sensors throughout the distribution network enables the identification of leaks and anomalies in real time, potentially reducing water losses by up to 40% (Mounirou et al., 2025). Additionally, digital twin models, such as those employed in EPANET simulations, facilitate scenario testing and infrastructure optimization, allowing municipalities to predict system failures and improve water distribution efficiency (Breil et al., 2022). Alongside these technologies, smart water metering solutions, including Advanced Metering Infrastructure (AMI), play a crucial role in improving monitoring accuracy. These systems allow for real-time tracking of household and commercial water usage, providing behavior-driven insights that help consumers reduce waste. Furthermore, automated billing and demand-based pricing strategies encourage conservation efforts by promoting more responsible water consumption practices (Rodríguez et al., 2021). By integrating these advanced monitoring and metering technologies, Chios can enhance the efficiency and sustainability of its water management system, while ensuring long-term resilience to climate variability and growing water demand.

Expected Outcomes: Reduction in NRW and Cost Savings

The implementation of smart water management technologies is expected to lead to significant reductions in non-revenue water (NRW) and generate substantial cost savings for Greek municipalities. By integrating decentralized water management and nature-based solutions, municipalities can reduce their reliance on traditional water sources while enhancing sustainability (Table 1).

Table 1: Expected Outcomes from Smart Water Management Technologies

Technology	Expected Water Savings (%)	Energy Savings (%)	Reduction in Operational Costs (%)	Estimated Reduction in Maintenance Costs (%)
IoT-Based Leak Detection	30	10	20	25
Smart Water Meters	25	8	15	20
Automated Pressure Management	20	12	18	22
Decision Support Systems (DSS)	15	5	12	18
Nature-Based Solutions (NBS)	10	4	8	10

One promising approach is rainwater harvesting combined with managed aquifer recharge, which offers a low-energy alternative to desalination for securing freshwater supplies (Monokrousou et al., 2024). Key interventions in this area include the installation of green rooftops and permeable pavements that help reduce stormwater runoff and replenish groundwater reserves (Wantzen et al., 2022). Additionally, wetland restoration can naturally filter pollutants while promoting biodiversity (Lewandowski et al., 2019), further supporting water quality and ecosystem health. Urban green infrastructure, such as bioswales and retention basins, also plays a crucial role in enhancing water management. These features reduce urban flood risks by absorbing and storing excess rainfall, improve water purification by filtering runoff before it enters water reservoirs (Meerkhan et al., 2021), and help mitigate the urban heat island effect, which is a growing concern under climate change (Hachem-Vermette, 2024). These solutions not only contribute to water conservation but also enhance urban resilience and adaptability.

Furthermore, the integration of digital water governance through Decision Support Systems (DSS) offers municipalities

tools for optimizing water distribution, energy use, and emergency responses (Jakovljević et al., 2021). Machine learning algorithms can be employed to forecast water demand based on climatic conditions (Chang et al., 2021), while geospatial mapping can help track and prevent groundwater depletion (Zounemat-Kermani et al., 2020). Finally, community-based water conservation programs play a vital role in driving long-term behavioral change. Public engagement through educational campaigns, digital water consumption dashboards, and municipal reward programs can encourage citizens to adopt water-saving practices and reduce domestic water consumption (Majumder and Kale, 2021).

The combined impact of these smart water management interventions is expected to significantly reduce NRW, lower operational costs, and foster more sustainable and resilient water systems, as demonstrated by similar successful practices in other municipalities across Greece (Table 2).

Table 2: Reduction of NRW Losses in Greek Municipalities with Smart Water Management

Municipality	Baseline NRW Losses (%)	Expected NRW Reduction (%)	Estimated Water Savings (m³/year)	Estimated Cost Savings (€/year)	Number of Beneficiaries
Aigio	48	35	600,000	21,000	20,422
Argos	54	40	1,200,000	42,000	22,209
Paramythia	72	50	600,000	20,000	3,032

(Data from: Chasiotis et al. 2023a; 2023b)

Case Study: Insights from the Island of Chios

Chios, a Greek island in the Aegean Sea, faces significant water management challenges due to seasonal variability, climate change, and high non-revenue water (NRW) losses. As a semi-arid island, Chios experiences long, dry summers and short, intense rainfall periods, which result in frequent water shortages and inefficient groundwater recharge. The municipal water system primarily relies on groundwater abstraction from local aquifers, limited rainwater harvesting, and seawater desalination to meet growing urban and tourism-related demand. However, these sources are increasingly vulnerable to climate variability, saline intrusion, and over-extraction, posing a threat to the island's long-term water security. The Municipal Water and Sewerage Company of Chios oversees the island's water supply and wastewater infrastructure (Table 3), drawing water from over 100 groundwater wells and boreholes, 160 natural springs, and 15 reservoirs, such as the Psaropetra Dam, which stores water during wet seasons. Additionally, four seawater desalination plants supplement supply, particularly during peak demand periods. Despite this diverse water network, Chios struggles with high NRW losses, reaching up to 50% in some areas due to aging pipelines, leaks, and unauthorized consumption. Outdated infrastructure, including asbestos cement and PVC pipes, requires urgent replacement, while the island's limited surface water storage capacity heightens its dependence on groundwater, leading to aquifer depletion and saline intrusion.

Table 3: Major settlements in Chios and their water supply characteristics

Municipal District	Main Water Sources	Challenges
Chios City	Groundwater, desalination, Psaropetra Dam	High seasonal demand, aging infrastructure
Kambos	Wells, springs	Overextraction, groundwater depletion
Mastichochoria	Reservoirs, springs	Insufficient supply during summer months
Volissos & Northern Chios	Springs, boreholes	High NRW losses, insufficient infrastructure
Oinousses Island	Desalination plant	Energy-intensive water production

(Data provided by the Municipal Enterprise for Water and Wastewater of Chios)

The water supply system serves both urban and rural settlements, each facing distinct challenges. Recent efforts to modernize infrastructure, such as replacing outdated asbestos cement pipes with high-density polyethylene (HDPE) alternatives, aim to improve water quality and reduce system inefficiencies. However, three primary challenges continue to impact Chios' water management. First, NRW levels remain high, with system inefficiencies caused by

aging pipelines, leaks, and inaccurate metering contributing to financial and operational losses. Second, climate change and rainfall variability have led to a 20% decline in annual precipitation over the past 30 years (Monokrousou et al., 2024), while rising temperatures and prolonged droughts increase reliance on groundwater, exacerbating the risk of saline intrusion in coastal aquifers. Third, tourism-driven demand surges place additional stress on the system, with water consumption increasing fivefold during peak summer months (Wendling et al., 2019).

The adoption of sustainable water management strategies offers significant environmental, social, and economic benefits for Chios. Environmentally, reducing groundwater over-extraction can help prevent saline intrusion, while minimizing water losses ensures efficient resource utilization. Improved wastewater treatment will further protect marine ecosystems by reducing coastal pollution. Social benefits include securing a continuous and safe water supply, enhancing climate resilience, and promoting water conservation awareness within the community. Economically, modernizing infrastructure and reducing NRW can lower operational costs, while improved water services and environmental sustainability can boost the island's attractiveness as a tourist destination. Additionally, investments in smart water technologies and infrastructure development can create new local employment opportunities.

By implementing smart leak detection systems, automated pressure regulation, expanded wastewater treatment capacity, and increased desalination and rainwater harvesting, Chios can enhance its water security and sustainability. The European Environment Agency in 2021 emphasized that digital water governance frameworks can significantly improve municipal decision-making, further supporting these interventions. Collectively, these measures could lead to a 30–40% reduction in NRW losses, strengthening the island's long-term water resilience. The success of these strategies depends on strong municipal governance, stakeholder collaboration, and sustained investment in digital water solutions, ensuring that Chios becomes a model for sustainable island water management.

Table 4: Expected Impact of Sustainable Water Interventions in Chios

Intervention	Expected Water Savings (%)	Energy Savings (%)	Cost Reduction (%)
Pipe replacement (HDPE)	20	10	25
Smart leak detection	30	8	20
Wastewater treatment upgrades	15	12	18
Rainwater harvesting	10	5	10
Desalination efficiency improvements	25	15	30

Conclusions

Ensuring a sustainable and resilient water management system in Chios requires a holistic approach that integrates technological innovations, nature-based solutions (NBS), and participatory governance. The combination of smart water technologies, such as IoT-enabled leak detection and digital twin modeling, with green infrastructure and adaptive governance frameworks presents a comprehensive strategy to mitigate non-revenue water (NRW) losses, enhance climate resilience, and secure long-term water availability for both residents and seasonal visitors.

The adoption of IoT-based monitoring systems and advanced metering infrastructure (AMI) has already demonstrated its potential in reducing water losses and improving operational efficiency. Simultaneously, investments in rainwater harvesting, managed aquifer recharge, and wetland restoration contribute to natural water retention and purification, reducing dependency on costly and energy-intensive solutions like desalination. These integrated solutions not only optimize water use but also promote ecological sustainability by restoring natural hydrological cycles.

However, for these interventions to achieve their full potential, a strong governance framework is essential. Aligning local policies with EU water management directives, promoting community engagement in conservation efforts, and fostering regional cooperation among Aegean islands will be crucial in ensuring long-term water sustainability. Effective governance will also support the scalability of these solutions and facilitate access to financial and technical resources.

Looking ahead, future research should focus on expanding smart water infrastructure, particularly through the development of digital twins and AI-driven demand forecasting, to optimize resource allocation and emergency response. Additionally, scaling up nature-based interventions can further enhance groundwater recharge and flood mitigation while reducing reliance on non-renewable water sources. Exploring funding opportunities through EU sustainability programs will also be key to supporting large-scale implementation and ensuring the financial viability of these initiatives.

By embracing an integrated and forward-thinking water management approach, Chios can serve as a model for other Mediterranean islands facing similar climatic and hydrological challenges. Sustainable water governance, combined with technological innovation and nature-based solutions, will not only safeguard the island's water security but also enhance its resilience to climate change and environmental pressures, ensuring a sustainable future for generations to come.

Acknowledgements
Authors would like to thank the Municipal Enterprise for Water and Wastewater of Chios for the provision of available data regarding the local water resources and water distribution network.

References

Breil, P., Pons, M.N., Armani, G., Amer, R., Pienaar, H., Oberholster, P. and Namour, P., 2022. Natural□Based Solutions for Bioremediation in Water Environment. Sustainable solutions for environmental pollution: Air, water and soil reclamation, pp.1-93.

Chasiotis, A., Feloni, E., & Nastos, P. 2023a. Strategies towards water leakage monitoring as a good practice under climate change adaptation in Argos City, Greece.

Chasiotis, A., Tsitsifli, S., Panytsidis, K., Nilsen, V., Mantas, N., Theodorou, D., Kyriakidis, T., Chasiotis, S., Bousdeki, M., Feloni, E. and Ratnaweera, H. 2023b. Building a smart green system to control water leakage and monitor drinking water quality in Paramythia city, Greece: the case of SMASH project. EGU General Assembly 2023.

Chang, N.B., Hossain, U., Valencia, A., Qiu, J., Zheng, Q.P., Gu, L., Chen, M., Lu, J.W., Pires, A., Kaandorp, C. and Abraham, E., 2021. Integrative technology hubs for urban food-energy-water nexuses and cost-benefit-risk tradeoffs (II): Design strategies for urban sustainability. Critical Reviews in Environmental Science and Technology, 51(14), pp.1533-1583.

Hachem-Vermette, C., 2024. Enhancing Urban Climate Resistance Through the Application of Selected Strategies and Technologies. Discover Cities, 1(1), p.17.

Jakovljević, D., Pešić, A.M. and Joksimović, D.M., 2021. Protection from harmful effects of water—examples from Serbia. In Water Engineering Modeling and Mathematic Tools (pp. 157-175). Elsevier.

Kumar, A., Button, C., Gupta, S. and Amezaga, J., 2023. Water Sensitive Planning for the Cities in the Global South. Water 2023, 15, 235 [online]

Lewandowski, J., Arnon, S., Banks, E., Batelaan, O., Betterle, A., Broecker, T., Coll, C., Drummond, J.D., Gaona Garcia, J., Galloway, J. and Gomez-Velez, J., 2019. Is the hyporheic zone relevant beyond the scientific community?. Water, 11(11), p.2230.

Majumder, M. and Kale, G.D. eds., 2021. Water and Energy Management in India: Artificial Neural Networks and Multi-Criteria Decision Making Approaches. Springer Nature.

Meerkhan, H., Freitas, L., Teixeira, J., Rocha, F., Pereira, A.J., Afonso, M.J. and Chaminé, H.I., 2021. DISCO-Urban: an updated GIS-based vulnerability mapping method for delineating groundwater protection zones in historic urban areas. Mediterranean Geoscience Reviews, 3, pp.361-377.

Monokrousou, K., Makropoulos, C., Eleftheriou, A., Vasilakos, I., Styllas, M., Dimitriadis, K., Kouris, N., Nyktari, E. and Malamis, S., 2024. From rain to resilience: rainwater harvesting coupled with subsurface storage and recovery as a nature-based solution for arid communities: the case of Mykonos. Urban Water Journal, pp.1-13.

Mounirou, L. A., Yonaba, R., & Faye, M. D. (2025). *Retention basins for urban flood mitigation: Insights from Ouagadougou in Burkina Faso.* ResearchGate.

Rodríguez, D.J., Paltán, H.A., García, L.E., Ray, P. and St. George Freeman, S., 2021. Water-related infrastructure investments in a changing environment: a perspective from the World Bank. Water Policy, 23(S1), pp.31-53.

Wantzen, K.M., Piednoir, T., Cao, Y., Vazhayil, A.M., Tan, C., Kari, F.G., Lagerström, M., Gerner, N.V. and Sommerhäuser, M.M., 2022. Back to the surface–Daylighting urban streams in a Global North–South comparison. Frontiers in Ecology and Evolution, 10, p.838794.

Wendling, L., Rinta-Hiiro, V., Jermakka, J., Fatima, Z., zu Castell Rüdenhausen, M., Ascenso, A., Miranda, A.I., Roebeling, P., Martins, R. and Mendonça, R., 2019. Performance and impact monitoring of nature-based solutions. UNaLab Project, EU H, 2020.

Mounirou, L.A., Yonaba, R., Faye, M.D., Biaou, A.C., Fowé, T., Coulibaly, G., Kafando, M.B. and Karambiri, H., 2025. Retention basins for Urban flood mitigation: Insights from Ouagadougou in Burkina Faso. World Journal of Advanced Research and Reviews, 25(1), pp.1497-1512.

Zounemat-Kermani, M., Matta, E., Cominola, A., Xia, X., Zhang, Q., Liang, Q. and Hinkelmann, R., 2020. Neurocomputing in surface water hydrology and hydraulics: A review of two decades retrospective, current status and future prospects. Journal of Hydrology, 588, p.125085.

17th INTERNATIONAL CONGRESS of the Geological Society of Greece

BULLETIN OF THE GEOLOGICAL SOCIETY OF GREECE, SP. PUBL.

EXTENDED ABSTRACT 046

Kentavros pluton (Thrace, Greece): Geochemistry and Petrogenesis

Chatzakou T.[1], Tsiri A.[1], Koroneos A.[1], Gerontidou I. [1], Drakoulis A. [1]

(1) Department of Mineralogy-Petrology-Economic Geology, Aristotle University of Thessaloniki, Thessaloniki, Greece, theodxat@gmail.com , atsirib@geo.auth.gr , koroneos@geo.auth.gr , ioangero@geo.auth.gr , alexdr@geo.auth.gr

Introduction

Rhodope massif is characterized by the extensive magmatism of Eocene - Miocene age. There are many plutonic rocks intruding the two units (Sidironero and Pangaion) of the Rhodope massif (e.g. Xanthi pluton, Kavala pluton, Vrondou pluton etc.) and most of them have been thoroughly studied (Christofides *et al*., 1998 and references therein). There is one pluton though, the pluton of Kentavros, which has not been petrologically and geochemically studied up to now. The pluton of Kentavros is located 26 km NNE of Xanthi city near the village of Kentavros. The pluton intrudes gneisses and gneiss-schists, marbles and occasionally amphibolites of the Sidironero unit, causing locally contact metamorphic phenomena (Fig.1) (IGME 1973). Liati (1986) using K-Ar method on hornblende gave a Late Eocene - Early Oligocene age (38±1 Ma) for the Kentavros pluton, similar to the age of Xanthi pluton which is 34±0.5 Ma (Christofides *et al*., 2012). The aim of this study is to present for the first time petrological, mineralogical and geochemical characteristics of the Kentavros pluton, to provide evidence on the origin of it as well as to compare it with the nearby Xanthi pluton of similar age.

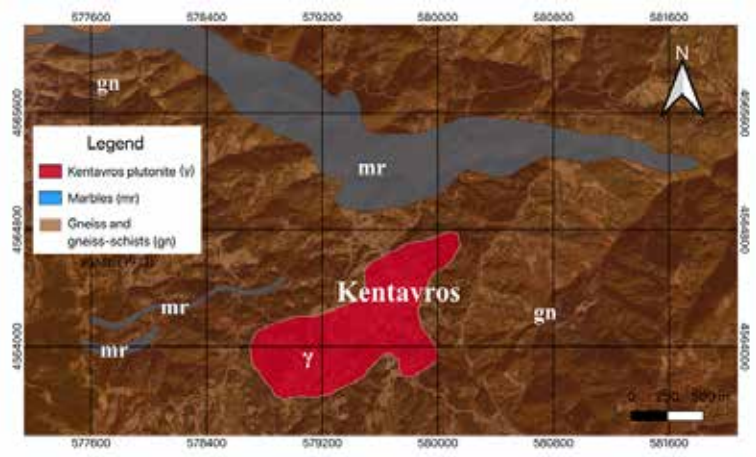

Figure 1: Geologic map of Kentavros area. (IGME, 1973 with modifications using QGIS.3.34, QGIS.org, 2023).

Geological Setting

The Rhodope massif is a thick (10-20 km) continental crust. It extends from southern Bulgaria to Thrace, Thassos, and eastern Macedonia. It is believed to originate either from the Eurasian plate or to be an ancient continental fragment of Gondwana, which was detached and incorporated into Eurasia (Mountrakis, 2021). Its western boundary is the Strymon fault, where it is separated from the Serbomacedonian massif, while to the east it is in contact with the Circum Rhodope zone. The Rhodope massif is divided into two units by Papanikolaou & Panagopoulos (1981): the Upper Tectonic Unit (Sidironero Unit) and the Lower Tectonic Unit (Pangaion Unit). The units were separated by the NE-SW trending and southwest-vergent Nestos thrust, from Xanthi to the Bulgarian border (Christofides *et al*., 2001). The Rhodope massif is intruded by igneous rocks, both plutonic and volcanic, with composition ranging from granitic to gabbroic (Christofides *et al*., 1998). The magmatism ranges from Eocene to Miocene in age and is related to an active continental margin (Mountrakis *et al*., 2006). According to Krohe & Mposkos (2002), Kentavros pluton is an intrusion into the upper Unit Sidironero Complex, which has been exhumed before 50-30 Ma. It is also associated with the Xanthi detachment system. Around the Kentavros pluton there is limited plastic elongation and rotation recrystallization of quartz. The pluton appears highly sheared and it is a syn-detachment intrusion into the Upper Sidironero Complex.

Analytical Methods

The laboratory research includes the determination of the mineralogical and chemical composition of the rocks. Regarding mineralogy, 11 thin sections were prepared and examined under a polarizing microscope. For the chemical analyses, 11 pressed pellets were prepared. The samples were ground to fine powder and mixed with a commercial cellulose based

binder (CEREOX®) at a ratio of 4 parts sample to 1 part binder. The final mixtures were then subjected to a pressure of 15 tons using a hydraulic press, in order to form pellets compatible with the wavelength-dispersive X-ray fluorescence (WDXRF) spectrometry system. The analyses were performed on a RIGAKU Supermini200 tabletop XRF instrument, which operates at 50kV and 4mA with 200W power.

Petrography and Mineralogy

The Kentavros pluton consists of different rock types, from basic to acid, differing to a certain extent in the mafic mineral contents and texture. Based on the TAS classification diagram of Cox *et al*. (1979) (Fig. 2), their texture and modal composition they are classified as: cumulates with pyroxene (Cum Px), cumulates with hornblende (Cum Hb) gabbros (Gb), diorites with hornblende (Hb-Dr) and diorites containing pyroxene and hornblende (Px, Hb-Dr), Qz monzodiorites (Qz-MzDr), tonalites (Ton) and pegmatite veins (Pgm).

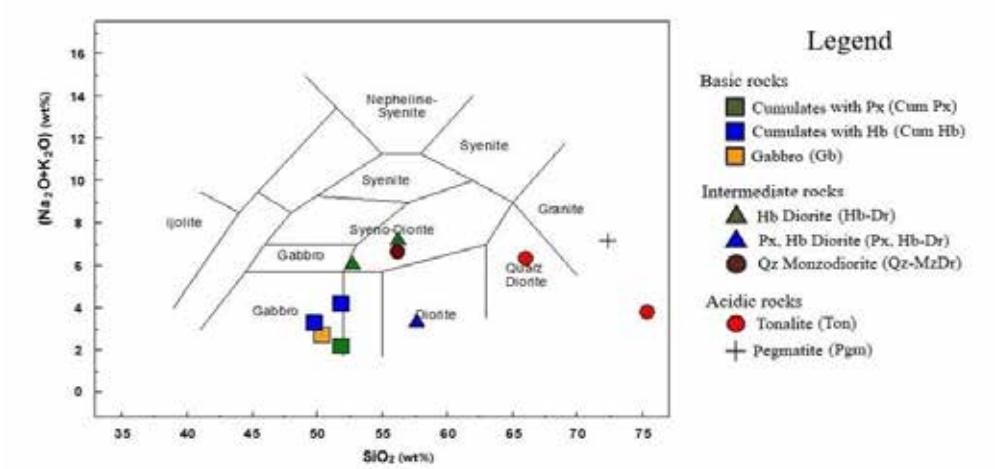

Figure 2: Chemical classification of the Kentavros pluton rock types (TAS after Cox *et al*., 1979).

All the rock types are medium grained apart from the Cum Hb rocks, which contain significantly large hornblende crystals (Fig. 3a). The cumulate rocks consist of hornblende, pyroxene, plagioclase (Fig. 3b), biotite (Fig. 3c) and contain minor amounts of orthoclase and quartz. The accessory minerals are titanite in remarkably large crystals (Fig. 3d), chlorite and apatite. The gabbros consist of plagioclase, hornblende and pyroxene. The diorites and quartz monzodiorites consist of plagioclase, orthoclase, hornblende, biotite, pyroxene and occasionally quartz. The accessory minerals are titanite, allanite, apatite, zircon and opaques. The tonalites consist of quartz, orthoclase, plagioclase, biotite, hornblende and occasionally pyroxene. The accessory minerals are chlorite, allanite and zircon. The pegmatite veins consist of quartz, microcline and plagioclase. The accessory minerals are epidote, clinozoisite and allanite.

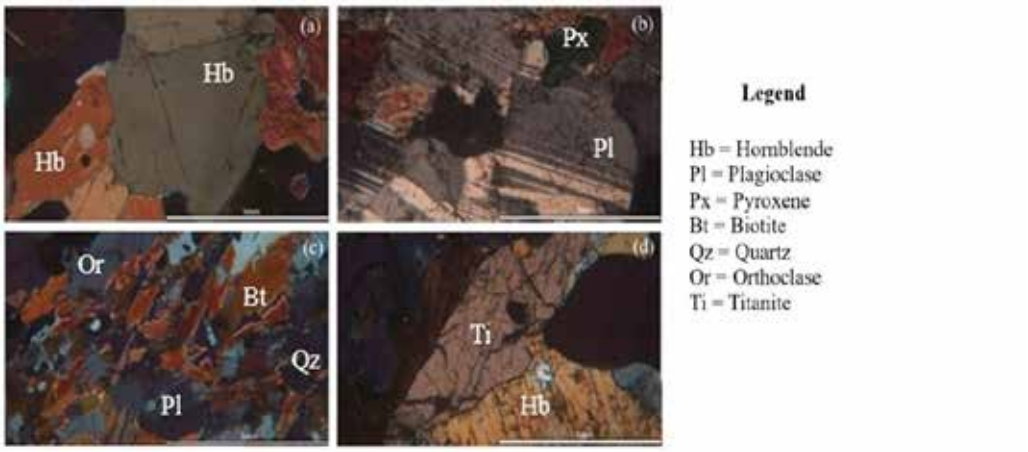

Figure 3: Representative minerals of the Kentavros pluton in N+. (a) Hb crystals, (b) Pl with Px, (c) Bt with Qz, Or and Pl, (d) Ti with Hb.

Geochemistry

The SiO_2 content of the basic rock samples (Cum and Gb) ranges from 49.08 to 51.35%. In the intermediate samples (Dr, Qz-MzDr) it ranges from 50.95 to 57.11%. In the acid samples (Ton, Pgm) it ranges from 65.60 to 71.92% (Table 1). TiO_2, FeO_{tot} (total Fe expressed as Fe^{2+}), MnO, MgO, CaO and P_2O_5 decrease with increasing SiO_2 (Fig. 4 and Table 1), while Al_2O_3, K_2O and Na_2O increase (Fig. 4 and Table 1). Regarding the trace elements, Sr, Ba, Cr, Ni, Zr, Y, Nb, V and Co decrease with increasing SiO_2 (Fig. 5 and Table 1), while Rb and Sc (Fig. 5 and Table 1) increase. According to the SiO_2 - K_2O diagram (Peccerillo & Taylor, 1976) the composition of the pluton varies mostly from calk-alkaline to high-K calc-alkaline (Fig. 4). Also, all the samples are metaluminous and characterized as I-type (Fig. 5).

Table 1: Whole-rock major (wt%) and trace (ppm) element analyses of representative samples from the Kentavros pluton.

Sample name	KE-12	KE-13	KE-03	KE-05	KE-08	KE-07	KE-10	KE-14	KE-11	KE-04	KE-06
Rock type	Cum	Cum	Cum	Gb	Dr	Dr	Dr	Qz-MzDr	Ton	Ton	Pgm
Major elements (wt%)											
SiO_2	49.08	51.29	51.35	49.27	50.95	55.01	57.11	55.80	65.60	74.77	71.92
TiO_2	1.43	1.10	1.01	0.33	0.86	0.42	0.81	1.13	0.18	0.14	0.06
Al_2O_3	8.68	11.45	4.34	18.77	13.97	18.33	7.59	16.09	17.46	11.41	16.14
FeO_{tot}	10.70	9.75	11.26	6.22	7.16	4.94	7.87	7.13	1.88	2.53	0.51
MnO	0.17	0.18	0.28	0.10	0.06	0.07	0.14	0.10	0.02	0.01	0.00
MgO	13.55	10.13	16.35	7.84	4.24	3.18	11.00	5.57	1.25	0.88	0.20
CaO	11.27	10.43	12.03	12.60	12.46	8.19	10.93	6.07	6.38	5.67	3.41
K_2O	0.99	1.07	0.80	0.53	2.18	0.98	0.99	2.54	1.17	0.79	1.23
Na_2O	2.21	3.04	1.36	2.13	3.73	6.12	2.32	4.02	5.04	2.94	5.86
P_2O_5	0.39	0.65	0.19	0.01	0.96	0.61	0.26	0.68	0.26	0.00	0.02
LOI	1.30	0.80	0.87	2.09	3.10	1.95	0.79	0.60	0.60	0.74	0.53
Total	99.77	99.89	99.84	99.89	99.67	99.80	99.81	99.73	99.84	99.88	99.88
Trace elements (ppm)											
Rb	7	4	5	11	50	0	7	47	3	13	5
Sr	646	751	169	210	1318	1308	570	1139	1162	358	836
Ba	234	141	29	18	868	375	124	83	154	18	241
Cr	582	306	576	297	40	38	569	48	27	36	32
Ni	165	103	228	99	18	8	176	30	11	15	10
Zr	128	93	80	36	411	101	102	213	78	464	57
Y	28	26	48	10	28	25	28	20	12	98	3
Nb	19	21	20	0	30	6	13	12	3	5	0
V	242	240	164	163	104	81	187	131	27	8	0
Co	44	38	48	24	25	16	32	25	2	4	0
Sc	21	27	34	39	30	20	30	17	23	27	9

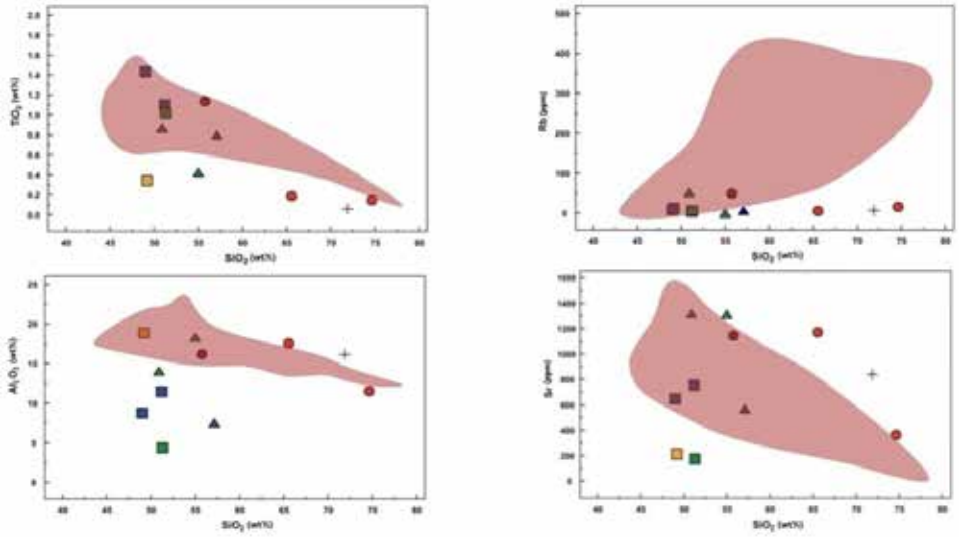

Figure 4: Harker diagrams of representative major and trace elements of the Kentavros pluton (red area: Xanthi pluton). Legend as in Fig. 2.

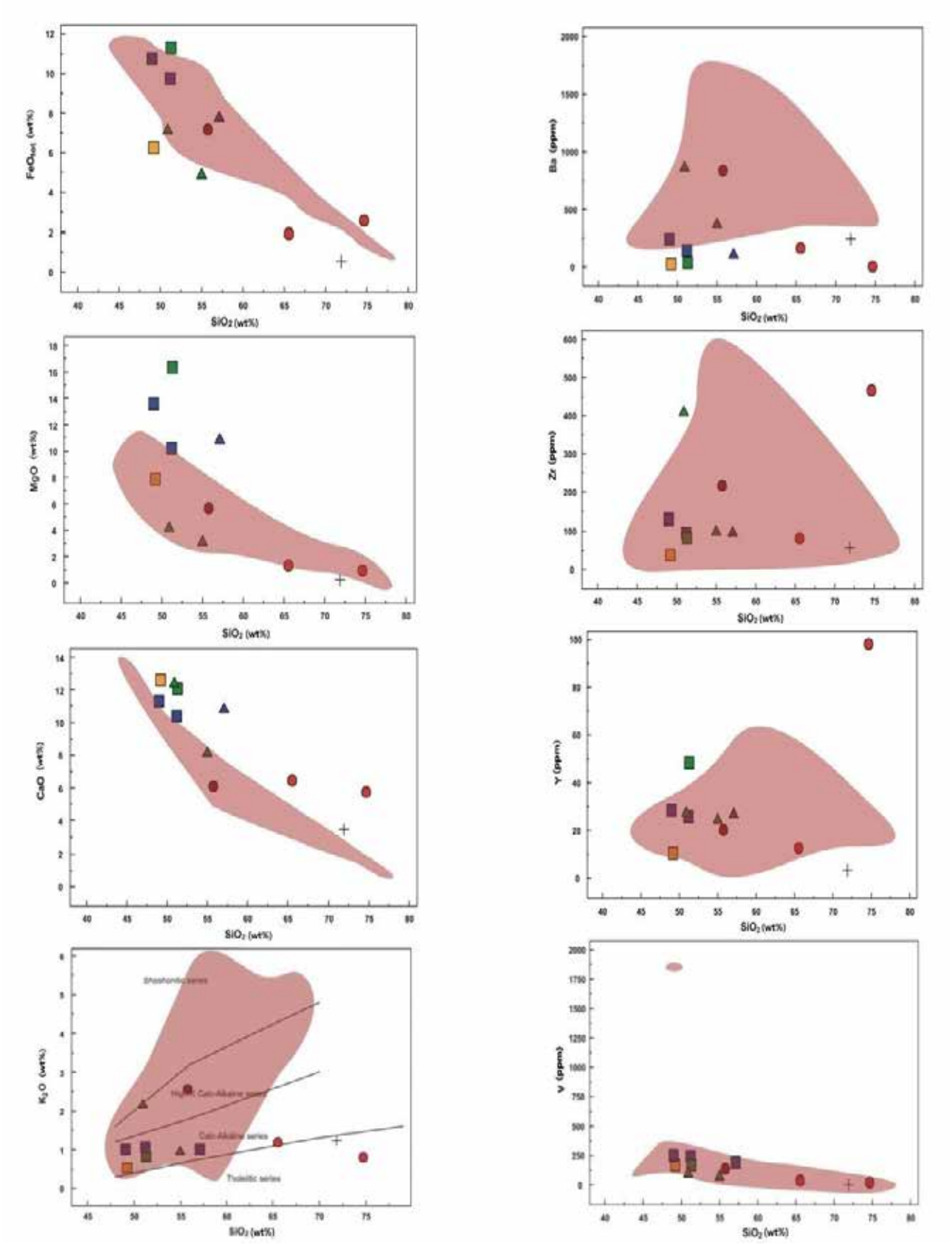

Figure 4 Cont.

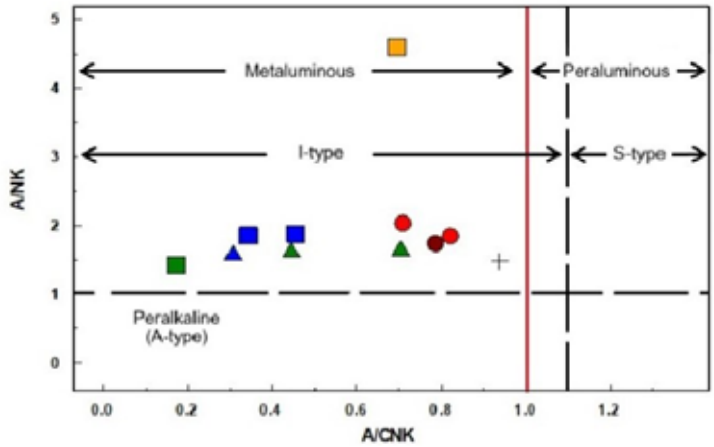

Figure 5: A/CNK - A/NK diagram. Legend as in Fig. 2.

Petrogenesis

According to the tectonic classification diagrams of Pearce *et al*. (1984) (Figs. 6 a and b) the analyzed samples plot mostly in the volcanic arc granitoids (VAG) field. This means that the magmatism of Kentavros is related to a subduction mechanism, which is typical for the Rhodope magmatic rocks of Eocene to Miocene age (Pipera *et al*., 2013).

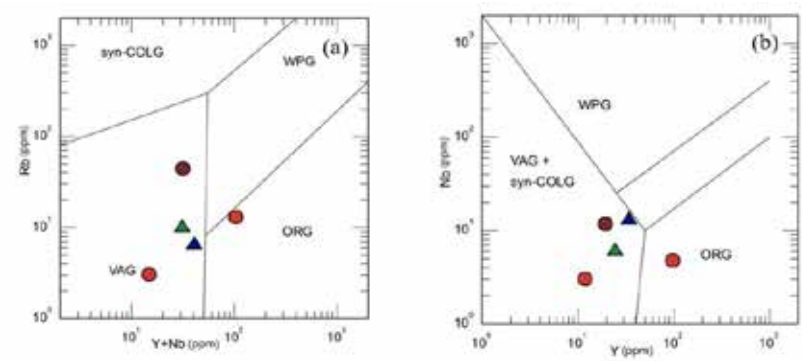

Figure 6: Tectonic classification diagrams (Pearce *et al*., 1984). Legend as in Fig. 2.

Kentavros gabbro represents a mantle-peridotite original melt (Fig. 7, brown area) and diorites are probably the results of evolution of the gabbroic magma although they might represent a high-Mg andesitic magma (Fig. 7, grey area). The tonalitic samples plot in the “Metagreywacke Sources” field (Fig. 7, pink area), indicating association with such sources. It is to note that, alternatively, the intermediate rocks can be probably a result of the metagreywacke’s melt interaction with peridotite melt during a mixing procedure.

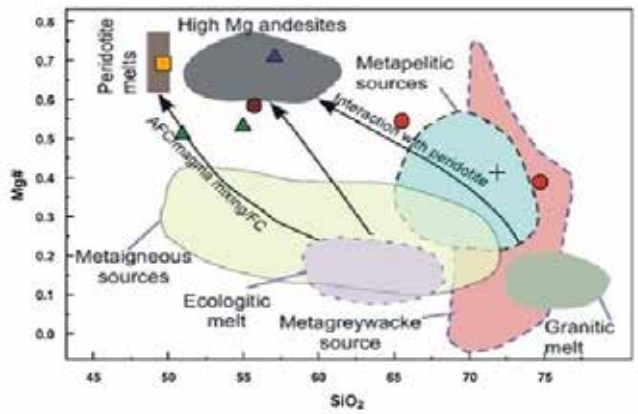

Figure 7: Mg# - SiO_2 diagram showing the melts’ origin (Sami *et al*., 2023 and references therein). Legend as in Fig. 2.

Comparison with Xanthi pluton

The fact that the Kentavros and Xanthi plutons are located close to each other (8.8 km apart) combined with their similar ages (Liati, 1986; Christofides *et al*., 2012), lead to the decision of comparing the two plutons, although the geochemical data are limited. Regarding the petrographic types they both contain Qz-MzDr, Dr and Gb, but they differ in the acid rock types. Xanthi pluton contains granodiorites (Gdr) and monzogranites (MzGr), while the Kentavros pluton contains Ton. It must be noted though that Gdr in Xanthi represents ~75% of the pluton. On the contrary, the amount of Ton in Kentavros pluton is limited. Major elements having similar behavior in both plutons are TiO_2, Al_2O_3, FeO_{tot}, MnO, MgO and P_2O_5 (Fig. 4). K_2O has lower values in Kentavros than Xanthi and Na_2O either lower and or higher values than Xanthi. Trace elements showing similar behavior in both plutons are Sr, Cr, Ni, Zr, Y, Co and V (Fig. 4). Rb and Ba have lower values in Kentavros than Xanthi, while Sc has higher values. Moreover, both plutons have calc-alkaline to high-K calc-alkaline affinity, even though Xanthi intermediate (monzonitic) rocks have higher K content (Fig. 4). Both plutons are associated to the same geotectonic environment (VAG) and to the Xanthi detachment system. It should be noted though, that Kentavros pluton is a syn-detachment intrusion while Xanthi pluton is characterized as late or post detachment intrusion (Krohe & Mposkos, 2002).

References

Christofides, G., Soldatos, T., Eleftheriadis, G., Koroneos, A., 1998. Chemical and isotopic evidence for source contamination and crustal assimilation in the Hellenic Rhodope plutonic rocks. Acta Vulcanologica, 10, 305-318.

Christofides, G., Koroneos, A., Soldatos, T., Eleftheriadis, G., Kilias, A., 2001. Eocene magmatism (Sithonia and Elatia plutons) in the Internal Hellenides and implications for Eocene-Miocene geological evolution of the Rhodope massif (Northern Greece). In: Downes, H., Orlando, V. (Eds.), Tertiary Magmatism in the Dinarides Acta Vulcanologica, 13, 73-89.

Christofides, G., Pipera, K., Koroneos, A., Papadopoulos, A., 2012. New geochronological data from the Xanthi pluton: Constraints on the Nestos thrust dating, The School of Prof. Zhivko Ivanov. In International Conference: Exhumation of High-grade Metamorphic Rocks (MCC), Magmatic Arc Systems and Strike-slip Zones (pp. 49-52).

Cox, K. G., Bell, J. D., Pankhurst, R. J., 1979. Compositional variation in magmas. In The interpretation of igneous rocks (pp. 12-41). Dordrecht: Springer Netherlands.

IGME, 1973. Geological map of Greece, Xanthi sheet. Institute of Geology and Mining Research, Athens.

Krohe, A., & Mposkos, E., (2002). Multiple generations of extensional detachments in the Rhodope Mountains (northern Greece): evidence of episodic exhumation of high-pressure rocks.

Liati, A., 1986. Regional metamorphism and overprinting contact metamorphism of the Rhodope Zone, near Xanthi (N. Greece) (Doctoral dissertation, PhD dissertation, Univ. Carolo-Wilhelmina, Braunschweig, Germany).

Mountrakis, D., Tranos, M., Papazachos, C., Thomaidou, E., Karagianni, E., Vamvakaris, D., 2006. Neotectonic and seismological data concerning major active faults, and the stress regimes of Northern Greece. Geological Society, London, Special Publications, 260(1), 649-670.

Mountrakis, D., 2021. Geology and Geotectonic Evolution of Greece. Thessaloniki: University Studio Press, 33-43.

Papanikolaou, D., Panagopoulos, A., 1981. On the structural style of Southern Rhodope, Greece.

Pipera, K., Koroneos, A., Soldatos, T., Poli, G., & Christofides, G., 2013. Origin of the High-K Tertiary magmatism in Northern Greece: Implications for mantle geochemistry and geotectonic setting. Bulletin of the Geological Society of Greece, 47(1), 416–426.

Pearce, J. A., Harris, N. B., Tindle, A. G., 1984. Trace element discrimination diagrams for the tectonic interpretation of granitic rocks. Journal of petrology, 25(4), 956-983.

Peccerillo, A., Taylor, S. R., 1976. Geochemistry of Eocene calc-alkaline volcanic rocks from the Kastamonu area, northern Turkey. Contributions to mineralogy and petrology, 58, 63-81.

Sami, M., Adam, M. M., Lv, X., Lasheen, E. S. R., Ene, A., Zakaly, H. M., Ali, S., 2023. Petrogenesis and tectonic implications of the cryogenian I-type granodiorites from Gabgaba Terrane (NE Sudan). Minerals, 13(3), 331.

17th INTERNATIONAL CONGRESS of the Geological Society of Greece

BULLETIN OF THE GEOLOGICAL SOCIETY OF GREECE, SP. PUBL.

EXTENDED ABSTRACT 047

The Impact of Urban Sprawl on Areas of Natural and Cultural Heritage and Geoheritage. Evidence of Lemnos Island, Greece

Chatzi Efstratia[1] , Derdemezi Evangelia - Theodora[1] , Tsilimigkas Georgios [1]
(1) University of the Aegean, Department of Geography, Mytilene, Greece
Email: efi.chatzi@geo.aegean.gr, ederde@geo.aegean.gr , gtsil@aegean.gr

Research Highlights

Quantitative rendering of the impact of urban sprawl on Natura 2000 areas, Wild Life Refuges, Small Islands Wetlands, Archeological areas and Monuments and the Petrified Forest in Lemnos island. Interpretation of results based on spatial planning system in Greece.

Introduction

Cultural and natural heritage and geoheritage sites are vital for preserving the identity and history of regions, but they are increasingly threatened by urban sprawl, particularly in areas with high development pressures (AbdelMaksoud 2020, Lagarias and Stratigea 2023). Islands are highly vulnerable to such pressures due to their small size and growing tourism (Baldacchino 2004, Spilanis 2012). The urban sprawl on islands is often expanded into critical heritage zones, which are already under pressure from both natural and human factors (Salvati 2013, Tsilimigkas et al.2022). Islands are characterized by spatial fragmentation, which on the one hand makes them fragile socio-spatial systems and on the other hand enhances endemism, creating ecosystems of particular value. This is recognized at the European level, and thus a large part of the island areas is included in the Natura 2000 network (EEC 1992, EC2009). The importance of the natural environment and the need for management and protection is also recognized at the national level with legislation under which, among other things, National Parks (OGG 1986, OGG 2020), Small Island Wetlands (MD 2010, OGG 2011) and Wild Life Refuges (OGG 1998, OGG 2011) are delineated. The cultural heritage of the islands is characterized by an extensive network of traditional settlements and archaeological areas and monuments. The need for cultural heritage protection and management is recognized at European and national level (Council of Europe 1995, OGG 2002, OGG 2021). An important part of the identity of the islands, and a valuable tourist resource is their geoheritage, which consists of physico-geographical elements of geological interest and at the same time, over the years, these areas acquire a cultural significance that makes them landscapes of special value (Sotiriou and Nunes 2024). At the international level, the importance of geoheritage has been recognized mainly through the UNESCO'S Global Geoparks Networks. At the national level, legislation concerning geoparks and geosites is fragmented and falls both within institutional arrangements for the protection of environment and habitats (OGG 2011, OGG 2020) and for the protection of the cultural environment and landscape (OGG 2010).

The study area for this paper is Lemnos Island of the Region of the North Aegean. Covering an area of 478,97 km² and the permanent population is 16409 people. Lemnos has notable natural and cultural heritage, including 3 areas integrated into the Natura 2000 network, 9 wildlife refuges areas, 3 sections of the Petrified Forest, 59 wetlands, 18 traditional settlements and 20 designated archaeological sites. One of the island's most unique features is the Petrified Forest of Lemnos, which contains subtropical vegetation remains dating back at least 20 million years (Dasarxeio, 2020). Designated as a "Preserved Natural Monument" (Decision No. 75247/4865/10-12-2013 by the Secretary General of the Decentralized Administration of the Aegean), this site is protected across three delineated areas and several individual fossil-bearing locations.

Objectives

The aim of this research is the quantitative rendering of urban sprawl in areas of natural and cultural value on the island of Lemnos and its interpretation within the framework of spatial planning. Specifically, the research questions are: (1) What percentage of built-up area is located within and outside settlements' boundaries? (2) What percentage of built-up area outside settlements' boundaries is located within (a) Natura 2000, (b) archaeological areas and (c) petrified forest? The results are interpreted based on spatial planning and applicable legislation.

Methods

To answer the research questions, acquiring the appropriate geospatial data was essential:

- Impervious Built-up (IBU) 2018, provided by the European Environment Agency (EEA) through Copernicus, was used to represent built-up areas. This raster layer contains binary information, with buildings classified as 1 and non-buildings as

0 (EEA 2018). The spatial resolution of IBU is 10m.

- For distinguishing built-up areas inside and outside settlements, the boundaries of official settlements were sourced from the open platform e-poleodomia (MEE 2025). In Lemnos there are 40 settlements of which 18 designated traditional settlements, three traditional settlements were found to lack official boundaries. To avoid considering these built-up areas as exurban, we digitized their boundaries aaccording to the compact residential fabric with reference map the Google Earth. Additionally, the settlement boundaries for Myrina, the capital of the island, were missing. These boundaries were digitized using the General Urban Plan (GUP), with topographical charts georeferenced using the Greek Geodetic Reference System 1987 (GGRS87) at a scale of 1:5.000. This ensures accurate and consistent mapping across all settlements.
- The Natura 2000 areas were retrieved from the EEA (EEA 2022). The Wildlife Refuges were sourced from the Forest Service and forest maps, while the Wetlands were obtained from the Greek Ministry of Environment and Energy. The delineation of archaeological areas came from the Archaeological Cadaster.
- The delineation of the Petrified Forest of Lemnos was based on the map included in the decision declaring it a “Preserved Natural Monument” (Official Decision 2013). To ensure spatial precision, we digitized the forest boundaries from the forest map provided by the Forest Service, georeferencing the map using GGRS87 at a scale of 1:5.000.

The methodology employed was based on raster analysis. Vector-format data were rasterized to align with the raster layers. The identification of exurban built-up areas was achieved by overlaying the layers of IBU and official settlement delineations. This analysis produced quantitative data, which was further examined to assess spatial relationships with the Natura 2000 areas, wildlife refuges areas, wetlands archaeological areas and the Petrified Forest of Lemnos. The resulting insights were interpreted within the framework of spatial planning to evaluate the impact of urban sprawl on these protected areas.

Results

In Lemnos, the total built-up area occupies 4.74 km², which corresponds to 0.99% of the island’s total area. Of this built-up area, 3.41 km² (or 0.71%) lies within the boundaries of settlements, while the remaining 1.33 km² (or 0.28%) is located outside settlement boundaries. Comparatively, the percentage of construction on Lemnos is significantly smaller than on other islands, such as Santorini, where construction occupies 4.04% of the total island area, with 2.08% in extra-urban areas (Tsilimigkas and Derdemezi 2020).

The distribution of built-up areas outside official and traditional settlements in Lemnos highlights their significant impact on zones of natural and cultural significance, as shown in Table 1.Urban sprawl has impacted 8 of the wildlife areas, 6 of the wetlands, 2 of the Natura 2000 sites and 11 of the archaeological sites. Archaeological areas, which cover an impressive 89.44% of the island, are among the most affected by this type of development, hosting a substantial portion of the built-up area outside settlements. This overlap underscores the need for careful management, as interventions within archaeological site boundaries must comply with strict regulations to prevent unplanned and unregulated development.

Table 1. Impact of Built-Up Areas Outside Settlements on Natural and Cultural Zones in Lemnos

Island of Lemnos	Percentage %
Petrified Forest Area B1	2,42
Petrified Forest Area B2	7,67
Wildlife Refuges Areas	32,57
Wetlands	0,61
Natura 2000	14,4
Archaeological	89,44

Other areas of natural significance also show varying degrees of impact from built-up areas outside settlements: Petrified Forest: Area B1 is affected by 2.42%, while Area B2 is affected by 7.67%. Wildlife Refuges Areas: These zones experience significant impact, with 32.57% affected by built-up areas outside settlements. Wetlands: Though wetlands occupy only 0.61% of the island, their exposure to built-up areas outside settlements highlights the need for protection from encroaching development. Natura 2000 Sites: These protected areas are also impacted with 14.4% affected by built-up areas outside settlements, further emphasizing the urgency of integrated spatial planning.

To better visualize the spatial distribution of built-up areas in relation to the zones of natural and cultural significance, Figure 1 provides an overview of Lemnos, while Figure 2 zooms in on two key areas of the island. The labels B1, B2, and B3 in Figure 2 correspond to areas of the Petrified Forest, which are among the zones impacted by built-up areas outside settlements.

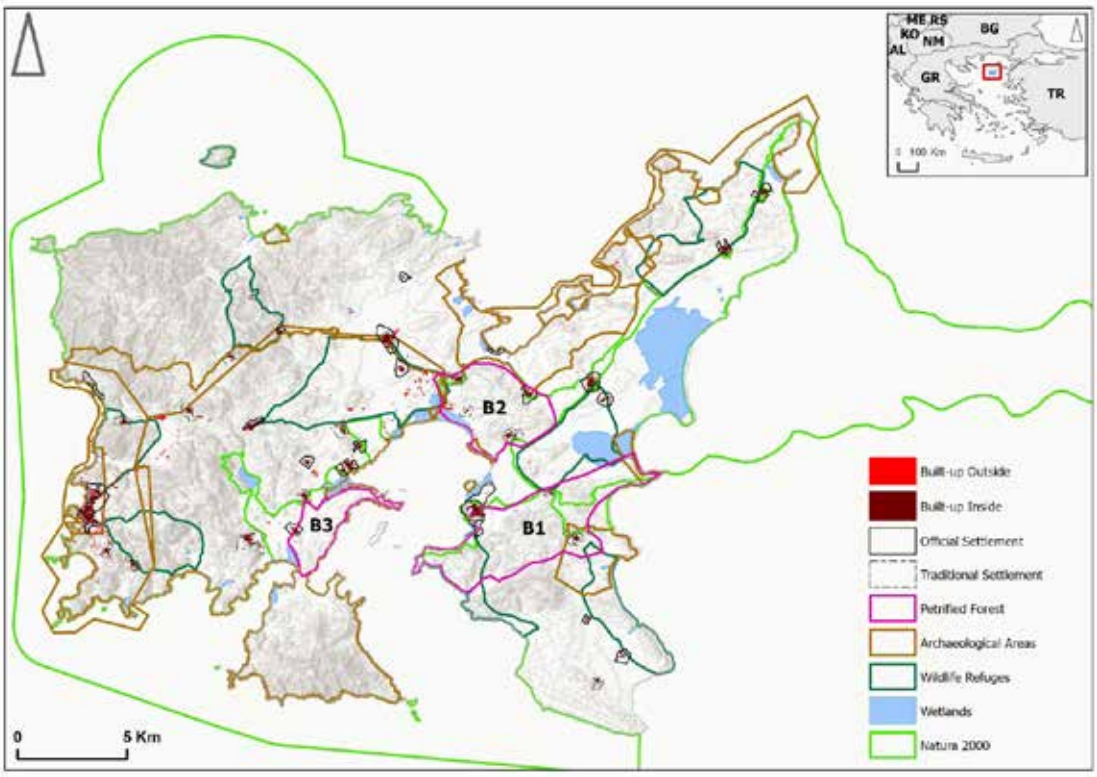

Figure 1: Overview of the Island of Lemnos, showing the spatial distribution of built-up areas, settlements, and protected zones.

Figure 1 provides a comprehensive view of the spatial distribution of built-up areas across Lemnos. The map highlights both built-up areas within settlements (dark red) and outside settlements (bright red). It also delineates key zones of natural and cultural significance, such as archaeological areas, wildlife refuges, wetlands, and Natura 2000 sites. This island-wide perspective allows for a clear visualization of how built-up areas intersect with these protected zones, underscoring the need for spatial planning to mitigate unregulated construction in sensitive areas. The map serves as a foundation for understanding the broader spatial dynamics of built-up development on Lemnos.

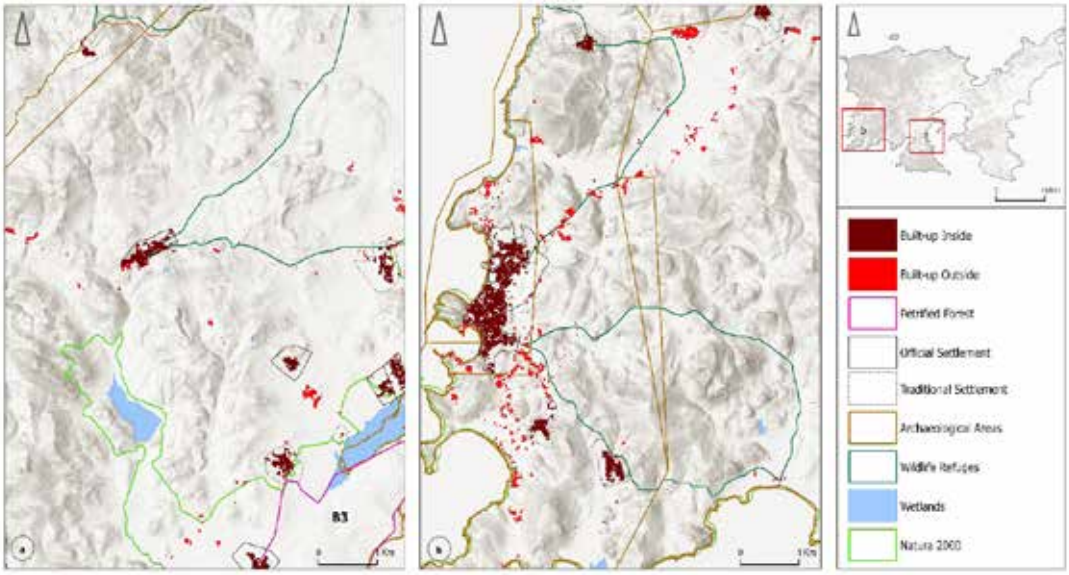

Figure 2: Zoomed-in views of two key areas in Lemnos, highlighting the overlap between built-up areas and protected zones. B1, B2, and B3 represent regions of the Petrified Forest.

Figure 2 zooms in on two critical regions of Lemnos, offering a closer examination of the overlap between built-up areas and zones of natural and cultural importance. The highlighted areas, B1, B2, and B3, represent sections of the Petrified Forest, a unique geological heritage site. The map illustrates the proximity of built-up areas to these sensitive zones, emphasizing the potential risks posed by unregulated construction. The focused view also shows how built-up areas extend beyond settlement boundaries into wildlife refuges, wetlands, and archaeological zones, providing a detailed context for the discussion on sustainable development and spatial planning.

In conclusion, these findings underscore the opportunity to implement a comprehensive and integrated spatial planning framework at the local level, aimed at regulating construction outside settlement boundaries. Such a framework is essential to align development with Lemnos' natural and cultural heritage and geoheritage, prevent the fragmentation of protected zones and balance growth with the preservation of archaeological sites and other critical areas.

Conclusions

This research underscores the critical need for an integrated and cohesive framework for the natural and cultural heritage and geoheritage While legal references and regulations exist, their fragmented nature, coupled with inconsistencies in spatial and temporal application, creates implementation challenges, fosters conflicts and leaves room for unregulated development in sensitive and significant areas (Tzeferis 2018; Tsilimigkas and Derdemezi 2020). A positive step was the inclusion of a section on landscape in the Regional Frameworks on Spatial Planning and Sustainable Development' (RFSPSD) according to European Landscape Convention principles. Although improvements are needed and especially for the island of Lemnos, geoheritage could be included more consistently in landscape zones. The directions of RFSPSD could form the basis to support downstream planning level regulations. The management and promotion of natural and cultural heritage, along with geoheritage, present significant opportunities for strengthening Lemnos' economy. Alternative forms of tourism, such as geotourism, can draw inspiration from neighboring Lesvos, where the Petrified Forest is part of the European Geoparks Network (Zouros 2004). Revised directions in the Special Spatial Framework for Tourism should focus on fostering such sustainable tourism development, emphasizing alternative and eco-friendly tourism models. At the same time, the RFSPSD should be revised to align with the upstream directions and plan a sustainable way of management and development. Finally,a significant challenge remains at the local spatial planning level, which is currently fragmented and incomplete, allowing unregulated built-up area expansion in exurban areas. The upcoming local plans are intented to restrain urban sprawl. . As highlighted in this study, such measures are imperative to prevent the pressures that urban expansion places on natural and cultural heritage and geoheritage.

References

AbdelMaksoud, K.M., El Metwaly, W. Maadi. (2020). Petrified Forest in Cairo, Egypt, as a Geologic Heritage Under Urbanization Pressure. Geoheritage. 12 (44). DOI: 10.1007/s12371-020-00465-4

Baldacchino, G. (2004). The coming of age of island studies. Tijdschrift voor Economische en Sociale Geografie, 95(3), 272–283. DOI:10.1111/j.1467-9663.2004.00307.x

Council of Europe (1995). The European Convention for the Protection of the Archaeological Heritage. Council of Europe Treaty Series no. 143

Dasarxeio. (2020). Giant eight-meter fossilized trunk discovered on Lemnos. Retrieved from https://dasarxeio.com/2013/12/11/10173/. Last Access 20/01/2025

EEA (European Environment Agency). (2022). Natura 2000. Spatial Data. Retrieved from: https://www.eea.europa.eu/data-and-maps/data/natura-14/natura-2000-spatial-data. Last Access 17/01/2025

EEA (European Environment Agency). (2018). Impervious Built - up 2018. Copernicus Land Monitoring Service

European Commission (EC). (2009). Directive 2009/147/EC of the European Parliament and of the Council of 30 November 2009 on the conservation of wild birds

European Economic Community (EEC). (1992). Council Directive 92/43/EEC of 21 May 1992 on the conservation of natural habitats and of wild fauna and flora

Lagarias, A., Stratigea, A. (2023). Coastalization patterns in the Mediterranean: a spatiotemporal analysis of coastal urban sprawl in tourism destination areas. GeoJournal . 88 (2529–2552). DOI:10.1007/s10708-022-10756-8

MD (Ministerial Decision). (2010). Approval of a list of small island wetlands, definition of conditions and restrictions for their protection. 518/2010. OGG B181/2010

Official Decision. (2013). No. 75247/4865/10-12-2013 Decision Declaring the Petrified Forest of Lemnos as a "Preserved

Natural Monument"
OGG (Official Government Gazette). (2021).Ratification of a Code of Legislation for the protection of antiquities and cultural heritage in general. Official Government Gazette 220/A/2021. Law 4858/2021
OGG (Official Government Gazette). (2020). Modernization of environmental legislation, incorporation into Greek legislation of Directives 2018/844 and 2019/692 of the European Parliament and of the Council and other provisions. Official Government Gazette 92/A/2020 Law 4685/2020
OGG (Official Government Gazette). (2011). Conservation of biodiversity and other provisions. Official Government Gazette 60/A/2011. Law 3937/2011
OGG (Official Government Gazette). (2010). 'Ratification of the European Landscape Convention'. Official Government Gazette. 30-A/25.02.2010. Law 3827/2010.
OGG (Official Government Gazette). (2002). 'Protection of Cultural Heritage'. Official Government Gazette 153-A/28.06.2002. Law 3028/2002.
OGG (Official Government Gazette). (1998). Establishment of the Account Certification Agency, the Payments and Control Agency for Community Aids, Guidance and Guarantees, the Certification and Supervision Agency for Agricultural Products, General Directorates and staff positions in the Ministry of Agriculture and "Agricultural Land Development Company" S.A. and other provisions. Official Government Gazette 200/A/1998. Law 2637/1998
OGG (Official Government Gazette). (1986). 'Environmental protection'. Official Government Gazette 160-A/16-10-86. Law 1650/1986.
MEE (Ministry of Environment and Energy). 2025. Geoporta e-poleodomia. Available at: http://gis.epoleodomia.gov.gr/v11/#/10.9313/39.8760/5
Salvati, L. (2013). 'Rural' sprawl, Mykonian style: A scaling paradox. International Journal of Sustainable Development & World Ecology, 20(2), 109–115. DOI:10.1080/13504509.2013.765522
Sotiriou, P. Nunes, P. (2024). The Geoheritage of Madeira: Implications for Natural Heritage and Geotourism. Geoheritage. 16 (74). DOI: 10.1007/s12371-024-00982-6
Spilanis, I. (2012). The islands development: what strategy and what policies to achieve territorial convergence. Gutenberg
Tsilimigkas, G. Gourgiotis, A. Derdemezi, E-T. (2022). Spatial planning incompetence to discourage urban sprawl on Greek Islands. Evidence from Paros, Greece. Journal of Coastal Conservation. 26 (2). DOI: 10.1007/s11852-022-00859-2
Tsilimigkas, G. Derdemezi, E-T. (2020). Unregulated built-up area expansion on Santorini island, Greece. European planning studies. 28 (9). pp. 1790 - 1811. DOI: 0.1080/09654313.2019.1687656
Tzeferis, P. (2018). Institutional framework for the protection of geological sites. Greek Mineral Wealth. Retrieved from: https://www.oryktosploutos.net/2018/04/blog-post_3-5/
Zouros, N. (2004). The European Geoparks Network - Geological heritage protection and local development. IUGS Episodes Journal of International Geoscience. 27(3). DOI: 10.18814/epiiugs/2004/v27i3/002

17th INTERNATIONAL CONGRESS of the Geological Society of Greece

BULLETIN OF THE GEOLOGICAL SOCIETY OF GREECE, SP. PUBL.

EXTENDED ABSTRACT 048

Slope failures of friable sandstone in coastal areas. A Case study from Western Greece.

Chatziangelis E.[1*], Boumpoulis V.[1], Depountis N.[1]
*(1) Department of Geology, University of Patras, 26504 Patras, Greece, *up1089644@upatras.gr*

Research Highlights: **Investigation of the failure mechanism of steep sandstone slopes in coastal areas**

Introduction

Coastal slope failures are major geological phenomena that often lead to environmental degradation, land loss and destruction of property and infrastructure. These failures occur predominantly in regions with weak geological formations, steep slopes and dynamic coastal processes. The Kalamaki coastal zone in Western Achaia, Greece, is a representative example, featuring a stratigraphy of friable sandstone formations overlaying clayey marls, which are inherently prone to weathering, erosion, and slope instability. The susceptibility of these geological formations to failure is exacerbated by structural discontinuities in the sandstone layers, allowing water infiltration and subsequent slope destabilization (Zhang *et al.,* 2020).

Since 2014, progressive slope instability in Kalamaki has been observed through satellite imagery (Figure 1), aerial surveys, and field investigations. The main causes of this instability include natural processes such as wave action and erosion, combined with anthropogenic activities such as irrigation and excavation for road and building construction. In addition, water infiltration along vertical cracks in the sandstone, combined with the penetration of vegetation roots, widens these cracks over time, causing translational slides, rockfalls, and earth flows. These processes deposit significant sediment loads along the coastline, altering beach dynamics (Delgado *et al.,* 2018; Poulos *et al.,* 2019).

Figure 1. Satellite image of Kalamaki in Western Achaia, Greece (Google Earth 05/2015) with the white line representing the failure area as determined in 9/5/2022.

Localized high-wave events and marine undercutting further destabilize the base of the coastal slopes, creating overhangs and weakening the upper geological layers. This underscores the necessity for targeted mitigation measures addressing both geological and marine influences. While prior studies suggest relative stability in some parts of the Kalamaki coastline, high-energy events have repeatedly triggered localized failures, highlighting the importance of assessing these vulnerabilities. For a better understanding of the failures on the coastal slopes of Kalamaki, this paper uses the results of the Coastal Vulnerability Index (CVI) estimation for specific areas (Boumpoulis, 2024; Boumpoulis *et al.,* 2025) in combination with the classical slope stability analysis. Using Hoek et al. (1981) two-dimensional slope stability analysis for weak rocks and general CVI considerations (Gornitz, 1991; Depountis *et al.,* 2023), , this study identifies slope destabilization hotspots in a coastal area, identifying the failure mechanism and providing critical information on areas requiring immediate protection.

Methodology and geological regime

The methodological framework for investigating the sandstone slope failures in the Kalamaki coastal area focuses on the identification of the geological characteristics and the mechanisms of driving slope instability. Fieldwork was conducted to document the state of the slope and identify signs of instability. Observations were made regarding the slope and coast morphology, the distribution of discontinuities in the sandstone mass and the vegetation cover. The field surveys conducted, using UAV and GPS equipment, helped in the production of high resolution orthoimages and mapping of the affected area (Figure 2).

Figure 2. Aerial photograph of the sandstone slope failure occurred in Kalamaki, Western Achaia (UAV campaign, 9/5/2022).

The geological framework of the affected area consists of Plio-Pleistocene sediments, mainly friable sandstones overlying clayey marls (Figure 3) – από το διδακτορικό του Βασίλη και τη δημοσίευση του 2025. Both formations are very susceptible to weathering and have the characteristics of soft rocks; hence, low Uniaxial Compressive Strength (UCS). Moreover, the sandstones exhibit high porosity and permeability, making them susceptible to water infiltration, and are intersected by vertical and sub-vertical cracks, which act as pathways for root penetration and water ingress; thus, further weakening the slope's integrity along the coastline.

Figure 3. Geological map of the study area.

The geological and field surveys carried out allowed the precise delineation of the landslide boundary and its characteristics (Figure 4).

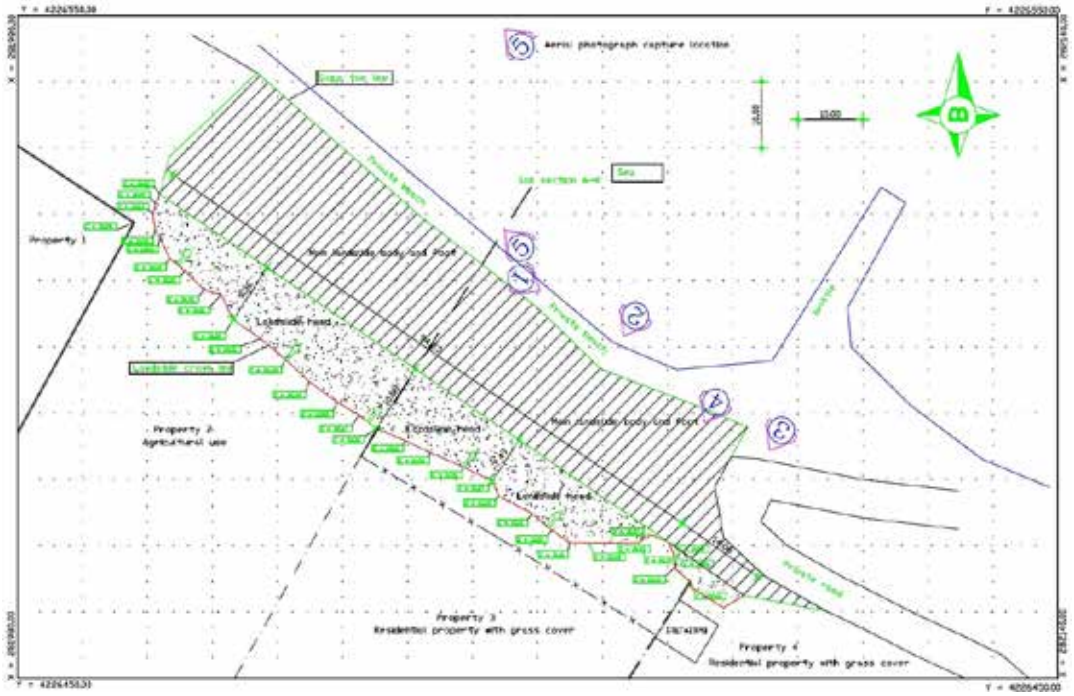

Figure 4. Plan view of the study area with the landslide delineation.

Measurements conducted during field surveys indicated that the landslide's total affected area was approximately 2,750 m², with the crown at an elevation of 18.5–22.5 meters above sea level. The landslide crown extended 120 meters in length, with a scarp of 3 meters and a head of 10.8 meters in width.

Analysis and Results

The failure mechanism was investigated based on the observed field data and geological regime, so a detailed two-dimensional geological cross-section was designed for further analysis (Figure 5).

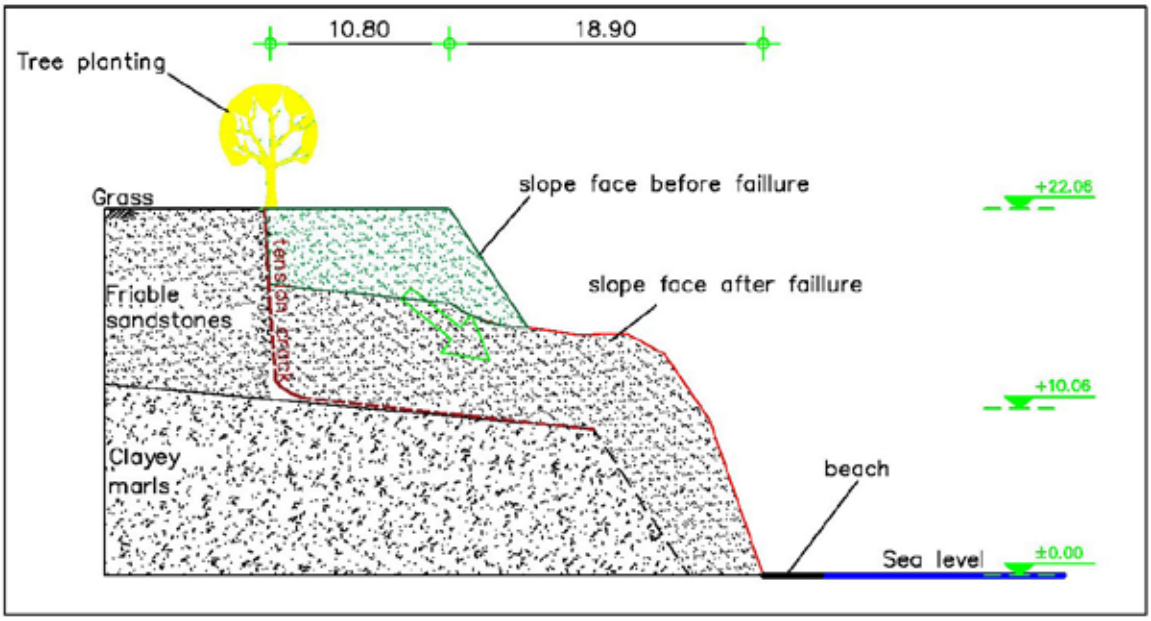

Figure 5. Geological cross-section presenting the landslide characteristics and the failure mechanism

The primary failure mode identified was translational sliding, where sandstone blocks detach along pre-existing discontinuities or tension cracks and slide over the underlying clay marls, even with low stratigraphic gradient between sandstones and clays. These discontinuities acted as tensile cracks, further widened by root penetration and water infiltration and facilitated block detachment and movement downslope. Earlier failure processes were also observed, such as sparse rock falls and earth flow, in places where marine undercutting had reduced the basic support of the slope.
Further destabilization of the slope occurred due to anthropogenic interventions, such as irrigation of vegetation and trees near the slope crest. These activities have contributed to the accumulation of water within the sandstone mass and its discontinuities, exacerbating the instability of the slope.
The failure analysis was based on the principle of a translational slide with tensile crack, as proposed by Hoek et al. (1981), as the most representative for the study area (Figure 6).

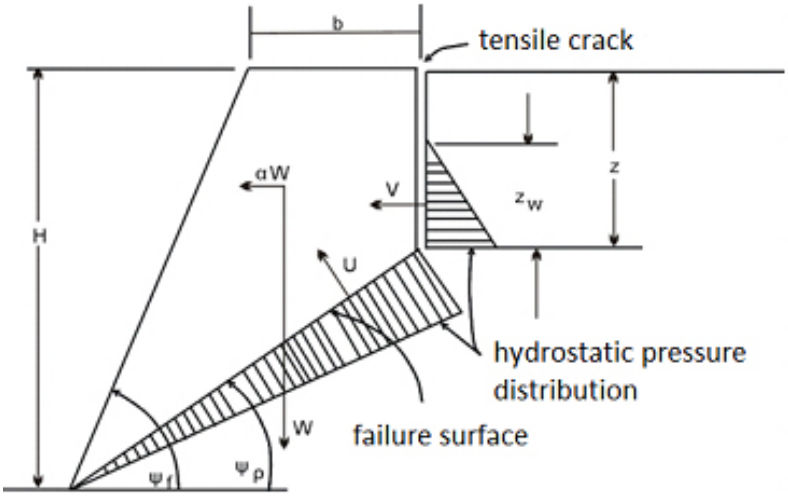

F	Factor of safety
H	Height of the sliding slope
W	Weight of the sliding block
U	Uplifting hydrostatic force
V	Hydrostatic tensile crack force
z	Depth of tensile crack
b	Width of the sliding block
z_w	Water level in tensile crack
ψ_p	Inclination angle of failure surface
ψ_f	Inclination angle of sliding slope
α	Seismic ground acceleration
γ	Unit weight of sliding block

Figure 6. Failure analysis of a rock mass in the form of translational slide with tensile crack (Hoek *et al.*, 1981)

The equations used for the calculation of the Factor of safety for this type of slide are (Hoek *et al.*, 1981):

$$F = \frac{cA + [W\ (\cos\psi_p - \alpha \sin\psi_p) - U - V\sin\psi_p]\ \tan\varphi}{W(\sin\psi_p + \alpha\cos\psi_p) + V\cos\psi_p}$$

$$Z = H(1 - \sqrt{\cot\psi_f \tan\psi_p})$$

$$A = (H - Z)cosec(\psi_p)$$

$$W = {}^1/_2\ \gamma\ H^2[(1 - (Z/H)^2)\cot\psi_p - \cot\psi_f]$$

$$U = {}^1/_2\ \gamma_w\ Z_w A$$

$$V = {}^1/_2\ \gamma_w\ Z_w^2$$

The data imported in the above equations are:
H = 12 m, z = 9,5 m, $\psi_\rho = 10^0$, $\psi_f = 80^0$, α = 0.12, γ = 23 kN/m^3, φ = 20^0, c = 10 kPa.
The geometrical data of slope derived by in-situ measurements and the geotechnical data (c and φ) of the sandstone material along the sliding surface considered to be similar to the residual state of a clayey sand with a minimum cohesion. The final calculation of the safety factor of the sandstone slope for three different scenarios is illustrated in Table 1, which shows that the main sliding force is hydrostatic uplift and lateral pressure. When the water level rises

within the discontinuities near the ground surface (0.5 m below the surface), failure occurs. This matches the actual conditions found in the research area and the moisture content of the samples that 1m from the ground surface was in a state of saturation.

Table 1. Factor of safety of the coastal sandstone slopes in the Kalamaki area

Scenario A (dry conditions)		Scenario B (hydrostatic fluctuation)		Scenario C (earthquake)	
Z_w	F	Z_w	F	Z_w	F
0	2.32	3	1.99	0	1.36
		5	1.64		
		7	1.3		
		9	**1**		
		10	0.88		

To exclude the hypothesis that this type of landslide was triggered by coastal erosion, the vulnerability status of the area was also analyzed, along with the calculation of the historical shoreline erosion changes in the coastline. The data was retrieved from two studies carried out in the Gulf of Patras by Boumpoulis (2024) and Boumpoulis *et al.* (2025).

In particular, the results of the Coastal Vulnerability Index (CVI) estimated by the previous studies indicate that the coastal zone of Kalamaki is characterized by very low vulnerability, represented by a green line in Figure 7 (Boumpoulis, 2024; Boumpoulis *et al.*, 2025). The green line in Figure 7 represents a stable coast, with an erosion rate ranging from -0.10 to -0.20 m/year, which suggests a low probability that the landslide event of 2022 was caused by coastal erosion. However, the sandy material of the beach has been created by past landslides, either due to undercutting of part of the slope by wave erosion or similar translational failures.

Figure 7. Coastal Vulnerability Index (CVI) along the Kalamaki coastline as adopted from a previous study conducted by Boumpoulis (2024). The image is a worldview 2018 aerial image and the red line indicates the landslide crown identified in 09/05/2022.

Conclusion/Discussion

This research bridges the perspectives of geology and coastal engineering by investigating the interaction between terrestrial and coastal processes in coastal slope failures. The research focused on finding the failure mechanism of a friable sandstone slope in the coastal area of Kalamaki and revealed that a combination of geological, hydraulic and anthropogenic factors contributed to the slope instability. The friable nature of the sandstone formations, combined with the increased hydrostatic pressure in the discontinuities of the sandstone mass, contributed to the instability of the slope. The vertical discontinuities within the sandstone mass serve as critical pathway for water infiltration, and hydrostatic pressure increases, while marine undercutting weakens the base of the slope; hence creating a complex geological environment for several types of instabilities that have occurred in the past, such as sparse rock falls and earth flows.

A key conclusion of this study is the role of anthropogenic activities in exacerbating slope instability. Practices such as irrigation of vegetation and trees near the top of the slope without any drainage, lead to water accumulation, further destabilizing the slope. These activities, combined with natural processes, highlight the progressive nature of slope failure in the area.

The results of this study underline the importance of an integrated approach to slope stabilization in coastal areas. Mitigation measures should prioritize the reduction of water infiltration in similar geological regimes by implementing appropriate drainage measures and preventing anthropogenic activities such as irrigation and excavation for road and building construction on the crest of coastal sandstone slopes.

References

Boumpoulis, V., 2024. Development of a coastal vulnerability assessment model: application in the pilot area of the Gulf of Patras, Greece. Ph.D. Thesis, University of Patras, 188 p.

Boumpoulis, V., Depountis, N., Dimas, A., Papatheodorou G., 2025. Presentation and analysis of the Geotechnical Coastal Vulnerability Index and validation of its application to coastal erosion problems. Sci Rep 15, 1424.

Delgado, G., Gómez, C., & Fernández, L., 2018. Coastal erosion processes and slope stability in sandy formations. Journal of Coastal Engineering, 42(3), 185-198.

Depountis N., Apostolopoulos D., Boumpoulis V., Christodoulou D., Dimas A., Fakiris E., Leftheriotis G., Menegatos A., Nikolakopoulos K., Pappatheodorou G., Sabatakakis N., 2023. Coastal Erosion Identification and Monitoring in the Patras Gulf (Greece) Using Multi-Discipline Approaches. J Mar Sci Eng 11:654.

Gornitz, V. 1991. Global coastal hazards from future sea level rise. Palaeogeogr Palaeoclimatol Palaeoecol 89:379–398.

Hoek, E., Bray, J., 1981. Rock Slope Engineering, 3rd ed., Inst. Mining and Metallurgy, London, UK, 372p.

Poulos, S.E., Collins, M.B., & Tsimplis, M.N., 2019. Sediment dynamics and slope failures in Mediterranean coastal zones. Coastal Sediments, 101-115.

Zhang, X., Li, Z., Chen, Y., 2020. Geological and geotechnical perspectives on slope failures in coastal regions. Geotechnical Journal, 38(4), 345-362.

17th INTERNATIONAL CONGRESS
of the Geological Society of Greece

BULLETIN OF THE GEOLOGICAL SOCIETY OF GREECE, SP. PUBL.

EXTENDED ABSTRACT 049

Settlements in residual soils

Nikolaos Chatzigogos[1] , Agisilaos Poulios[2], Thomas Makedon[3],
(1) Geology, Aristotle University of Thessaloniki, Thessaloniki, Greece (e-mail: chatzi12@gmail.com)
(2) Geology, Aristotle University of Thessaloniki, Thessaloniki, Greece (e-mail: pouliosa@geo.auth.gr)
(3) Geology, Aristotle University of Thessaloniki, Thessaloniki, Greece (e-mail: thomas@geo.auth.gr)

Introduction

The conservation and restoration of cultural heritage structures requires a complete and detailed analysis of the geological and geotechnical hazards that affect them. Thus, it is possible to clarify the failure mechanisms that act upon them or might be activated due to technical interventions and to carry out detailed planning of measures to mitigate their effect at a time scale longer than conventional construction works. In the present paper, geological and geotechnical data from site investigation are presented and evaluated relating to the failure mechanisms affecting the foundation of the Holy Monastery of Chilandari mainly the western wing of the Monastery. The Monastery was founded on artificial backfill material followed by weathered soil formations - most probably residual soils of weathered granodiorite – that lay on top of granodiorite and marble rocks. Specifically, the paper presents the results of the geotechnical investigation carried out via sample drilling in situ and laboratory tests and the formulation of the geotechnical model of the foundation area of Monastery. Based on the model, the nature and mechanical behavior of the foundation soil is investigated against mass movements, deformations and settlement. Finally, the main failure mechanism of the subsoil foundation of the Monastery is established and mitigating measures are proposed.

Methodology

For the purposes of this investigation, a methodology of in situ along with laboratory investigation was followed to examine the physical and mechanical properties of the foundation subsoil of the buildings, aiming to assess its origin and mechanical behavior and identify the failure mechanism responsible for the deformations observed in the western wall of the Monastery. The main steps of this methodology are as follows:

1. Determination of the nature and origin of subsoil formations.
2. Evaluation of in-situ test results and design of a conventional Soil Mechanics testing program.
3. Comparison of in-situ test results with the results of laboratory tests. Tests conducted included the determination of physical properties, soil classification tests, and calculations of mechanical properties.

Based on the above, the following steps were taken:

1. Evaluation of shear strength so as to clarify the mechanical behavior of the foundation subsoil and produce design parameters.
2. Bearing capacity and settlement analysis using specialized software, including the calculation of the safety factor against shear failure and the estimation of expected settlements.
3. Interpretation of computational analyses and assessment of the main geotechnical hazards on site.

Geotechnical Model - Calculations

Based on the results of the geotechnical investigation the geotechnical model is derived via the respective steps and calculations:

- Description of the geological-geotechnical formations.
- Compilation of geotechnical sections of the foundation subsoil based on strength and compressibility parameters, the effect of groundwater levels (maximum annual and 50-year period), foundation levels of the main and neighboring constructions, etc.
- Indication of the main/critical conditions to be observed.

- Calculation of bearing capacity (short-term and long-term). Control of settlement due to consolidation and or hydroconsolidation, estimation of differential settlement etc.
- Full dimensioning of all required retaining and soil improvement works with references to the calculation assumptions and the way of analysis.
- Detailed description of the proposal for the type, level and dimensions of the foundation and a description of the sequence of construction works.
- Investigation and description of suitable alternative construction solutions for the foundation and improvement of

the subsoil, among which the best technically and economically optimal solution will be described.

Discussion

The subsoil formations are residual soils of weathered granodiorite, and the failures recorded to the structures of the western part of the compound of the Monastery are due to differential settlements.

- The differential settlements are due to the subsoils' volumetric change behavior under constant loading as well as changes in the moisture content.
- The changes in moisture content are caused by the seasonal fluctuations of the water table that were measured during the dry and wet periods of the year.
- The stratigraphy is dipping to the west which creates a thicker soil cover of the bedrock to that direction, thus producing differential settlement and failures.
- The drying of the foundation soils causes significant settlements because of swelling under wetting and shrinkage under drying. Overall, it is estimated that wetting affects the surficial deposits (S1, S2 and possibly R1) and drying affects the deeper deposits (layers S3 and C1), resulting in a total amount of settlements throughout a wetting-drying circle over a period of one year.
- No data that indicates possible creep - sliding phenomena or any short of horizontal deformations were observed.

Based on the above, it is suggested that remedial measures against the buildings' failures should adopt an approach to limit vertical deformations. Since it is very difficult to fully control the groundwater regime and the seasonal fluctuations, it is suggested that every structure's foundation separately should be connected to the solid bedrock, so that any further volume changes of the overlain soil layer could not affect them. It must be noted that at a certain point of investigation (location of borehole G3) the compressible layer has a small thickness and therefore the total final settlements in time will not be of great magnitude.

Mitigation Measures

Based on the above and to ensure the safety of the significant and historical structures of the Monastery against further settlements it is proposed that mitigation measures should be implemented along with a monitoring program that can assist possible future interventions. Due to the significance of the structure the suggested measures should have minimal disturbance or effect on the character of the construction and that of the broader area of the Monastery. The solution of micro-piles has several advantages relating to the above considerations:

- They are underground and thus hidden interventions that can be constructed on the perimeter and/or sides of the constructions and anchored to the existing foundations where possible, for further support.
- They can be linked with a capping beam to increase bearing capacity and prevent further differential settlements.

The monitoring should include crack gauges for potential deformations and piezometers for groundwater table measurements. These should be intercorrelated so as to verify the failure mechanism by correlating the rate of deformation with the groundwater levels and its seasonal variations.

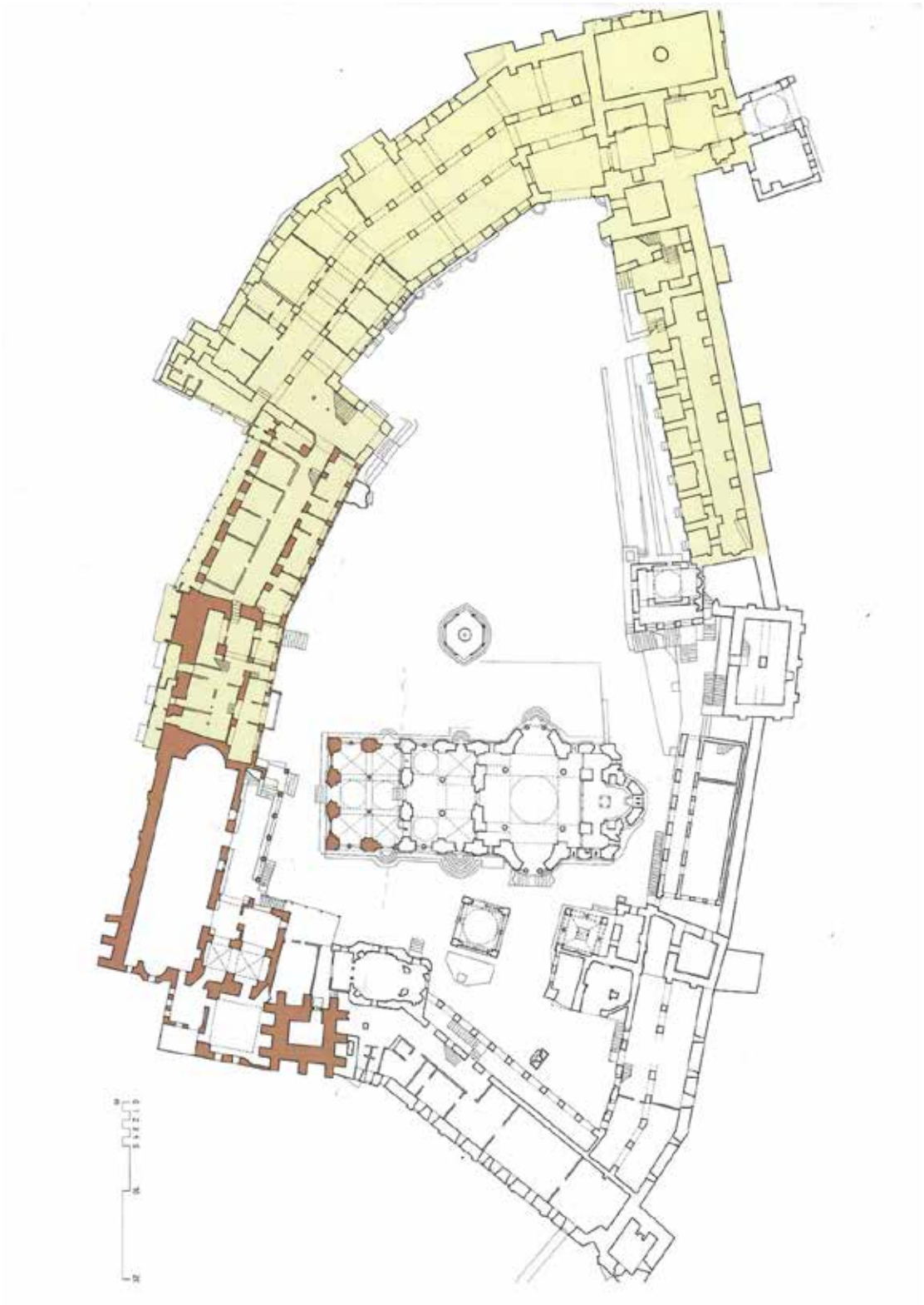

Figure 1: Location of mentioned failures

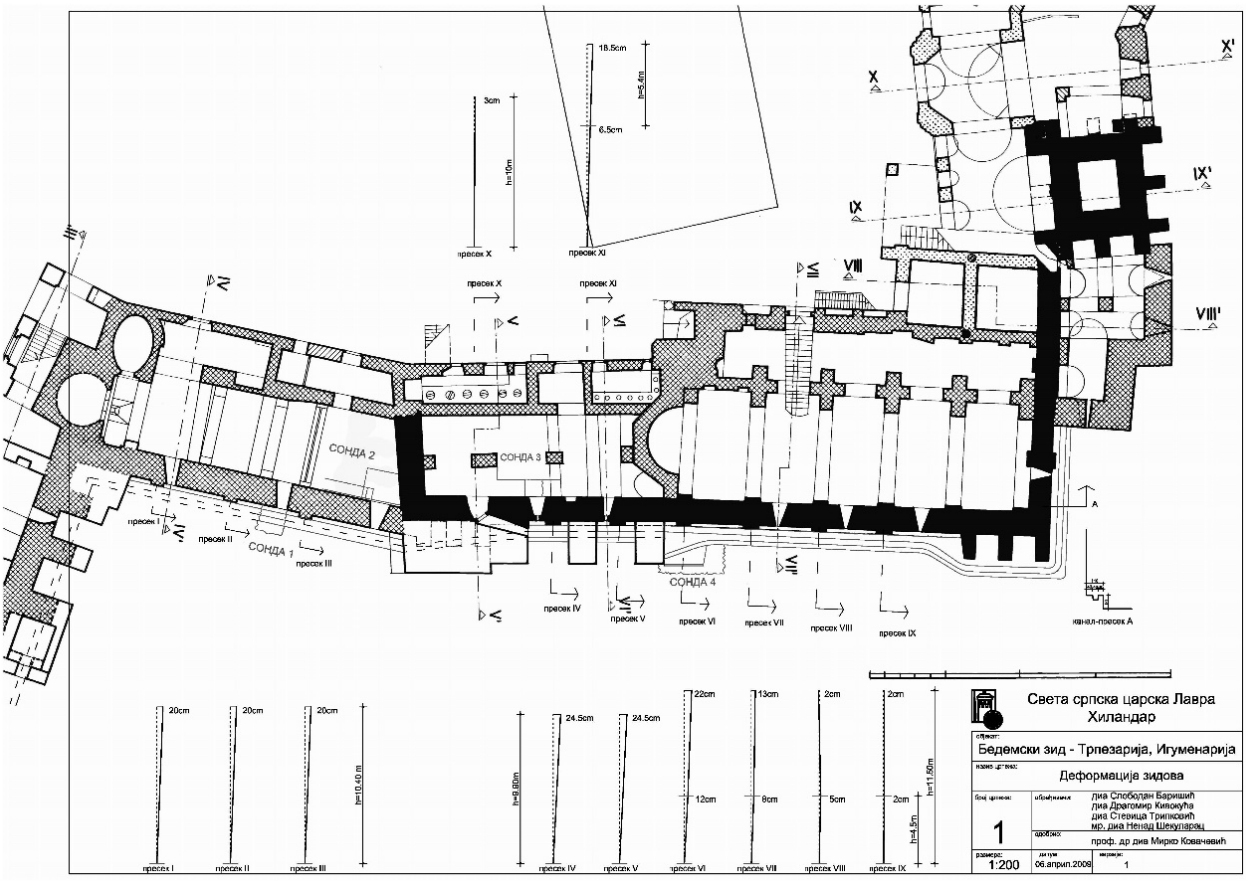

Figure 2: Locations and extent of deviation of structures

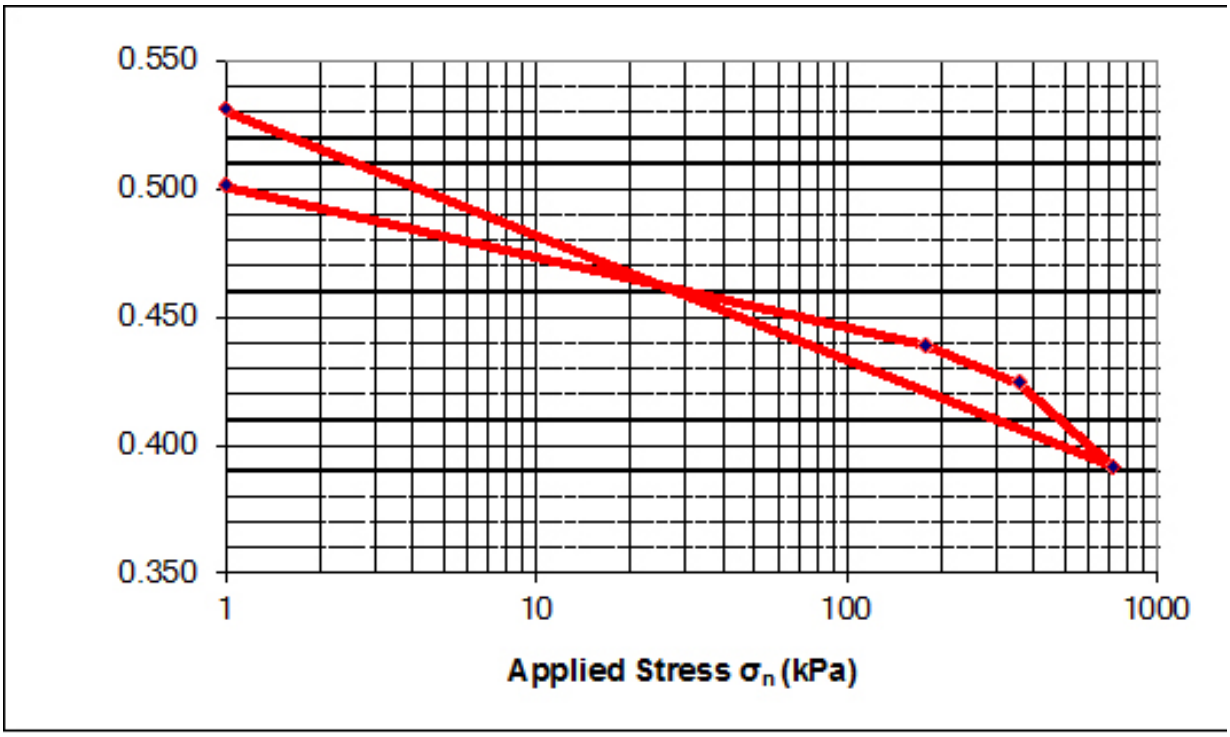

Figure 3:Swelling behavior of layer C1

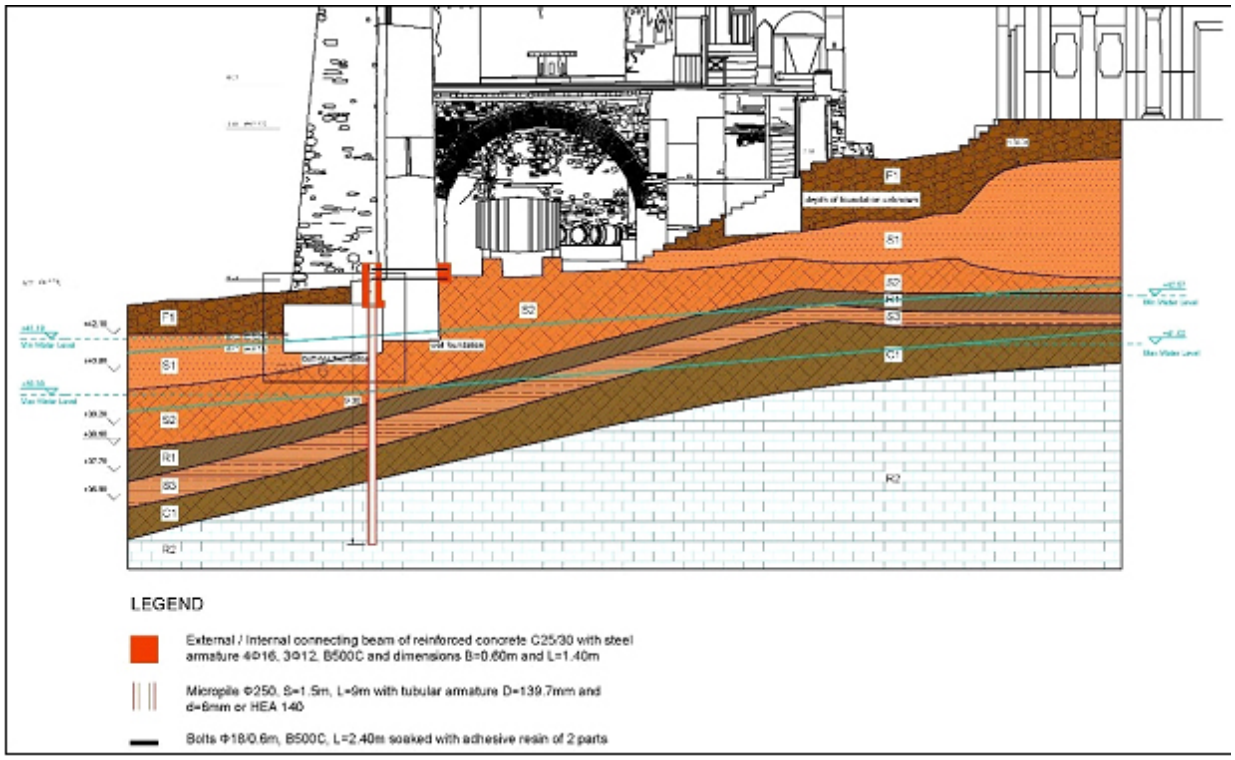

Figure 4:Geotechnical cross section 1-1' with proposed remedial measures

References

Blight, G. E. (1965). A study of effective stresses for volume change. Στο Moisture Equilibria and Moisture Changes in Soils. Beneath Covered Areas (σσ. 259-269). Butterworth, Australia.

Blight, G. E. (1987). Lowering the groundwatertable by deep-rooted vegetation-The geotechnical effects of groundwater recovery. Proc. 9th European Conf. On Soil Mech. and Found. Eng., 1, σσ. 285-288. Dublin.

Blight, G. E. (1997). Mechanics of Residual Soils. Rotterdam, Netherlands: Balkema. Bowles, J. (1957). Foundation Analysis and Design., (σ. 308). New York.

Budhu, M. (2000). Soil Mechanics and Foundations. New York: Wiley.

Craig, R. F. (1992). Soil Mechanics (5 εκδ.). London: Chapman & Hall.

Jennings, J. E., & Knight, K. (1975). A guide to construction on or with materials exhibiting additional settlement due to collapse of grain structure. Proc. 6th Reg. Conf. For Africa on Soil Mech and Found. Eng., 1, σσ. 99-105. Durban.

Knight, K. (1961). The collapse of structure of sandy sub-soils on wetting. PHD Thesis, University of the Witwatersrand, Johannesburg.

Pillissier, J. P. (1991). Piles in deep residual soils. Proc. 10th Conf. For Africa on Soil Mech. and Found. Eng., 1, σσ. 31-40. Maseru, Lesotho.

Tromp, B. E. (1985). Design of stiffened raft foundations for houses on collapsing sands. Johannesburg: Schwarz, Tromp and Associates.

Wesley, L. D. (2010). Geotechnical Engineering in Residual Soils. Hoboken, New Jersey: John Wiley & Sons Inc.

Williams, A. A. (1991). The extraordinary phenomenon of chemical heaving and its effect on buildings and roads. Proc. 10th Reg. Conf. for Africa on Soil Mech. and Found. Eng., 1, σσ. 91-98. Maseru, Lesotho.

17th INTERNATIONAL CONGRESS of the Geological Society of Greece

BULLETIN OF THE GEOLOGICAL SOCIETY OF GREECE, SP. PUBL.

EXTENDED ABSTRACT 050

Geotopes of Thessaly (central Greece) and their educational approach

Chatzipetros A.[1], Samantzi V.[2]

(1) Department of Structural, Historical and Applied Geology, School of Geology, Aristotle University of Thessaloniki, 54124, Greece, ac@geo.auth.gr (2) Department of Geography, University of Aegean, Mytilene, Greece

Introduction / Background

Geotopes play an important role in deducing the geological history and evolution of an area and can contribute to the understanding of geological processes that take place daily. Geotopes can be used for educational purposes, since they can function as natural laboratories in which citizens can come into contact with Geology and understand how the Earth works, thus contributing to the protection of natural monuments. At the same time, economic benefits can also potentially stem from the promotion of a geotope.

Thessaly is an area located in central Greece and is abundant with important geotopes. Tectonic structures, such as faults and folds, rocks, gorges, quarries, caves, monasteries, traditional settlements and more, are some of the impressive locations of Thessaly. Every year there are thousands of visitors in the broader region of Thessaly, who come to admire the treasures of nature and, at the same time, have the potential to come into contact with Geology and its principles.

For this project, six geosites of Thessaly were selected, which are related to different areas of Geology. Each selected geotope is related to a geological phenomenon, which can be presented and analyzed to secondary school students in the context of the course of “Geology – Geography”.

Objectives

This paper aims to help teachers who intend to organize educational trips to the region of Thessaly and for this reason these characteristic landforms have been selected, which have the potential to impress students and attract their interest.

At the same time, the Worksheets and Evaluation Sheets, which correspond to each geotope, include activities and tasks that can be done independently of the educational trip, but can be part of the teaching of the course of “Geology – Geography” of the first and second grade of High School, in order to understand geological concepts, such as weathering and erosion, deposition, faults and earthquakes, volcanos, fossilization, etc. that are phenomena that take place daily in areas of the planet and affect people’s lives.

It is important to mention that by completing the tasks during teaching of the selected geotopes and activities, students will have practiced writing and speaking, team collaboration, and will have developed their self-confidence.

Methods

Geotopes

Geotopes can be used as a source for collecting information about the geological history and paleoenvironment of an area, aiding science, research and education. At the same time, they are of archaeological, historical and folklore importance, while in many cases they host local ecosystems and contribute to the development of tourism in the area. Greece presents great geodiversity with complex geological structures due to geomorphological processes that have taken place and have shaped the image of the country on the surface and the interior of the Earth, thus creating a large number of geotopes throughout the country.

Geosites can contribute to the education of students through activities that lead to an understanding of Geology. Student visits to geological structures can make geotopes a means of understanding geological processes that have taken place in the past (Theodosiou et al., 2006). Educational (geo)tourism can support geoeducation, as geosites are open to the public and are “living museums”. The combination of a geotope with local history and mythology, with archaeology, religion, folk tradition and geological history, can attract the interest of young and old visitors.

Education

Today, courses of environmental interest are taught in Primary and Secondary Education, which bring students into contact with nature and the problems it faces and will face in the future, with the ultimate goal of raising students’ awareness about the protection of natural and geological heritage (Fermeli, 2023).

For the better consolidation of geological concepts, the teacher, in addition to the theoretical approach of the subject, is required to use other assignments or outdoor exercises, in order for the new knowledge to become the property of

the students. Although Greece has a rich geological and geomorphological heritage, few schools form environmental groups to implement environmental programs during the school year that will help students get in touch with the natural environment and love it. Educational activities in the context of Geoeducation, Environmental Education and Education on Natural Disasters is essential for students. Phenomena, such as earthquakes and volcanoes, can affect people's daily lives and even cause human losses.
The proper teaching of a lesson requires proper planning by the teacher, taking into account the general objectives of the course based on the Curriculum. When teaching a lesson, the teacher uses the Lesson Plan and the Worksheets and Evaluation Sheets, which complete the textbooks, for a better understanding and consolidation of the lesson. Initially, the teacher must start with the preexisting knowledge, then continue with the presentation of the lesson, follow the Worksheets for the application of the new knowledge, continue with the evaluation of the lesson through the Evaluation Sheets and finally, after summing up, connect the lesson with the next (Tzovla, 2021).

Geotopes of Thessaly

Thessaly is located in central Greece. It presents a simple geomorphological picture, with the mountainous parts bordering the lowlands in the central areas. Strong earthquakes have occurred in the region from time to time, causing problems, such as the great earthquakes of 1892, 1901, 1941 and the most recent ones of 2021, while the recent floods of 2023 have still left fresh memories, having created serious problems.
Thessaly is an area that combines geological, historical, archaeological and cultural elements. It has many characteristic geological sites, which attract the interest of visitors and scientists. Some geotopes of Thessaly are world famous.
For this paper, six (6) representative geosites of the geological history of Thessaly were selected, in order to develop the interest of students of the first two grades of High School in Geology in general and its individual fields, such as Structural Geology, Physical Geography, Seismology, Volcanology and Palaeobotany. Eventually, students develop into responsible and aware citizens. Initially, general data are given for each geotope, then the necessary geological knowledge is determined, required for the understanding of each geotope by the students, followed by an indicative Lesson Plan for the organization of the teaching of the geological phenomenon and, finally, the Worksheets and Evaluation with activities and homework for the best possible consolidation of the topic.

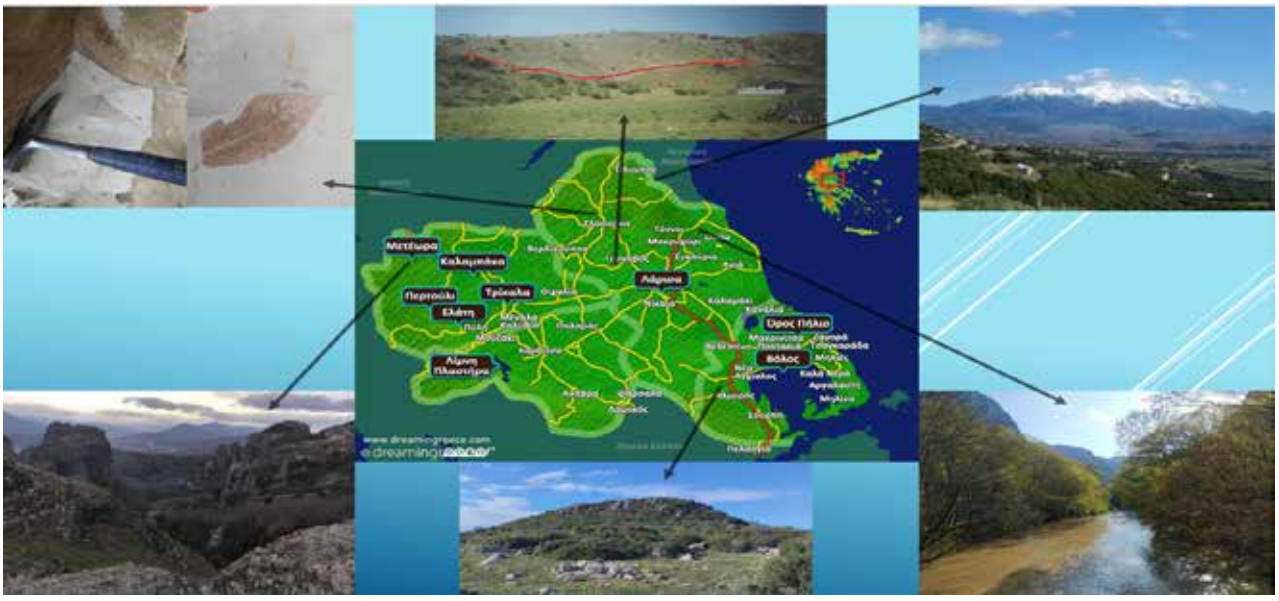

Fig. 1: The six selected geotopes of Thessaly.

The six (6) geotopes are the following (fig. 1, clockwise from top right):

- The **tectonic window of Mount Olympus**, a characteristic geological and tectonic form of Greece,
- The **valley of Tempi**, a characteristic geomorphological form of unique beauty, associated with the mythology of the whole wider area of Olympus and the river Pinios, which flows through it,
- The **volcano of Mikrothives**, as volcanism affected the region of Thessaly in the geological past,
- **Meteora**, a unique global natural monument, with the characteristic huge boulders of conglomerates, which are

a source of awe and admiration,
- The **Neogene basin of Elassona** with numerous flora fossils and
- The **Tyrnavos fault**, which is associated with the seismicity of the wider area, having being the source of a significant number of seismic events in the past.

As part of the work, field work was carried out on Olympus and Ossa mountains, from where one can admire the valley of Tempi, Meteora for the observation of the imposing volumes in western Thessaly, in the area of Tyrnavos – Damasi – Vlachogianni after the earthquakes of March 2021, in the area of Elassona (Sarantaporo, Lykoudi), in order to locate the plant fossils of the Neogene Basin of Elassona, as well as in the interesting, unexploited - but with growth prospects - area of the volcano of Mikrothives.

OLYMPUS

Mount Olympus is an important symbol and monument of Greece, as it is the highest mountain in Greece, known worldwide from Greek mythology, since on its top lived the Twelve "Olympian" Gods, according to the religion of the ancient Greeks. In 1938 it was declared as the first National Park in Greece, for the protection of the area, while later the Ministry of Culture declared Mount Olympus as an archaeological and historical site due to the number of its monuments. It is a compact, relatively small in size, multi-peaked and rocky mountain with an almost circular shape. It hosts about 1,700 plant species, i.e. about 25% of the Greek flora, as well as a multitude of vertebrates.

The "Olympus tectonic window" is of great geological value to scientists and was formed due to the intense pressures and temperatures, but also the intense tectonism, that the region of Greece undergoes. The area is mainly covered by limestone and dolomites of the autochthonous Olympus Unit, but also marble, shale, gneiss and amphibolite of the Pelagonian Zone, intruded by later magnetic products (granitic bodies).

Students of Greek schools come into contact with mythology and the Olympian gods already from the third grade of Primary School. Mount Olympus has a number of characteristic sites that show its geotectonic evolution. However, the concept of "tectonic window" and geological time in Geology is a difficult concept, even for students of Geological Departments. High School students, within the framework of the course of "Geology – Geography", taught in the first and second grades, can come into contact with simpler concepts of Structural Geology, such as faults and folds, which can be found in nature and make a reference to the tectonic window.

For the educational approach of the Geotope of Mount Olympus, the necessary knowledge is provided, which students should know and is mainly related to faults. Geological concepts related to tectonics, endogenous and exogenous factors that shape the relief of the Earth, lithospheric plates, earthquakes and seismicity, are interesting subjects for the students. The teacher can follow the respective lesson plan, which will be called *"Faulting in Greece"*, will be addressed to students of the first grade and will use Worksheets and Evaluation Sheets on faults.

TEMPI VALLEY

The well-known valley of Tempi is in the eastern part of Thessaly plain and located between the mountains of Olympus to the north and Ossa or Kissavos to the south. Along the valley, which has a NE-SW direction, Pinios River flows, which drains the waters of Thessaly into the Aegean Sea with intense meanderings through the plain and flows into the Aegean Sea forming its Delta near Stomio, creating a rich ecosystem. The valley of Tempi consists of mainly limestone, dolomites and marbles, while caves have been created in places, some of which have impressive decoration with stalactites.

The valley of Tempi is inextricably linked to Mount Olympus and mythology. Today the geotope of the Tempi Valley continues to attract visitors, but fewer than in the past, since it is easily accessible to everyone. The picturesque church of Agia Paraskevi, a landmark of the area, continues to attract visitors, who can come into contact with history, mythology, culture, religion and nature. The combination of the above with certain concepts of Geology can attract the interest of students during a visit to the area.

The educational approach of the Tempi Valley Geotope requires knowledge related to concepts of Physical Geography and Geomorphology. The Lesson Plan is related to concepts such as erosion, transport, deposition, weathering, drainage systems, estuary and river delta, but also floods, which in recent years have caused great disasters and human losses in the area. The relevant Lesson Plan with the corresponding Worksheets and Evaluation Sheets can be called *"How water affects the terrain of the Earth"* and addresses students of the second grade of High School.

THE MIKROTHIVES VOLCANO

In the prefecture of Magnesia near Nea Anchialos and Mikrothives is the hill "Kastro", visible and easily accessible from the Volos – Athens National Road, covered by volcanic rocks of the Pleistocene from the volcanic action of the now inactive Mikrothives volcano. The area is of great geological and historical interest, as the lavas of the volcano

cover a large area, while excavations have brought to light parts of an ancient theater, where the sites are made of volcanic rocks, as well as parts of ancient walls of the "Fthiotides Thebes" of the Hellenistic period (Clapsopoulos, 1991, Vavaliou, 2014, Samantzi, 2024).
It is a small low volcano of typical Maar form, where the volcanic cone is absent (Bournovas, 1999). To the SE there is a dome up to 50 meters thick, which is the main crater, from where lava is believed to have flowed and is called "Magoula". Fragments of volcanic rocks are scattered throughout the area of the "Castle" (basalt, andesite) (Clapsopoulos, 1991). The ancient basalt quarries of Phthiotides Thebes operated in the past in the area, probably during the Hellenistic and Roman times, as there are several sites where it seems that healthy rock has been processed and removed. The original rock was solid and hard and could be processed by workers and, in addition, very close was the Pagasetic Gulf and the ancient port of Pyrasos for the transportation of boulders (Vavaliou, 2014). During field work in the area, large basaltic blocks were observed with obvious marks from the tools used by the workers to carve and cut them off the natural rock, which have been altered mainly by wind erosion. The hill "Kastro" perfectly combines Geology with History and Culture, since the ancient inhabitants of the area utilized the "materials" offered by nature for the economic development of the area and come from the volcano.
The educational approach of the Geotope of the volcano of Mikrothebes requires students to possess knowledge of Volcanology, related to the interior of the Earth, lithospheric plates, volcanoes, as well as the volcanism of Greece. The Lesson Plan can be entitled: *"Volcanic activity in Europe and Greece"* and addressed to students of the second grade of High School with the corresponding Worksheets and Evaluation.

METEORA

Meteora is one of the most important geotopes in Greece, being a UNESCO World Heritage Site. It is a geological monument of exceptional value in terms of aesthetics and science, which is the object of study, promotion and protection. More than 50 vertical, steep and cut off dark rocks are located north of the city of Kalambaka and west of the village of Kastraki in the prefecture of Trikala, at the exact point where Pinios enters the plain of Thessaly. At the top of the rocks are the famous Monasteries of Meteora, which attract thousands of visitors every year. Nimas (1987) likens the area of Meteora to a unique in the world *"stone forest",* which during the post-Byzantine era was transformed into *"Lithopolis",* as hundreds of monks settled in the area.
The conglomerates of Meteora (Miocene) are marine sediments of great thickness, in which many marine fossils have been found. Rounded pebbles are of varying consistency, size and origin. The matrix is a fine-grained clay material rich in carbonates. Holes of various sizes are observed in places, created due to the corrosive action of water and wind and in some cases have formed caves (Rassios et al., 2020).
The flora and fauna in the area of Meteora are important. In addition, the Museum of Geological Formations of Meteora operates in Kastraki since 2018, which contributes to Environmental Education. Since 2024, the Meteora-Pyli Geopark has joined the UNESCO Global Geoparks network, where visitors can take part in various activities that will bring them into contact with the natural environment of the area.
For the educational approach of the Geotope of Meteora, concepts of Sedimentology, Physical Geography and Geomorphology are required. Concepts such as Sedimentary Rocks and Sedimentation, exogenous factors that affect the Earth's relief, such as weathering and erosion, lithification and diagenesis, can help students understand how to create forms, like Meteora. The relevant Lesson Plan can be called *"How weathering and erosion affect the relief of the Earth"* and addressed to students of the first grade of High School, while the Worksheets and Evaluation are about weathering and erosion.

NEOGENE BASIN OF ELASSONA

The basin of Elassona hosts a particularly rare and rich fossilized flora assemblage. This is a rare subtropical flora, having forest plants and swamp plants. The Neogene basin of Elassona is the southern part of a NW-SE trending elongated graben consisting also of the Florina, Ptolemaida – Amyntaio and Kozani – Servia ones. Neogene deposits in the region include Miocene, Pliocene and Quaternary sediments. Fossils of leaves, fruits, pollen and seeds have been found in the area and it is one of the most remarkable sites in Europe. However, the area has not yet been exploited (Samantzi, 2024).
'Sequoia', 'Cryptomeria', 'Cathaya', 'Egeria' fossils have been found (Velitzelos and Gregor, 1990; Velitzelos et al., 2014; Bouchal et al., 2020). In the basin of Elassona, plant fossils are enclosed in diatomites of white to yellowish – whitish color and occur in various places, such as Lykoudi, Drymos and Sarantaporos. Diatomite resembles chalk and forms an extremely fine-grained, soft and usually light-colored and friable sedimentary rock, which consists of fossilized diatomaceous remains (Aivaliotis, 2011, Stefanou, 2016). In the basin of Elassona, clay diatomites were deposited in a lagoon environment and their plant fossils correspond to a humid and warm climate in a clean water

lake environment, displaying a brownish yellow to brown color on the surface, while in depth they have a gray color (Stamatakis and Koukouzas, 2001).
For the educational approach of the Geotope of the Neogene Basin of Elassona, students must possess certain knowledge related to Palaeobotany, such as plant fossils, ways of fossilization, petrified forests in Greece. The Lesson Plan can be called *"Plant fossils in Greece"* and addressed to students of the first grade of High School, while the Worksheets and Evaluation Sheets will be related to fossilization and plant fossils.

TYRNAVOS FAULT

The region of Northern Thessaly is of particular interest to scientists, as it consists of several active normal fault zones. In 2021 two large earthquakes of magnitude 6.3 and 5.9 respectively took place in the region between the cities of Tyrnavos and Elassona and were felt in most of mainland Greece, causing significant damage in the epicentral area. Tyrnavos fault, although not directly related to the earthquakes of 2021, is an active normal ENE striking fault, activated during the Middle Pleistocene (Caputo et al., 1993, Kotsis, 1995, Caputo et al., 2004). The trace of the fault is clearly visible and has been mapped for more than 12 km (Koukouvelas et al., 2021), while it is characterized by seismicity of low to moderate magnitude. The maximum expected earthquake is of the order of 6.5R, while it is thought that the fault caused an earthquake of magnitude 6.0 in 1731 (Belesis, 2012).
The School of Geology, Aristotle University of Thessaloniki, the University of Ferrara and the Municipality of Tyrnavos collaborated for the construction of the Palaeoseismological Museum of Tyrnavos, a model research and educational center of Geology and Seismology at the 7th km of Tyrnavos – Damasi road within the valley of the Titarisios River in the middle of the Tyrnavos fault. Paleoseismic trenches in the site show successive reactivations of the fault, aswhile research instruments (seismograph and GNSS) have also been installed (Belesis, 2012). It is the only open museum park in Europe for the geology of earthquakes. Unfortunately, it is still not open to visitors, while today it shows signs of abandonment.
Tyrnavos fault is an important geotope for the region of Thessaly, but also for the whole country due to its seismic potential. The preparation of citizens of all ages is necessary so that their reaction before, during and after the earthquake is optimum and human losses are avoided. Secondary school students can visit the geotope of the Tyrnavos fault, as it is easily accessible, and be informed about the earthquakes of the past.
For the educational approach of the Tyrnavos Fault Geotope, students are required to know about seismology, earthquakes and their characteristics, seismic waves, seismographs, as well as about the surface manifestations of an earthquake (ground ruptures, rockfalls, landslides, subsidence, soil liquefaction). The lesson plan may be entitled: *"The earthquake in everyday life"* and addressed to students of the first grade of High School, while the Worksheets and Evaluation refer to earthquakes.

Results and Conclusions

Several, if not all, geosites can be classified as educational and, in the context of field trips, used by teachers to transfer geological concepts to students. The subject of "Geology – Geography", taught in the first and the second grades of the Greek High Schools, is linked to the natural environment, natural disasters and landforms and can instill a sense of responsibility in students towards the geoenvironment. Students can understand the value of geotopes, get in touch with the place where they live and how they were created.
In addition, the teaching of the subject of "Geology – Geography" needs to change to attract the interest of students. The school must be in accordance with the needs of the time and the students to become efficient and able to prepare them for the new challenges of the future. At the same time, teachers should teach their students topics that interest them and will activate them for the protection of natural and geological heritage, instead of providing them with sterile knowledge. For the above reasons, proper preparation and organization of the lesson by the teacher is required (Iliopoulou, 2006).
In conclusion, it should be mentioned that of the geotopes chosen, Mount Olympus and Meteora are places world famous with thousands of visitors every year. The other four geotopes (Valley of Tempi, Tyrnavos fault, Neogene basin of Elassona, Volcano of Mikrothives) are places that need support, empowerment and promotion in order to attract visitors of all ages while developing Geotourism and economic benefits.

Acknowledgements

This paper is part of the second author's MSc Thesis at the University of the Aegean, completed under the Inter – Institutional "Natural Hazards and Disaster Mitigation" Master Course programme. The authors would like to thank Professor Emeritus Spyros Pavlides, Dr. Charalambos Fassoulas and Professor Nickolas Zouros for their contribution towards the completion of the Postgraduate Program and the MSc Thesis.

References

Aivalioti M. (2011). Remediation of water contaminated by BTEX and MTBE using natural and modified diatomite – Comparison and combination with other natural adsorbents. Doctoral Thesis. Department of Environmental Engineering. Technical University of Crete. Chania.

Belesis A. (2012). Revision and modification of the General Urban Plan (GSP) of the Municipality of Tyrnavos (Stage A – Preliminary Geological Suitability Study.

Bouchal JM, Güner TH, Velitzelos D, Velitzelos E and Denk T. (2020). Messinian vegetation and climate of the intermontane Florina–Ptolemais–Servia Basin, NW Greece inferred from palaeobotanical data: how well do plant fossils reflect past environments? R. Soc. Open Sci. 7: 192067, http://dx.doi.org/10.1098/rsos.192067.

Bournovas, I. (1999). The natural monuments of Greece. Publications: KACTOS.

Caputo, R. and Pavlides, S. (1993). Late Cainozoic geodynamic evolution of Thessaly and surroundings (central-northern Greece). Tectonophysics 223. 339–362, https://doi.org/10.1016/0040-1951(93)90144-9.

Caputo R., Helly B., Pavlides S. and Papadopoulos G. (2004). Palaeoseismological investigation of the Tyrnavos Fault (Thessaly, Central Greece). Tectonophysics 394. 1 –20.

Clapsopoulos I. (1991). Petrology, Geochemistry and origin of Pliocene – Pleistocene potassium – rich volcanic rocks from Greece. Ph.D. Thesis, Department of Geology. Faculty of Science. University of Manchester.

Fermeli, G. (2023). The teaching of geosciences in Greece, through school textbooks: A historical review (1830-2021).

Iliopoulou If. (2006). Storyline: An interdisciplinary approach to the development of environmental issues. 2nd Conference of School Programs of Environmental Education. 15-17/12/2006. Athens.

Kotsis, H. (1998). Neotectonics and paleoseismology in the area of Tyrnavos and Rodia (Thessaly)- Seismic risk assessment for the city of Larissa with geological data. Master's Thesis. Department of Geology. Aristotle University of Thessaloniki.

Koukouvelas I., Nikolakopoulos K., Kyriou A., Caputo R., Belesis A. Zygouri V., Verroios S., Apostolopoulos D. and Tsentzos I. (2021). Damasi Earthquake Sequence, Central Greece. Reactivation Evidence across the Westward Propagating Tyrnavos Graben. Geosciences, 11, 328, https://doi.org/10.3390/geosciences11080328.

Lampaki O., Zouros N. (2007). Geoconservation: Promotion and management of natural monuments – geotopes. The case of the Petrified Forest Geopark of Lesvos. Proceedings of the 8th Panhellenic Geographical Conference of the Hellenic Geographical Society. Athens.

Nimas, T. (1987). Trikala – Kalampaka – Meteora – Pindos – Chasia (Geography – History – Monuments – Tourism). Kyriakides Bros Publications. Thessaloniki.

Rassios Ewing A., Ghikas D., Dilek Y., Vamvaka A., Batsi A. and Koutsovitis P. (2020). Meteora: a Billion Years of Geological History in Greece to Create a World Heritage Site. Geoheritage.

Stamatakis M.G. and Koukouzas N.K. (2001). The occurrence of phosphate minerals in lacustrine clayey diatomite deposits, Thessaly, Central Greece. Sedimentary Geology 139. 33-47.

Stefanou C. E. (2016). The diatomites of Lemnos and their environmental applications. Postgraduate Thesis. Department of Geology. Aristotle University of Thessaloniki. Thessaloniki.

Theodosiou E., Fermeli G. and Koutsouveli A. (2006). Our geological heritage. Publications: Kaleidoscope.

Tzovla E. (2021-22). Teaching Methodology: Lesson Plan – Worksheets. Department of Molecular Biology & Genetics, School of Health Sciences. Democritus University of Thrace.

Vavaliou, M. (2014). Archaeological, mineralogical and geochemical study of the ancient basalt quarries in Mikrothives, Magnesia. Analysis of archaeological basalt material in the wider area. Diploma thesis. Interdepartmental Postgraduate Program "Protection, conservation, restoration of cultural monuments". Aristotle University of Thessaloniki Thessaloniki.

Velitzelos E. and Gregor H.J. (1990). Some aspects of the Neogene floral history in Greece. Review of Palaeobotany and Palynology. 62: 291-307.

Velitzelos D., Bouchal M. J. and Denk T. (2014). Review of the Cenozoic floras and vegetation of Greece. Review of Palaeobotany and Palynology 204. 56–117, http://dx.doi.org/10.1016/j.revpalbo.2014.02.006.

17th INTERNATIONAL CONGRESS of the Geological Society of Greece

BULLETIN OF THE GEOLOGICAL SOCIETY OF GREECE, SP. PUBL.

EXTENDED ABSTRACT 051

Flood risk of a touristic island beach under Climate Change: Komi beach Chios

Chatzistratis D[1]., Monioudi I.N.[1], Chalazas T.[1], Andreadis O.P.[1], Moschopoulos K.[1], Chatzipavlis A.E.[1,2], Psarros F.[1], Velegrakis A.F.[1]

(1) Department of Marine Sciences, University of the Aegean, University Hill, 81100 Mytilene, Greece, mard20007@aegean.gr (2) Department of Physics and Earth Sciences, University of Ferrara, Via Saragat 1, 44122 Ferrara, Italy

Research Highlights

Assessment of beach flood risk using open source geospatial data and models.

Introduction

Coastal floods from extreme marine events have had increasing impacts on the coastal natural and human ecosystems, causing coastline changes, biodiversity losses, human mortality, increased health risks and poverty and induced coastal infrastructure/asset damages (IPCC, 2023). Under climate change, the frequency of extreme events is projected to increase and expose annually a large part of the global coastline to the current 1 in 100 years Extreme Sea Level by 2100 (Vousdoukas *et al*., 2018). 'Sandy' shorelines (i.e., the low-lying coasts built on sediments—beaches), which comprise a large segment of the global coastline (Luijendijk *et al*., 2021) will be particularly vulnerable. In addition to their own importance as ecosystems, beaches form natural buffers that protect backshore ecosystems, infrastructure, and assets from coastal flooding (Toimil *et al*., 2023); they also have high hedonic/recreational value, contributing very significantly to the tourism sector due to the current dominance of the 'Sun, Sea, and Sand—3S' model (UNWTO, 2024). Beaches in touristic islands face increased vulnerability to coastal flooding, due to their generally limited width, scarce sediment supply and the high potential exposure to coastal flooding of their backshore infrastructure and services (Brett, 2021). However, the flood assessment of beaches, presents certain challenges due to the need for accurate geospatial information, as well as the accuracy/costs of the used models (Almar *et al*., 2021).

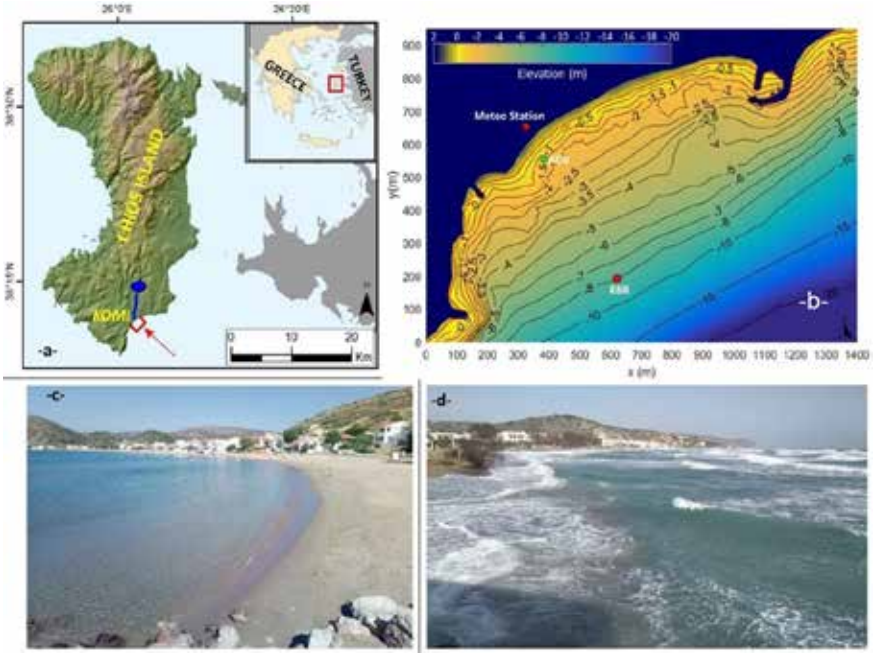

Figure 1. (a) Chios island and Komi beach, showing Katraris river and dam (blue line and circle). (b) Beach nearshore topography/bathymetry. Photos of Komi beach, (c) from the ENE under calm conditions and (d) from WSW during a storm.

Therefore, the objective of this short contribution has been to assess the flood risk of an island beach (Komi, Chios; Fig. 1), using readily available geo-spatial information and an open - source numerical model. Komi is a 1.2 km long barrier beach with a maximum dry width of 38 m. Its backshore hosts a coastal road and many residential and touristic assets, sometimes at a distance of <10 m from the coastline. The beach is characterized by low slopes with elevations that in many areas do not exceed 1.5 m (slopes of approximately 3%). In addition, the backshore elevations are in many areas <1 m. A stream is present at the western segment of the beach, whereas at its eastern end there is a small fishing port. The stream is the outlet of the Katraris river, the land sediment supply of which has been diminished due to the construction of the Kalamoti-Katraris Dam (Andreadis *et al*., 2021).

Methods

In addition to the simple static inundation 'bathtub' model, a simplified two-dimensional finite difference hydrodynamic model LISFLOOD-FP (Bates and de Roo, 2000) was also used. This simulates flood dynamics in a pre-designed grid using a Digital Elevation Model (DEM). Specifically, LISFLOOD-FP applies fluid continuity to calculate the depth at each grid cell while the water flow is channeled along the ground using a simple storage algorithm based on the difference in hydraulic head between adjacent cells (Bates *et al*, 2005). In each cell, the calculated height of the water surface above the topographic elevation as well as the Manning soil friction coefficient are used to calculate the flow rate. The water flow is described by the momentum conservation and mass continuity equations:

$$h_{(i,j)}^{(t+\Delta t)} = h_{(i,j)}^{t} + \frac{\Delta t * Q_{(xi,j-1)}^{t} - Q_{(xi,j-1)}^{t} - Q_{(yi,j-1)}^{t} - Q_{(yi,j)}^{t}}{\Delta x^2} \quad [1]$$

$$Q^{t} = \frac{q_t - \frac{g h_{flow}^{t} * \Delta t * \Delta (h^{t} + z)}{\Delta x}}{1 + g h_{flow}^{t} * \Delta t n^2 * |q^{(t-\Delta t)}| \left(h_{flow}^{t}\right)^{(10/3)}} \Delta x \quad [2]$$

where, (Q^t) is the flow at time (t) between cells, calculated using a centered difference scheme resolved in the (x) or (y) direction; (h_{ij}) is the water depth at the center of cell (i, j); (h_{flow}) is the depth between cells where flow is possible; (z) is the topographic height in the cell; (n) is the ground friction coefficient; (g) is the acceleration of gravity; (q) is the flow from the previous time step; and (Δt, Δx) is the width of the cell.

The flood flows are discretized into a grid of square cells, thus allowing the model to represent two-dimensional flows on the ground surface. LISFLOOD-FP results (ascii files) can be easily imported into a GIS environment for further analysis. The model had been originally designed to simulate river floods, but, in recent years, has been also successfully used to simulate coastal floods (e.g., Monioudi *et al*., 2018; Le Gal *et al*., 2023).

The DEM of Komi beach used the 'Digital Terrain Model of the LSO25 project' (LSO - Large Scale Orthophotos) of the Hellenic Cadastre, which was constructed using high-resolution aerial photographs (2014-2016). The Cadastre DEM has a resolution of 2 m, which allows capture of both the slopes of the coastal topography and adjacent coastal works with much greater accuracy than the EU-DEM (resolution of 25 m, spacedata.copernicus.eu/documents/20123/121239/GEO1988-CopernicusDEM-RP-001Validation_Report_I3.0.pdf). Application of the model at a local level allows the use of this specific spatial resolution with a very reasonable computational cost. The DEM were processed in QGIS software. The Manning friction coefficient was calculated on the basis of the land uses recorded in the Coastal Zone Land Use/Land Cover (LU/LC) geospatial file of the European Copernicus service (https://land.copernicus.eu/en/products/coastal-zones). Manual corrections were applied, which mainly concerned the more accurate design of the beach boundaries (and coastal works and port facilities). As an additional check, the corrections were also taken into account in the DEM of the area to ensure that there were no significant discrepancies between the land uses and the topography, e.g. the polygon corresponding to the sea was checked to overlap pixels with zero elevation. Then, a value for the Manning coefficient was entered for each land use, using the calculations of Papaioannou *et al*. (2018).

The model was driven by the projected Extreme Sea Levels (ESLs) for Chios under the RCP8.5 climatic scenario for 2050 and 2100 extracted from the EU-JRC (Joint Research Centre) database https://webcritech.jrc.ec.europa.eu/SeaLevelsDb detailed in Vousdoukas *et al*. (2018). ESLs were projected using the numerical hydrodynamic model Delft3D-Flow driven by the wind and atmospheric pressure fields corresponding to the climate conditions

of the RCP4.5 and RCP8.5 scenarios calculated by an ensemble of 8 climate models; model performance was assessed for the period 1980 – 2014 (baseline) driven by wind/atmospheric pressure fields extracted from the ERA – Interim database. The ESLs form the sum of the future long-term relative mean sea level rise (RSLR), the astronomical tide (n_t) and the episodic sea level rise (n_{ce}) due to meteorological tides (storm surge) and the storm wave set-up; the latter, which can be quite significant during an energetic event, is set using a generic approximation of 0.2 Hs, i.e., of the offshore significant wave height projected for the same scenarios.

Results

The ESLSs with return period of 100 years (ESL_{100}) projected for the area were 1.12 m and 1.77 m for 2050 and 2100, respectively. The bathtub model results showed inundation of 70,850 and 128,300 m^2 for 2050 and 2100, respectively, with maximum flood extent more than 220 m and 260 m.

The projections show that a large part of the area will be flooded (Fig. 2), with maximum flood extents of 118 m and 190 m for 2050 and 2100 respectively, The beach itself is projected to be completely inundated, presenting a flood risk to all assets at its immediate backshore. Already from 2050 the flood appears to significantly penetrate inshore at the western beach, affecting assets along and to the west of the stream. By 2100, the flood is projected to reach >100 m to the east and west of the stream affecting considerable infrastructure/assets, while the small fishing port will be completely flooded. Overall, it is clear that due to the low relief and many backshore infrastructures/assets there is a high food risk that can cause serious damages/losses, especially if combined floods (i.e., from land and the sea) are considered, which is a likely occurrence during extreme storms.

Figure 2. Flood extent at Komi beach in 2050 (left) and 2100 (right) under theRCP8.5 scenario. The different colors correspond to the estimated beach width that will be flooded.

Discussion and Conclusions

The results show considerable inundation for Komi beach which is projected to be worse by the 'bathtub' approach. However, the static method is considered to overpredict the flood extent, mainly because it ignores bed friction effects on the flood flow as well as its flood inundation predictions for cells are not hydraulically connected with the rest of the flooded area. Similar discrepancies between the two approaches have been found also in other island beaches (Chatzistratis *et al*., 2024). In general, flood simulations with numerical models appear more appropriate for local scales while on regional assessment the bathtub approach may be used as fine grids for numerical modelling increase substantially the computation cost (Seenath *et al*., 2016). Moreover, LISFLOOD-FP provides outputs of flood characteristics at user defined timesteps, providing significant information for flood risk preparedness.

It should be noted that the coastal flood risk in Komi is likely to be exacerbated by the beach erosion/retreat due to the relative sea level rise (RSLR). Andreadis *et al*. (2021) have estimated that Komi beach retreat due to the RSLR will be 3-9 m and 6-9 m by 2050 and 2100, respectively, even under the moderate RCP4.5 climatic scenario. It is noted that these beach erosion/retreat projections are even more conservative, as they

do not take into account the (cumulative) effects of storm events (which, both observations and modeling suggest, could be significant at Komi beach), or the effects of the diminished land-sourced sediment supply due to the construction of the Kalamoti-Katraris Dam. Therefore, in order to assess the flood risk more accurately, coupled beach erosion/flood models will be required. Although such models present large challenges, particularly due to uncertainties at the land/sea boundary condition, future efforts should be focused on it as a response to the major flood disaster risks under climate change.

Acknowledgements

This work was supported by the Project 'Coastal Environment Observatory and Risk Management in island Regions AEGIS+' (MIS 5047038), implemented within the Operational Programme 'Competitiveness, Entrepreneurship and Innovation' (NSRF 2014-2020), co-financed by the Hellenic Government (Ministry of Development and Investments) and the European Union (European Regional Development Fund).

References

Almar, R., Ranasinghe, R., Bergsma, E.W.J. *et al*., 2021. A global analysis of extreme coastal water levels with implications for potential coastal overtopping. Nat. Commun. 12, 3775. https://doi.org/10.1038/s41467-021-24008-9

Andreadis, O., Chatzipavlis, A., Hasiotis, T., Monioudi, I., *et al*., 2021. Assessment of and Adaptation to Beach Erosion in Islands: An Integrated Approach.. J. Mar. Sci. Eng. 9(8), 859. https://doi.org/10.3390/jmse9080859

Bates, Paul D., De Roo, A.P.J., 2000. A simple raster-based model for flood inundation simulation. J. Hydrology 236, 54-77 https://doi.org/10.1016/S0022-1694(00)00278-X

Bates, P., Dawson, R., Hall, J., *et al*., 2005. Simplified two-dimensional numerical modelling of coastal flooding and example applications. Coast. Eng. 52 (9), 793-810. https://doi.org/10.1016/j.coastaleng.2005.06.001

Brett, R., 2021. How Important Is Coastal Tourism for Island Nations? An Assessment of African and Indian Ocean Islands. J. Coast. Res. 37, 568–575. https://doi.org/10.2112/JCOASTRES-D-20-00011.1

Chatzistratis, D., Monioudi, I., Velegrakis, A.F., Chalazas, Th., Tragou, E., 2024. Exposure to coastal erosion and flooding in the Northeastern Aegean islands, Greece, in Briand F. (Ed.), CIESM Monograph 52, Marine hazards, coastal vulnerability, risk (mis)perceptions – a Mediterranean perspective, CIESM Publisher, Paris, Monaco, 115- 130.

IPCC, 2023. Climate Change 2023: Synthesis Report. Contribution of Working Groups I, II and III to the Sixth Assessment Report of the Intergovernmental Panel on Climate Change, Core Writing Team, Lee, H., Romero, J. (Eds.), IPCC: Geneva, Switzerland.

Le Gal, M., Fernández-Montblanc, T., Duo, E., Montes Perez, J., Cabrita, P., Souto Ceccon, P., Gastal, V., Ciavola, P., Armaroli, C., 2023. A new European coastal flood database for low–medium intensity events. Natural Hazards and Earth System Sciences 23, 3585–3602. https://doi.org/10.5194/nhess-23-3585-2023

Luijendijk, A., Hagenaars, G., Ranasinghe, R. *et al*., 2018. The State of the World's Beaches. Sci. Rep. 8, 6641. https://doi.org/10.1038/s41598-018-24630-6

Monioudi, I.N., Asariotis, R., Becker, A., *et al*., 2018. Climate change impacts on critical international transportation assets of Caribbean Small Island Developing States (SIDS): the case of Jamaica and Saint Lucia. Regional Environmental Change 18, 2211-2225. https://doi.org/10.1007/s10113-018-1360-4

Papaioannou, G., Efstratiadis A., Vasiliades, L., Loukas, A., Papalexiou, S.M., Koukouvinos, A., Tsoukalas, I., Kossieris, P., 2018. An operational method for flood directive implementation in ungauged urban areas. Hydrology 5, 24. https://doi.org/10.3390/hydrology5020024

Seenath, A., Wilson, M., Miller, K., 2016. Hydrodyanmic versus GIS modelling for coastal flood vulnerability assessment: Which is better for guiding coastal management? Ocean & Coastal Management 120, 99-109. https://doi.org/10.1016/j.ocecoaman.2015.11.019

Toimil, A., Losada, I.J., Álvarez-Cuesta, M., Le Cozannet, G., 2023. Demonstrating the Value of Beaches for Adaptation to Future Coastal Flood Risk. Nat. Commun. 14, 3474. https://doi.org/10.1038/s41467-023-39168-z

UNWTO, 2024. International Tourism Highlights. World Tourism Organization: Madrid, Spain, ISBN 978-92-844-2579-2.

Vousdoukas, M.I., Mentaschi, L., Voukouvalas, E., *et al*., 2018. Global probabilistic projections of extreme sea levels show intensification of coastal flood hazard. Nat Commun 9, 2360. https://doi.org/10.1038/s41467-018-04692-w

17th INTERNATIONAL CONGRESS of the Geological Society of Greece

BULLETIN OF THE GEOLOGICAL SOCIETY OF GREECE, SP. PUBL.

EXTENDED ABSTRACT 052

Three Years of Progress in Digital Applications and Monitoring Utilizing 3D Reality Capture Technologies for Landslide Hazard Mitigation, the Case in Evritania, Central Greece

Chatzitheodosiou T.[1], Farmakis I.[2], Papouli D.[1], Stoumpos G.[1], Prountzopoulos G.[3], Marinos V.[1]
(1) National Technical University of Athens, Athens, Greece, chatzitheodosiou@mail.ntua.gr
(2) Sapienza University of Rome, Italy
(3) Independent Geotechnical Engineering Consultant, Greece

Introduction / Background

Rockfall and landslide hazards pose significant challenges for mountainous road networks in Central Greece, particularly in the region of Evritania, which is recognized as one of the most susceptible areas to landslides in Greece (Marinos et al., 2015). In cooperation with the Region of Central Greece, the NTUA Engineering Geology & Geohazards Research Group initiated a targeted research program focusing on several key sites in the region. These areas were selected due to their geological complexity, different mechanisms of failure, challenging terrain, and history of documented landslides. Detailed investigations have been conducted to assess slope stability and analyze the mechanisms contributing to slope instability.

Building on these investigations, this study highlights advancements achieved through the research program over the past three years, focusing on the application of innovative technologies and the development of methodologies for geotechnical analysis and hazard monitoring. By leveraging advanced 3D reality capture technologies, the research integrated high-resolution aerial and terrestrial data to produce precise digital replicas of the investigated areas. These replicas enabled the extraction of critical engineering geological information and supported the development of advanced digital tools for terrain analysis and hazard assessment.

Furthermore, the digital replicas formed the foundation of a comprehensive monitoring program designed and implemented by the research team. When combined with ground-based instrument monitoring (e.g., inclinometers), this program provided a continuous stream of data, enabling regular updates to datasets and significantly improving the accuracy and reliability of detailed 2D geotechnical simulations. These analyses, along with 3D numerical simulations, offered valuable insights into slope behavior, advancing landslide hazard assessment and informing the development of site-specific mitigation measures.

Finally, the study evaluates key limitations encountered during data acquisition, processing, and analysis. These insights are examined in the context of each site, demonstrating how challenges were addressed or remain to be resolved to further enhance hazard assessment and optimize mitigation strategies.

Methodology

The methodological framework for this study builds on the integration of advanced digital tools with systematic monitoring programs, aiming to continuously refine geotechnical analyses and optimize solutions to address landslide and rockfall hazards in mountainous terrains. The workflow, illustrated in **Figure 1** begins with detailed engineering geological investigations, including field and laboratory assessments. These investigations enabled the classification of engineering geological units (EGUs) and the development of preliminary hazard maps, geotechnical models and stability analyses that delineated zones of instability and proposed conceptual mitigation designs.

To enhance the accuracy of the preliminary analyses, high-resolution topographic and geospatial data were acquired through UAV-based photogrammetry (Westoby et al., 2012) and terrestrial laser scanning (TLS). UAV surveys using DJI Phantom 4 Pro RTK and Mavic 3 Enterprise drones generated point clouds, digital surface models (DSMs), and orthomosaics with sub-centimeter accuracy, while TLS LiDAR scanning with the Leica ScanStation P40 provided millimeter-level precision for capturing detailed discontinuity characteristics, such as orientation, spacing, and persistence. These datasets facilitated advanced discontinuity mapping using techniques like Principal Component Analysis (PCA) and DBSCAN clustering (Riquelme et al., 2015; Farmakis et al., 2020), as well as the creation of Slope Relief Models (Chatzitheodosiou et al., 2024) to identify overhangs and undercuts. Semantic segmentation tools further refined the analysis by distinguishing vegetation, bedrock, and infrastructure, optimizing the detection of unstable zones and supporting rockfall trajectory analyses (Chatzitheodosiou et al., 2023).

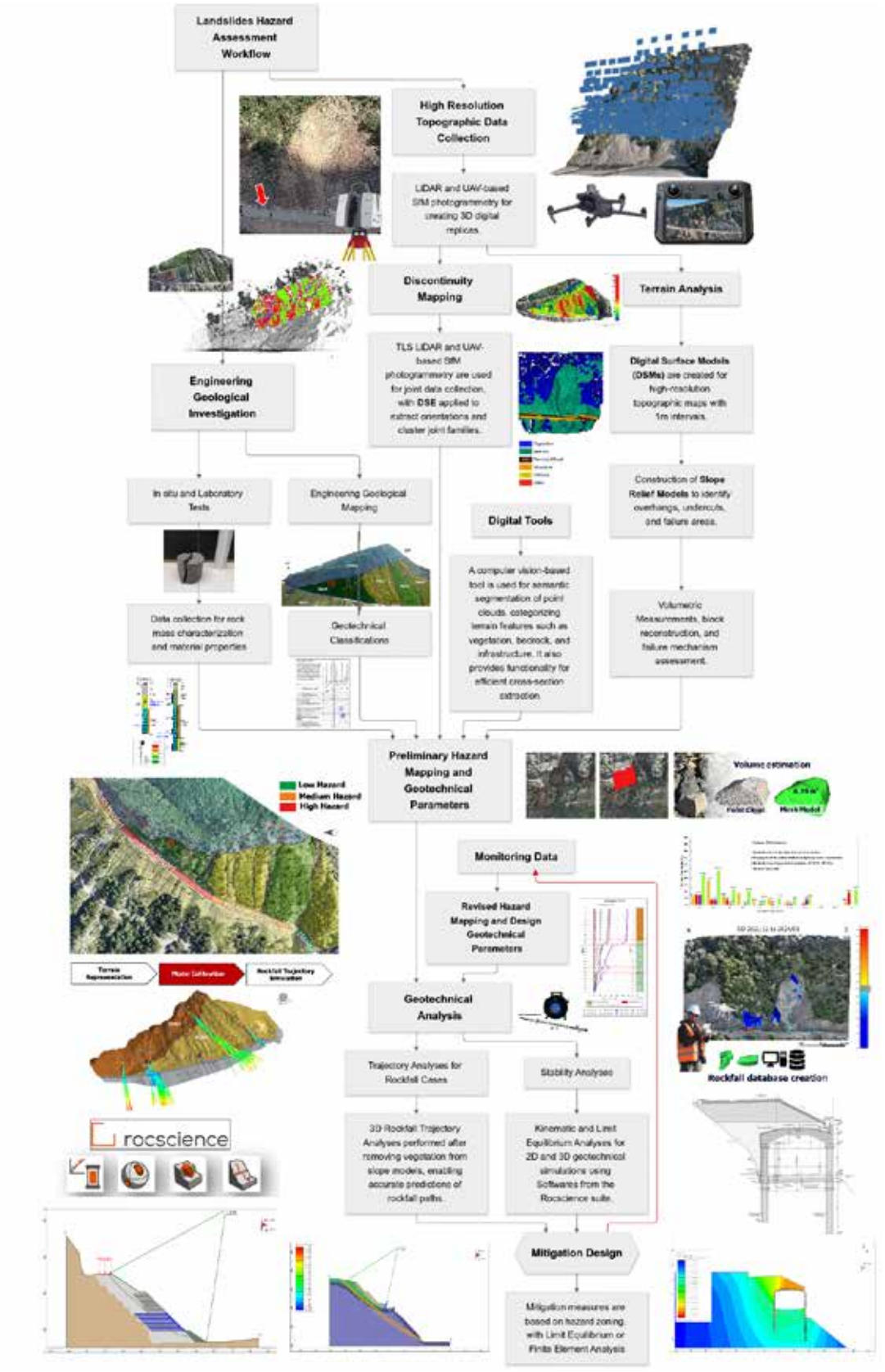

Figure 1. Integrated workflow for Landslide Hazard Assessment.

Monitoring, as illustrated in **Figure 2,** formed a crucial part of the methodology, implemented through a hybrid approach combining UAV surveys (Chatzitheodosiou, 2023) and ground-based instruments. Sequential UAV campaigns produced multi-temporal datasets that were analyzed using the Multiscale Model-to-Model Cloud Comparison (M3C2) algorithm (Lague et al., 2013) to detect and quantify surface deformations and rockfall volumes. Spatial changes were clustered using the Density-Based Spatial Clustering of Applications with Noise (DBSCAN) algorithm (Ester et al., 1996), enabling the identification of discrete events. To enhance volume reconstructions of rockfall events, 3D mesh models were generated using the Iterative Alpha Shape algorithms (Edelsbrunner and Mücke, 1994). Additionally, the VoxFall non-parametric volumetric change detection method (Farmakis et al., 2024) provided an unbiased approach for volumetric rockfall measurements directly between mesh models, cataloging key metrics such as size and location with high accuracy.
Ground-based instruments, such as inclinometers, offered complementary data on subsurface movements, particularly in rotational landslides, where a comparative analysis revealed the attenuation of subsurface displacements near the surface due to material properties and failure plane stratification. The integration of these datasets refined kinematic models and enhanced hazard assessments. Over a three-year period, this dynamic monitoring workflow informed iterative updates to hazard maps and geotechnical models, incorporating stability analyses with kinematic, limit equilibrium, and numerical methods from the Rocscience suite. These analyses, combined with real-time data on rockfall trajectories, guided the design of effective, targeted mitigation measures tailored to the evolving conditions of the study areas.

Results and Conclusions

High-resolution datasets generated through UAV-based photogrammetry and TLS LiDAR enabled the precise identification of critical geohazards, including overhanging rock masses, undercuts, and structurally controlled failure zones in the mountainous terrains of Central Greece. These results underscore the value of combining advanced digital tools with traditional geotechnical methods, providing a robust foundation for hazard mapping, geotechnical modeling, and the classification of engineering geological units (EGUs) with millimeter-level precision. The multitemporal monitoring program provided valuable insights into the dynamic behavior of slopes. The M3C2 change detection algorithm successfully quantified surface deformations and detected rockfall volumes over time. The use of VoxFall for volumetric change detection ensured accurate modeling of these events, minimizing user bias and enhancing the overall reliability of the analysis. The database enabled the team to characterize the frequency, magnitude, and spatial distribution of rockfall events, offering a detailed understanding of hazard zones. For rotational landslides, the comparison between inclinometric data and UAV-based change detection revealed how movement attenuates as it approaches the surface. This attenuation pattern was linked to the geotechnical properties of the subsurface materials and provided critical data for refining stability models and estimating the depth of the failure plane.
Geotechnical analyses, informed by these datasets, identified the predominant failure mechanisms in the study areas. For instance, in structurally controlled limestone slopes, wedge sliding and toppling failures emerged as the dominant modes of instability. Physically based trajectory modeling, calibrated with real-time data, accurately predicted the impact zones of these rockfalls, thereby supporting the design of targeted mitigation measures. Similarly, rotational landslides in weak flysch formations were classified using a modified Geological Strength Index (GSI) tailored for heterogeneous rock masses like flysch (Marinos, 2019) and analyzed in detail, with stability simulations indicating the zones most susceptible to failure and highlighting the effectiveness of potential stabilization interventions. To address the specific challenges at each site, various mitigation measures were proposed to enhance slope stability and safeguard infrastructure. These measures included the installation of rockfall nets and anchored rock bolts to stabilize critical rock masses. Where space constraints limited conventional approaches, reinforced embankments or lane covers were recommended. In areas requiring additional structural support, deep reinforced piles were proposed to provide both lateral and vertical stability by anchoring into stable substrata. Hazard zoning, informed by refined analyses, facilitated proactive planning, while real-time monitoring ensured timely evaluations of the effectiveness of each intervention and allowed for iterative improvements.
Finally, the study addressed several challenges encountered during data collection and processing, such as suboptimal lighting conditions, vegetation interference, and noise in point cloud data. These obstacles were mitigated through adaptive methodologies, including optimized flight paths, advanced clustering algorithms, and rigorous manual validation procedures. Overall, the integration of digital tools with traditional engineering geological and geotechnical approaches has produced significant advances in landslide and rockfall hazard assessment, emphasizing the importance of continuous monitoring, dynamic hazard mapping, and data-driven design proposals for managing geohazards in complex mountainous regions.

Acknowledgements
The authors sincerely thank the Region of Central Greece and the Regional Unit of Evritania for their invaluable support in this research. Their collaboration with the National Technical University of Athens highlights the important role local governments play in advancing scientific efforts to improve infrastructure safety and address geohazards. We are especially grateful for their assistance in facilitating access to key sites, providing logistical support, and contributing to the successful completion of this research.

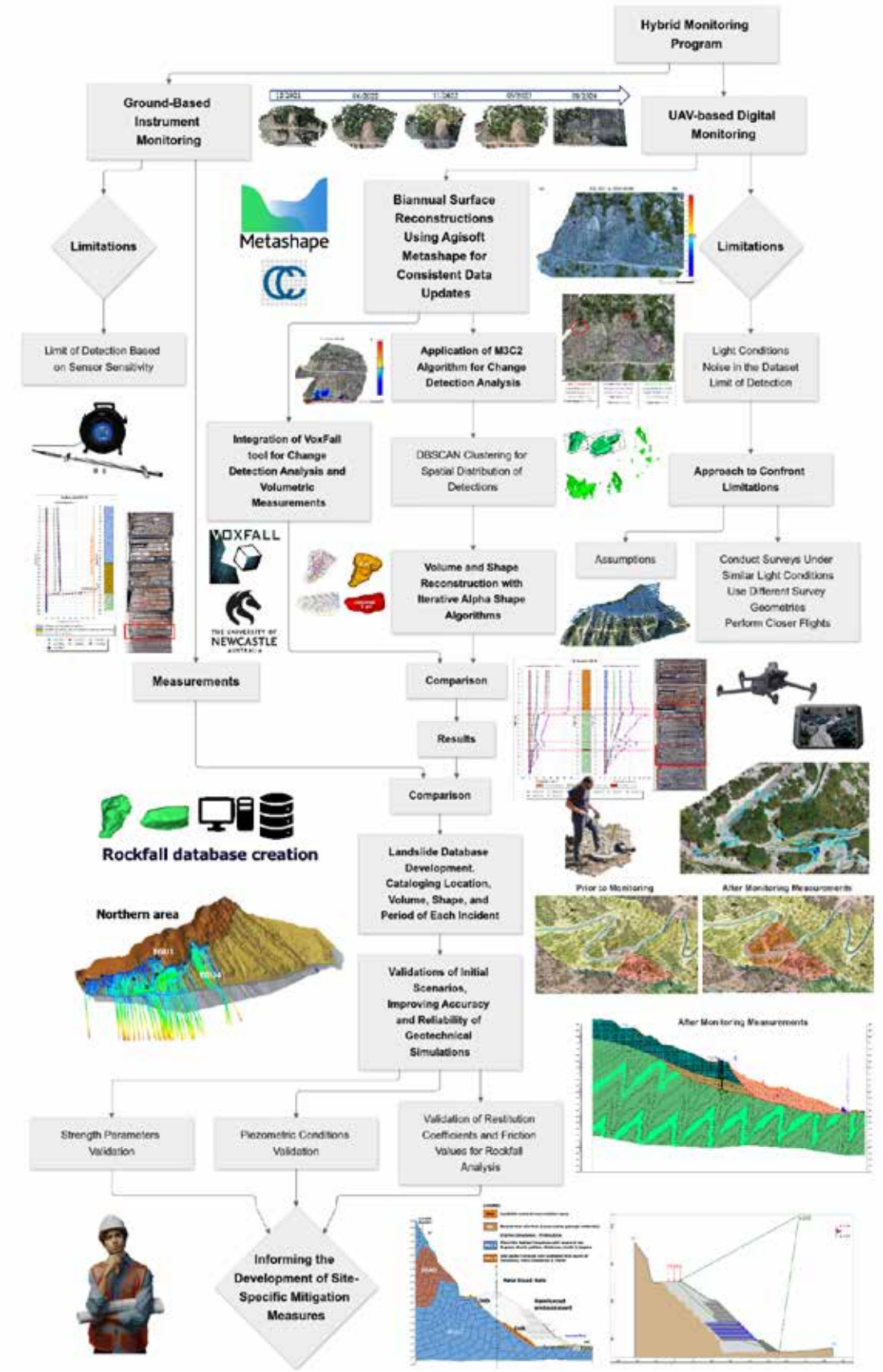

Figure 2. Hybrid monitoring program refining Landslide Hazard Assessment.

References

Chatzitheodosiou, T., Farmakis, I., Prountzopoulos, G., I., Papouli, D., Stoumpos, G., Thomaidis, T., & Marinos, V. (2023). Addressing rockfall challenges in flysch environments – A case study from Greece. In Proceedings of the 6th Regional Symposium on Landslides in the Adriatic-Balkan Region.

Chatzitheodosiou, T. (2023). "One rock at a time" 3D Geology Mini-Series. Available at: https://sketchfab.com/themisto123 [Website]

Chatzitheodosiou, T., Farmakis, I., Papouli, D., Stoumpos, G., & Marinos, V. (2024). SfM photogrammetry for rockfall monitoring and hazard assessment along the Agia Varvara-Agrafa road in Central Greece. 4th European Regional Conference of IAEG – EUROENGEO 2024.

Edelsbrunner, H., & Mücke, E. P., 1994. Three-dimensional alpha shapes. ACM Transactions on Graphics (TOG), 13(1), 43–72.

Ester, M., Kriegel, H. P., Sander, J., & Xu, X., 1996. A density-based algorithm for discovering clusters in large spatial databases with noise. In Proceedings of the 2nd International Conference on Knowledge Discovery and Data Mining (KDD-96), Portland, Oregon, 226–231.

Farmakis, I., Marinos, V., Papathanassiou, G., et al., 2020. Automated 3D jointed rock mass structural analysis and characterization using LiDAR terrestrial laser scanner for rockfall susceptibility assessment. Geotechnical and Geological Engineering, 38(3), 3007–3024.

Farmakis, I., Guccione, D. E., Thoeni, K., & Giacomini, A., 2024. VoxFall: Non-parametric volumetric change detection for rockfalls. Preprint submitted to Elsevier.

Lague, D., Brodu, N., & Leroux, J., 2013. Accurate 3D comparison of complex topography with terrestrial laser scanner: Application to the Rangitikei Canyon (New Zealand). ISPRS Journal of Photogrammetry and Remote Sensing, 82, 10–26. **[Journal Article]**

Marinos, V.; Papathanassiou, G.; Vougiouka, E.; Karantanellis, E., 2015. Towards the Evaluation of Landslide Hazard in the Mountainous Area of Evritania, Central Greece. In: Engineering Geology for Society and Territory, Lollino et al. (eds.), Published by Springer – Volume 2, pp. 989–993.

Marinos, V., 2019. A revised, geotechnical classification GSI system for tectonically disturbed heterogeneous rock masses, such as flysch. Bulletin of Engineering Geology and the Environment, 78(2), 899–912.

Riquelme, A., Abellán, A., & Tomás, R. (2015). Discontinuity spacing analysis in rock masses using 3D point clouds. Engineering Geology, 195, 10.1016/j.enggeo.2015.06.009.

Westoby, M. J., Brasington, J., Glasser, N. F., Hambrey, M. J., & Reynolds, J. M., 2012. Structure-from-Motion photogrammetry: A low-cost, effective tool for geoscience applications. Geomorphology, 179, 300–314.

17th INTERNATIONAL CONGRESS of the Geological Society of Greece

BULLETIN OF THE GEOLOGICAL SOCIETY OF GREECE, SP. PUBL.

EXTENDED ABSTRACT 053

Mapping and Categorization of damage on the built and natural environment caused by the 2023 Daniel and Elias storms in MountPelion, Greece

Eleftheria Christodoulopoulou[1], Olga-Joan Ktenidou[2], Grigorios Tsinidis[3]
1 University of the Aegean, Mytilene, Greece, christodoulopoulouleftheria@gmail.com
2 Institute of Geodynamics, National Observatory of Athens, Athens, Greece
3 University of Thessaly, Volos, Greece

Introduction and motivation

Storms Daniel and Elias occurred in September 2023 with only a 20-day gap between them and left a severe impact on the affected areas, since their aftermath is still clearly visible to date, 16 months later. The meteorological station in Zagora at Mount Pelion recorded the highest daily rainfall value in the country (around 760 mm) during Daniel storm, breaking the previous record of Paliki, Kefalonia (645 mm) recorded during the mediterranean cyclone Ianos in 2020 (Ντάφης κ.ά., 2023; Βουγιούκας κ.ά., 2023). Figure 1 shows the total amount of rainfall (in mm) for September over a period of ten years, as recorded by three different meteorological stations in the vicinity, namely Volos, Zagora and Makrinitsa (see Figure 4 for station locations). Studies exist already analysing the effects of these storms on various aspects of the community and ecosystem; e.g., Dimoudi *et al*. (2024) performed analyses to examine the effect on water quality, He *et al*. (2024) used SAR technologies to map effects on crops and livestock, while Mavroulis *et al*. (2024) highlighted all the risk factors that favor the occurrence of infectious diseases. Here, we consider effects on the built environment and infrastructures through in-situ visits.

In this study we focus on the types of damage that these storms caused in the Pelion region. Through photographic documentation the damage was categorized into six key categories referring to: loss of life, damage to the road network, damage to bridges and other structural elements, soil erosion, debris accumulation, and property loss. These findings provide valuable insights into the diverse and severe impacts of storms and their effects on communities and the environment. We aim to showcase the extent of this destruction caused to the villages and communities of Pelion and provide a comparison between Pelion's three municipalities and the types of damage each one suffered. We also point to the degree to which reparation actions have progressed at the time of writing this abstract, which is 16 months after the incident.

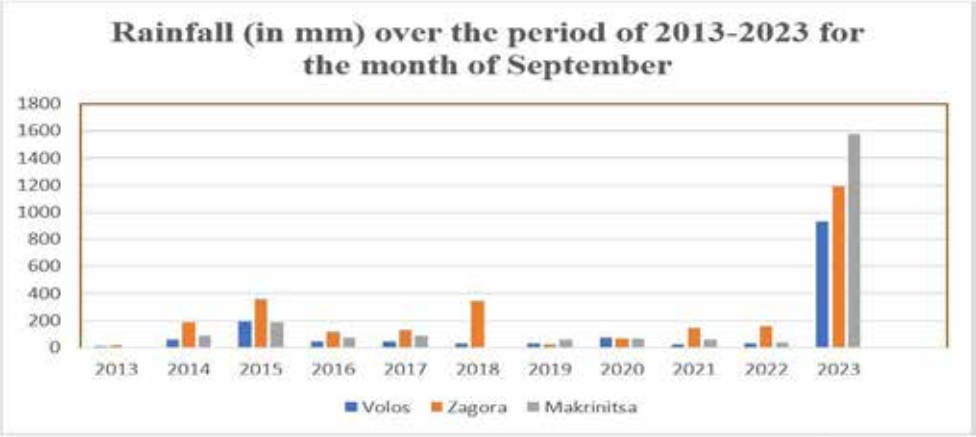

Figure 1. Rainfall of the study area over a ten-year period for the month of September (data from: https://meteo.gr/climatic.cfm)

Method and data collection

In total, seven routes were arranged based on news reports of extensive damage in the region. Data was collected on site through geotagged photographs. A total of 554 photographs were taken, of which 137 were included in the study's detailed analysis. ArcGIS Pro software was used in order to create a map that visualizes the relation between the seven survey routes and the location of damages recorded during field visits. Then, damages were sorted and categorised depending on their content alone, i.e., disregarding their coordinates. Lastly, another map was created to feature the relation between the spatial distribution of damage depending on their type and municipality.

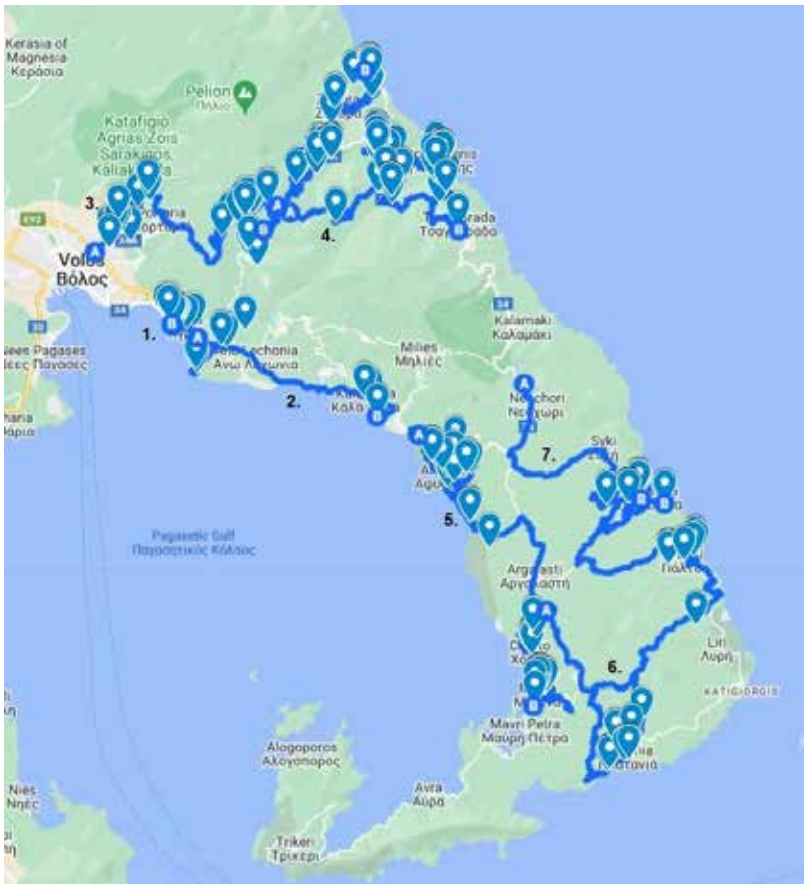

Figure 2. The seven routes that were followed in relation to all damages recorded

Results

Every photograph had georeference through its coordinates, as is standard practice for all post-disaster reconnaissance activities in order for photographs taken in the field to be acceptable for use in the desk analysis. This rendered it possible to visualise all damages and map locations where they were concentrated (Figure 2). After studying the available data, these were categorized into six groups according to the type of damage they were depicting. The groups were formed as shown below:

- Loss of Life: Four fatalities were recorded in the Pelion region alone during Storm Daniel.
- Road Networks: Significant damage was observed, especially near streams and water bodies. Roads were washed away or severely eroded due to the discharge and the high speed of water flow.
- Bridges and Infrastructure: Bridges collapsed or were rendered unsafe, as their structural foundations were compromised. Key access routes were severed. The damage was mainly attributed to scouring phenomena at the approaching embankments of the bridges.
- Property Loss: Houses, vehicles and businesses suffered extensive damage, particularly in areas close to riverbeds.
- Soil Erosion: Landslides and mudflows led to large volumes of soil being moved, exacerbating the damage.
- Debris Deposition: Tree trunks, stones, and other debris clogged waterways, damaged vehicles, and destroyed public spaces.

Figure 3 shows some of the damages recorded, namely: road network destruction in Kala Nera, structural damage of a bridge in Horto, debris deposition on a playground in Agios Onoufrios, extensive damages to a house in Platanias and lastly a large volume of soil that was moved due to a landslide in between Chania and Drakia village. Finally, it was deemed necessary for this study, to create a map where all groups of damages were shown in relation to municipalities (Figure 4), since each one differs from the other regarding environmental conditions (vegetation, gradient).

Figure 3. Different types of damages recorded on site during field visits

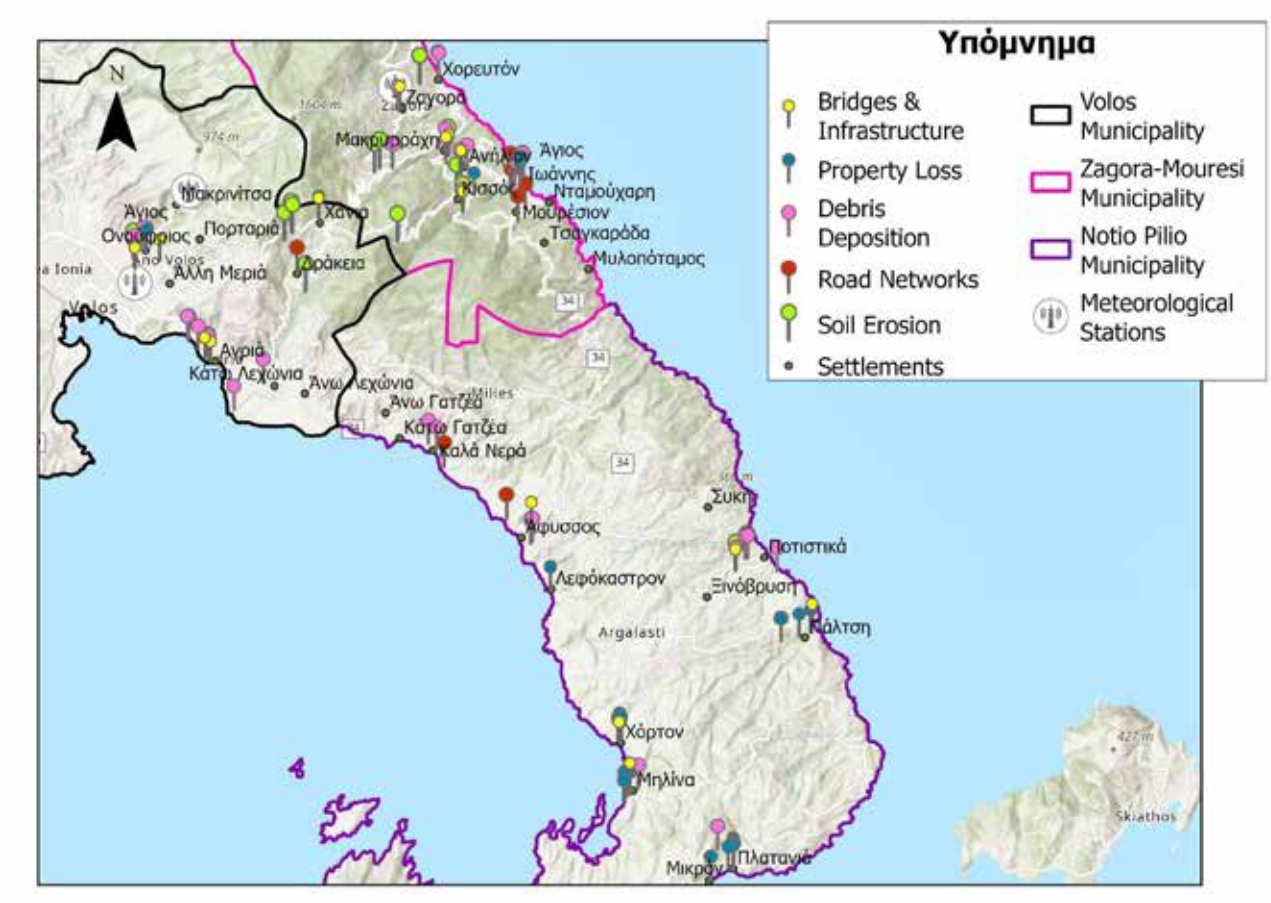

Figure 4. Distribution of types of damages in relation to each municipality of the study area

Conclusions

Proximity of infrastructure and settlements to water bodies played a crucial role in the severity and extensiveness of the damages recorded. Four people lost their lives in Pelion region alone, due to the violent water flow of the torrents. Huge amounts of soil were removed, especially from locations with great inclination (mostly in municipality of Zagora – Mouresi, followed by Volos municipality), and were carried away violently by the water, finally redepositing within riverbeds, private houses, public spaces and the sea. Bridges were washed away or severely damaged, roads were eroded and some settlements were cut off for a few days because of it. These findings highlight the need for improved urban planning and infrastructure resilience in flood-prone areas, but also updated, well-known to all residents evacuation plans. Recovery efforts, one year after these events, indicate slow progress in rebuilding and rehabilitation. In most cases temporary rehabilitation measures have been applied. This study underscores the importance of better disaster management practices, followed by everyone involved, in order to mitigate future risks.

References

Dimoudi, A., Voulgaris, K., Varkoulis, A., Georgiou, K., (2024). The impacts of "DANIEL" and "ELIAS" storms on water quality of Pagasitikos Gulf – a first record. Available at: https://www.researchgate.net/publication/382220692

He, K., Yang Q., Shen, X., Dimitriou, E., Mentzafou, A., Papadaki, C., Stoumboudi, M., Anagnostou, E.N., (2023). 'Brief communication: Storm Daniel Flood Impact in Greece 2023: Mapping Crop and Livestock Exposure from SAR'. Available at: https://doi.org/10.5194/nhess-2023-173.

Mavroulis, S., Mavrouli, M., Lekkas, E., Tsakris, A. Impact of the September 2023 Storm Daniel and Subsequent Flooding in Thessaly (Greece) on the Natural and Built Environment and on Infectious Disease Emergence. Environments 2024, 11, 163. https://doi.org/10.3390/environments11080163

Hewson, T., Ashoor, A., Boussetta, S., Emanuel, K., Lagouvardos, K., Lavers, D., Magnusson, L., Pillosu, F., Zsoter, E., (2024). Medicane Daniel: an extraordinary cyclone with devastating impacts. Available at: https://www.ecmwf.int/en/newsletter/179/earth-system-science/medicane-daniel-extraordinary-cyclone-devastating-impacts

Βουγιούκας, Στρ., Κωλέτσης, Ι., Λαγουβάρδος, Κ., (2023). Αποτίμηση της κακοκαιρίας DANIEL, μέρος 1ο: Ξεπέρασε κατά πολύ τα ύψη βροχόπτωσης του Μεσογειακού Κυκλώνα ΙΑΝΟΥ του 2020. https://meteo.gr/article_view.cfm?entryID=2923

Ντάφης, Σ., Κύρος, Γ., Λαγουβάρδος, Κ. (2023). Κακοκαιρία Daniel: Καταρρίφθηκε το ρεκόρ ημερήσιου ύψους βροχής στη χώρα μας. https://www.meteo.gr/article_view.cfm?entryID=2913

BULLETIN OF THE GEOLOGICAL SOCIETY OF GREECE, SP. PUBL.

EXTENDED ABSTRACT 054

ERBE SYMPOSIUM 2027– LAVRION GREECE: Honouring the Values of Geo-Mining Heritage

Demetrios C. Constantinides, RNDr.
Exploration Geologist, Nicosia, Cyprus, email: dimkon46@gmail.com

Introduction

The word Symposium is very understandable to the Greeks, since their ancestors had started organising these events already in the 7th century BC. At such gatherings, the more experienced members of the community were expected to impart practical guidance to younger generations. This mentorship helped maintain the steadiness of certain cultural traditions. A symposium usually took place in a men's dining room of a nobleman. The room was called "andron" and was specially designed for such meetings, with couches placed around the perimeter for guests to lie down, while they while they were eating and drinking (Fig. 1).

Fig. 1: Relief depicting a scene from a symposium in ancient Greece[1]

The ERBE Symposium

An ERBE Symposium has a strong element in common with the ancient Greek symposia: it aims to bring out the cultural heritage of those "who crawl like worms in the earth, denying the sun and the air", as the Cypriot poet Costas Montis describes the miners in one of his poems.

ERBE is a German word that means heritage. The International "ERBE" Symposium, exploring the cultural heritage of geology, mining and metallurgy, has a tradition that goes back more than three decades, since the first one was organised in Freiberg of Germany in 1993. Since then, the Symposium has been organised 15 more times to return to Freiberg in 2023. So far, it has been held in the following cities and countries:

Freiberg/Saxony – Germany (1993)
Leoben – Austria (1995)
St. Petersburg – Russia (1997)
Banská Štiavnica – Slovakia (1999)
Golden/Colorado – USA (2000)
Idrija – Slovenia (2002)
Leiden – The Netherlands (2003)
Schwaz – Austria (2005)
Quebec-City – Canada (2007)
Freiberg/Saxony – Germany (2009)
Real del Monte – Mexiko (2011)
Bozen/Bolzano – Italy (2013)
Banská Štiavnica – Slovakia (2015)
Ravne na Koroskem – Slovenia (2018)
Eggenburg – Austria (2021)
Freiberg/Saxony – Germany (2023)

The next city to host the Symposium will be again Ravne na Koroskem on 22nd – 27th September 2025. Here are some scenes from previous symposia (Fig. 2-6). The source of figures 2 to 6 is https://photos.erbe-symposium.org/index.php?/categories.

Fig. 2: Participants of the last ERBE Symposium in Freiberg during a city sightseeing tour.

Fig. 3: The building of the Old Castle in Banská Štiavnica, the venue of the 13th ERBE Symposium.

Fig. 4-5: Children's performance and miner's choir at the 13th ERBE Symposium.

Fig.6: An old mining locomotive that was exhibited at the ERBE Symposium in Quebec (2007).

For those interested in enjoying thousands of images from all the sixteen symposia, a visit to the website of the ERBE Association is recommended[2].

The Main Goals of an ERBE Symposium

The main objective of an ERBE Symposium is to exhibit the cultural heritage in Geosciences, Mining and Metallurgy. However, each symposium tried to highlight more specific cultural characteristics relating to the local mining tradition. For example, the last Symposium held in Freiberg, focused on libraries, archives and museums associated with historic mining industry. The Principles of the Cultural Heritage of Geosciences, Mining, Metallurgy and Archaeology have been established some time ago[3].

The aim of both international and national commissions of the Symposia is to make available the entire human cultural heritage relating to the earth's crust, including geo-memorials. The committees are made up of personalities who promote and develop the values and the heritage of mining culture.

We could go on presenting the objectives of the Symposia held to date. However, this is not the subject of this paper. What really needs to be highlighted here is the decision of a small group of people to take over the 2027 Symposium that we would like to organise in Lavrion.

Our Initiative

The author of this paper has joined the 13th ERBE Symposium in Banská Štiavnica, where he lived for about 10 years. It is a town of 16,000 inhabitants whose economy is heavily dependent on the tourism generated by its mining heritage.

The idea of applying for one of the next ERBE Symposia, which could be organised by the Lavreotiki Geopark and

the Committee of Geological-Geomorphological Heritage of the Greek Geological Society, was strengthened in our minds after the inclusion of the Lavrion area in the UNESCO Geoparks Group. Nevertheless, the maintenance of a Geopark on this List and its potential inscription on the UNESCO World Heritage Register, will require a great deal of effort. That is why we believe that, apart from the fact that we will be able to present the history, incredible monuments and natural beauty of Lavrion so broadly, the organisation of such a symposium would help us to gain international supporters for the inclusion of the area in the UNESCO World Heritage List.

Why Lavrion?

The beginning of mining and metallurgy in Lavreotiki is placed in the 5th millennium BC. In particular, the inhabitants of Velatouri hill are thought to have been there since the Middle Neolithic, around 4500 BC. At the foot of the hill was the oldest theatre in ancient Greece, that of Thorikos (Fig. 7).

Fig. 7: Thorikon theatre and an ore washing plant.

Next to the amphitheatre is the entrance to the adit where the Ag-Pb ores were mined (Fig. 8). Photo @Richard Kaňa

Fig. 8: The entrance of a mining adit. Photo @Richard Kaňa

The most important technological achievement of this period was mining and metallurgical processing. The archaeological remains of these activities can be found and visited in Souriza (Fig. 9).

Fig. 9: Ruins of the water management system at Souriza. Photo @Richard Kaňa

Not to be missed

Apart from being famous for the exploitation of silver and funding the famous projects of the "Golden Age of Pericles", as well as the fleet of the Naval Battle of Salamis, this mining area contains more minerals than any other region of the Earth, making it also a unique site of mineral heritage.

According to the Mindat Organisation 805 mineral species and varietal names are listed in the abandoned mines of Lavreotiki district[4], whilst it is the type-locality for 23 of them.

Fig. 10: Minerals from Hercules Katsaros collection. Photo @H. Katsaros

Circulars, Sessions and Tours

As soon as our proposal to hold the ERBE Symposium in Greece is officially accepted, the Organising and Scientific Committee of the Symposium will be set up so that the sessions of the Symposium can be decided and the first Circular Letter can be sent out. Of course, the Symposium will include excursions to geological and mining monuments of Lavrion and the surrounding archaeological sites (Sounion and the Temple of Poseidon, the ancient marble quarry at Agrileza and others).

Obviously, the programme will include a full-day trip to Athens including a visit to Acropolis and its modern museum, as well as a lunch in Plaka. Perhaps some delegates who have the time could be offered more distant excursions, e.g., to Serifos and/or Milos.

The Venue

The proposed venue is an important part of the cultural heritage of Lavrion. The buildings are located within the Lavrion Technological and Cultural Park, which was established in 1992 on the site of the former French Mining Company of Lavrion, on the initiative of the National Technical University of Athens. The premises are of high aesthetic and architectural value (Figs. 11), although most of them were built between 1875 and 1940. They include the processing facilities, as well as administrative and other buildings. The site was the location of the company's operations until 1988.

Fig. 11: Historical buildings of the French Mining Company of Lavrion. Photos: @H. Katsaros

The proposed emblem for ERBE Lavrion Symposium

The concept of the ERBE Symposia banner was established at the Freiberg Conference in 1993. With three exceptions, the rest of the countries respected the original emblem by adding only the city and date of the event. It is for this reason that we are proposing the following emblem for the ERBE Symposium to be held in Lavrion in September 2027 (Fig. 12). The exact dates will be added to the logo once they have been finalised in consultation with the International Committee.

Fig. 12: The proposed emblem for the 2027 ERBE Symposium in Lavrion.

What are we looking forward to?

What are we looking forward to?

As the promoters of this initiative, we expect the following:

- The acceptance by the international geological and mining ERBE community of our proposal to hold the 2027 Symposium in Lavrion.
- Effective cooperation between the organising bodies of the Symposium to ensure its success. And above all, to properly promote the cultural heritage of the geological and mining Lavreotiki.
- The General Directorate of Mineral Resources of the Greek Ministry of Environment and Energy to support the efforts of the organisers in an un-bureaucratic way.
- The Greek Geological Society, the Union of Greek Geologists, the Technical Chamber of Greece, the Association of Mining Enterprises, the Eastern Attica Region, the National Technical University of Athens and other relevant bodies to support this initiative.

If all goes well, we believe that Lavrion and its Geopark will not only establish its reputation as one of the world's most Historical Mining Centres and become better known around the world, but also raise the bar for a place on the UNESCO World Heritage List.

(Endnotes)

1 National Geographic.
2 https://photos.erbe-symposium.org/index.php?/categories
3 https://www.erbe-symposium.org/executive-board-committee/cultural-heritage-principles/
4 https://www.mindat.org/search.php?search=Lavrion

17th INTERNATIONAL CONGRESS of the Geological Society of Greece

BULLETIN OF THE GEOLOGICAL SOCIETY OF GREECE, SP. PUBL.

EXTENDED ABSTRACT 055

The Geoheritage of the "Atlantic Geopark" Project (Central Portugal) at a Glance

Custódio, S.C.[1], Henriques, M.H.[2], Sá, A.A.[3]

(1) Geosciences Center, Department of Earth Sciences, University of Coimbra, Rua Sílvio Lima s/n, 3030-070 Coimbra, Portugal; scmcustodio@student.uc.pt

(2) Geosciences Center, Department of Earth Sciences, University of Coimbra, Rua Sílvio Lima s/n, 3030-070 Coimbra, Portugal

(3) Department of Geology and Pole of the Geosciences Center, University of Trás-os-Montes e Alto Douro, Quinta de Prados, 5000-801 Vila Real, Portugal

Introduction

The history of the Proto-Atlantic and the opening up of the Atlantic are particularly well expressed on the Western Iberian Margin (WIM) and are of interest to many geosciences' experts and curiosity to many citizens. The expressiveness of the last 600 million years of the WIM's geological history is particularly eloquent in a territory that covers an east-west strip of the Beira Litoral (Central Portugal), comprising the municipalities of Figueira da Foz, Mira, Cantanhede, Mealhada, Montemor-o-Velho and Penacova (Fig. 1).

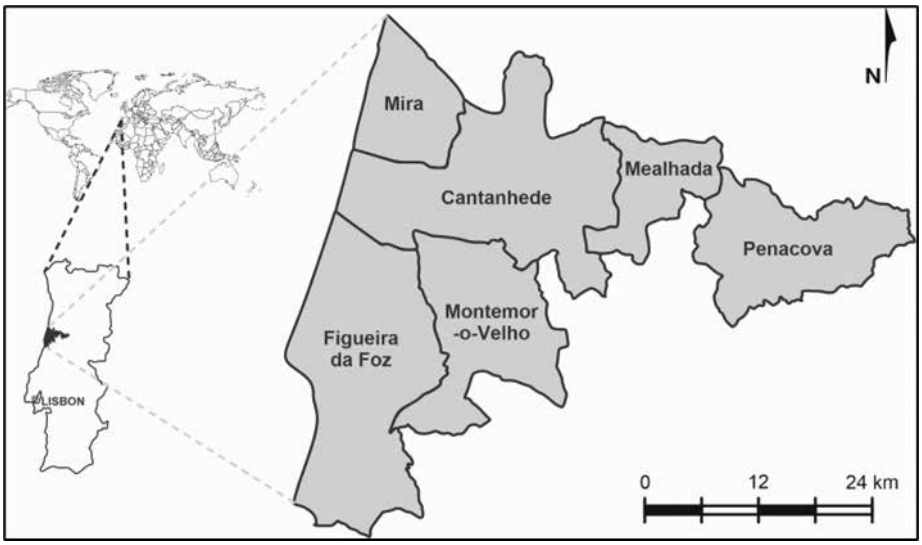

Figure 1: Location map of the "Atlantic Geopark" territory.

The "Atlantic Geopark" Project consists of inventorying and evaluating the geological heritage of those six municipalities, with a view to its conservation, valuation and monitoring for a future application to the Global Geoparks Network (GGN). The results obtained will provide technical support for the application dossier, that has to also include a sustainable management plan for the territory aiming at fostering socio-economic development, conserving the geological heritage and inspirating its replication in similar transatlantic territories.

Conceptual framework

This research assumes that the Earth's natural heritage includes two components - abiotic and biotic - which must be preserved namely through local, regional and national actions/organizations, as well as supranational ones, of which the current UNESCO programs are an example (e.g., Man and the Biosphere Program (since 1971); Convention for the Protection of the World Cultural and Natural Heritage (since 1972) and the International Geosciences and Geoparks Program (since 2015)).

The abiotic component of nature is reflected in its geodiversity, which can be defined as the variety of geological characteristics/features that can be identified in a given territory and taking into account their frequency and distribution, as well as their expressiveness as a reflection of the geological evolution of that territory. When they have scientific, educational and tourist value, such geological sites and elements take on heritage value and are part of the Earth's geological heritage (Carcavilla *et al.*, 2007; Brilha, 2016).

Geoconservation is a geological science that, based on the geodiversity of any territory and/or geological element

(e.g., fossils, rocks and minerals), seeks to safeguard the Earth's geological heritage through specific methods and techniques of inventorying, evaluating, conserving, valuation and monitoring (Henriques *et al*., 2011). From this need emerged the concept of geopark, whose historical foundations date back to the Digne Convention (1991), where an international declaration to protect the geological heritage as a legacy for future generations was approved (IDRME, 1995).

UNESCO defines a geopark as a single, unified area, where sites and landscapes of international geological importance are managed in a holistic concept of protection, education and sustainable development (UNESCO, 2024). UNESCO's link with geoparks officially began in 2004. However, numerous previous initiatives, such as the creation of the European Geoparks Network in 2000, contributed to UNESCO's commitment to the dynamics of geoparks. In 2015, UNESCO enshrined the UNESCO Global Geopark concept within the framework of the new International Geosciences and Geoparks Programme (Henriques & Brilha, 2017).

In 2024, Portugal has six UNESCO Global Geoparks - Azores, Arouca, Estrela, Naturtejo, Terras de Cavaleiros and Oeste (CNU, 2024) – and two Aspirants - Litoral de Viana do Castelo and Algarvensis. The "Atlantic Geopark", which is still in the design phase, emerged from the willingness of six municipalities located in Central Portugal (Cantanhede, Mealhada, Mira, Montemor-o-Velho, Figueira da Foz and Penacova) to apply for their territory to become a UNESCO Global Geopark. To this end, it is necessary to inventory, assess, conserve, valuate and monitor the geological heritage of its territory with a view to incorporating it into the application file for the GGN. This is the main goal of this project which have already produced some relevant results.

First results

The geodiversity of this area, which comprises a strip that crosses Portugal in an approximately east-west direction, allows us to recognize the main episodes in the geological history of the WIM over the last 600 million years (Fig. 2). This is supported by a set of sites of geological interest that illustrate the main episodes related to the opening and closing of the Rheic Ocean, the fragmentation of Pangea, the opening of the North Atlantic Ocean and the Quaternary geodynamics of the North Atlantic Ocean (Custódio *et al.,* 2024; Table 1).

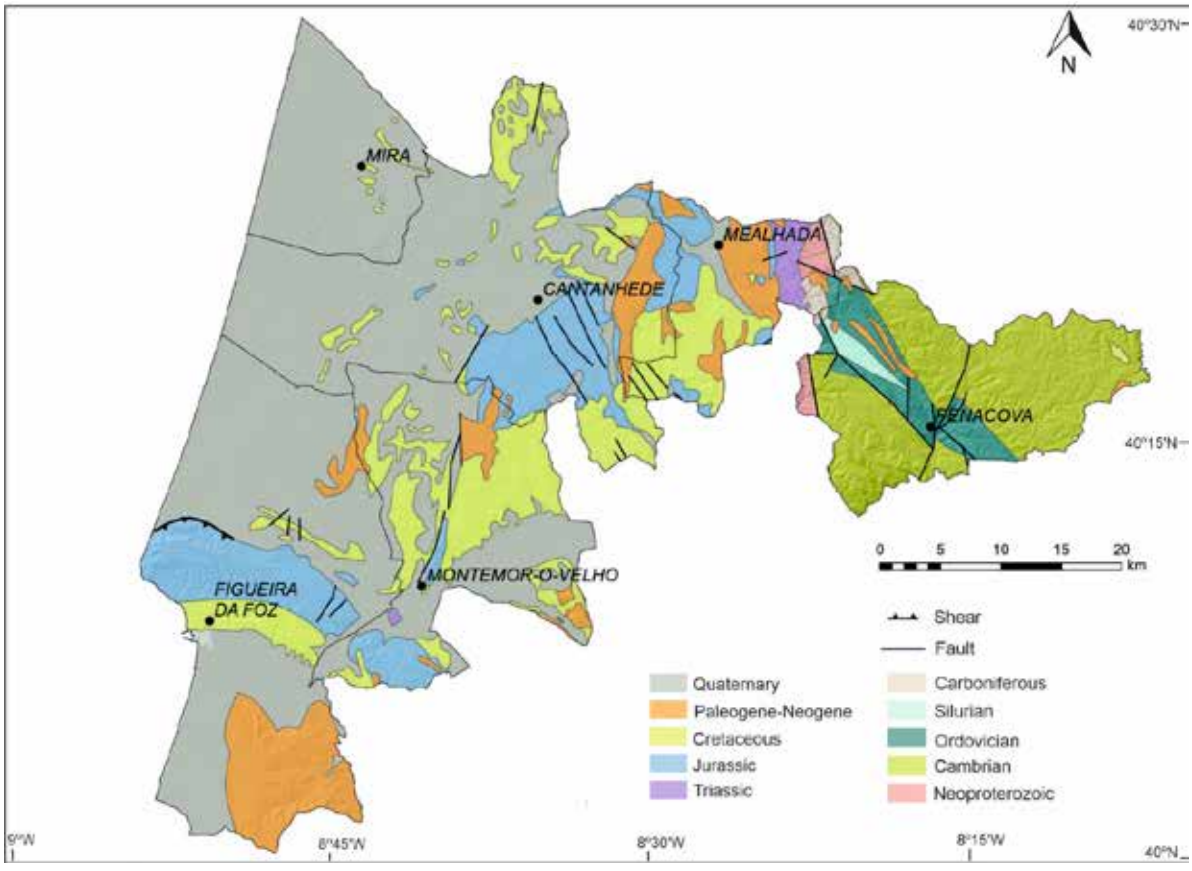

Figure 2: Geological map of the study area. It covers materials from the Neoproterozoic (600 Ma) to the Cenozoic (Vaz *et al*., 2023).

The first geological framework in the study area is the Beiras Supergroup (635 Ma), that represents the oldest record in the study area, outcropping in Penacova Municipality (Fig. 3A). This record is associated with the evolution of a volcanic arc (Cadamian Orogeny; 650-550 Ma) on the margin of the Gondwana continent. It was later inverted by the beginning of the Variscan Cycle (Cambrian—Ordovician; 495–485 Ma), and another deformation episode which is related to the closing of the Rheic Ocean and the Pangea assembly.
The geological record of the Buçaco Synclinal (Lower Ordovician - Silurian; 485-423 Ma) was deposited in a passive margin context of the Rhein Ocean, and it outcrops in Penacova and Mealhada Municipalities (Fig. 3B). In Mealhada Municipality it also crops out the east sector of the Buçaco Carboniferous Basin (Early Ghzelian - 303 Ma), whose units were deposited in a continental basin context located between the Variscan mountains (Fig. 3C).
The next geological framework is represented by the Silves Group (Upper Triassic; Mealhada Municipality a siliciclastic unit that can attest to the central position that Iberia occupied in Pangea just before the opening of the North Atlantic Ocean, marking the break-up of that supercontinent (Fig. 3D).
The Jurassic Carbonate platform of the Proto-Atlantic is well represented in Cantanhede and in Figueira da Foz Municipalities (Figs. 3E and 3F). The reference section of Cabo Mondego (Figueira da Foz) includes the GSSP for Bajocian (170 Ma) and the ASSP for the Bathonian (168 Ma), which represents geoheritage of global relevance. The same section provides a continuous record from the Middle Jurassic fossiliferous marly limestones interpreted as a sag episode of the first rift to the syn-rift episode of the Late Jurassic second rift.
The transition to a passive margin is represented by the next geological framework of the “Atlantic Geopark”, the Carbonate Platform of the Atlantic (Cenomanian—Turonian, 100–93 Ma), which is also well recorded in Figueira da Foz, and in Montemor-o-Velho Municipalities (Fig. 3H).
The Quaternary geodynamics of the Atlantic Margin is well represented throughout the territory, with extensive superficial deposits that cover most of the littoral, dated from the Pleistocene to the Holocene (Fig. 3I).

Table 1. The geological frameworks of the “Atlantic Geopark” and its representative geological site.

Geological framework	Episode	Geological site	Relevance	Municipality
Beiras Supergroup (Neoproterozoic)	Opening of the Rheic Ocean	Aguieira Dam (40°20’24.5”N 8°11’54.6”W)	Regional	Penacova
Buçaco Synclinal (Ordovician - Silurian)	Evolution of the Passive Margin	Livraria do Mondego (40°17’00.9”N 8°15’58.0”W)	Nacional	Penacova
Buçaco Carboniferous Basin (Carboniferous)	Closing of the Rheic Ocean	Santa Cristina Fountain (40°20’55.2”N 8°23’02.8”W)	Regional	Mealhada
Silves Group (Triassic)	Fragmentation of Pangea	Vacariça (40°20’53.6”N 8°23’23.0”W)	Local	Mealhada
Carbonate platform of the Proto-Atlantic (Jurassic)	Opening of the North Atlantic Ocean	Cabo Mondego (40°10’48.4”N 8°54’20.7”W); Ançã limestone (40°17’17.6”N 8°32’22.5”W)	Global	Figueira da Foz; Cantanhede
Carbonate Platform of the Atlantic (Cretaceous)	Marine transgression of the North Atlantic Ocean	Nossa Sra. dos Olivais Chapel (40°14’12.4”N 8°35’20.3”W)	Regional	Montemor-o-Velho
Quaternary Dunes	Quaternary geodynamics of the Atlantic Margin	Barrinha de Mira (Ria de Aveiro; 40°27’05.5”N 8°47’53.3”W)	Local	Mira

Figure 3: The representative geological site of each geological framework recorded at the "Atlantic Geopark". A) Aguieira Dam (Penacova); B) Livraria do Mondego (Penacova); C) Santa Cristina Fountain (Mealhada); D) Vacariça (Mealhada); E) Ançã (Cantanhede); F) Cabo Mondego (Figueira da Foz); G) Nossa Sra. dos Olivais Chapel (Montemor-o-Velho); H) Barrinha de Mira (Mira).

These preliminary results have been reported in several scientific forums, and as geoeducative and geoturistic products (Fig. 4). A promotional video was produced in 2021 by AD ELO, the organization in charge of implementing the future application to GGN (https://youtu.be/NFVJGIL4PX8?si=vPztmIP6BM6vRuMT). The most emblematic geological sites for each municipality were described in detail by Custódio *et al*. (2024). They feature the Oceans Route, a set of outcrops that make it possible to reconstruct the geological history of two oceans—Rheic and Atlantic. Other geo-itineraries (the water route, the stone route and the beach route) were created and are available online (AD ELO, 2024) and as a book in the region's tourist offices (Vaz *et al*., 2024). Other initiatives promoted by municipal authorities regarding the conservation and valuation of local geoheritage resources include the recent designation of the Ançã Limestone as Global Heritage Stone (David Lista *et al*., 2024) and the classification of Livraria do Mondego (in the Buçaco Syncline) as Local Natural Monument included in the National Network of Protected Areas of Portugal (Henriques *et al*., this volume).

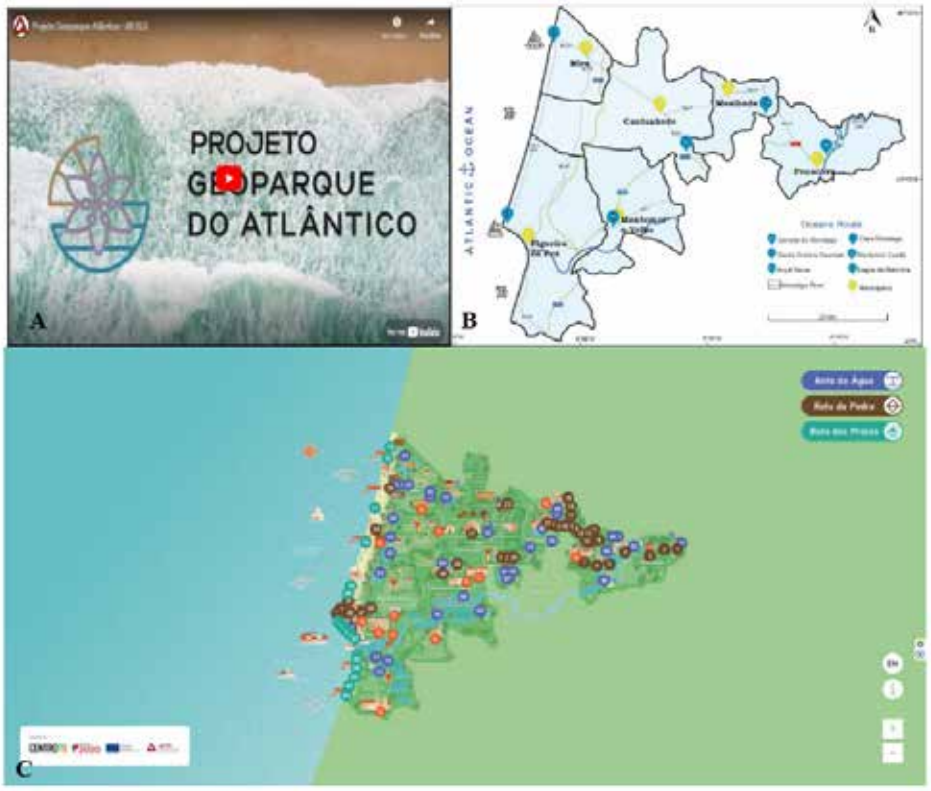

Figure 4: Different types of products resulted from the ongoing "Atlantic Geopark" Project. A: the promotional video (AD ELO, 2021); B: the geo-itinerary with selected geological sites (Custódio *et al*., 2024); C: the geo-itinerary of the heritage routes comprising the water route, the stone route and the beach route (Vaz *et al*., 2024).

Next steps

The results obtained so far allow us to conclude that the territory related to the "Atlantic Geopark" project has geological heritage of international importance, as required by the GGN guidelines (UNESCO, 2022). The geological sites that have been identified so far make it possible to create geotourism routes that tell the story of the various episodes of the geological history of the WIM. But a successful application seeking recognition as a UNESCO Global Geopark requires go through other steps, namely the design and implementation of a comprehensive management plan, covering governance, development, communication, protection, infrastructure, finance, and partnership issues (UNESCO, 2024). This task falls to AD ELO, which has been developing a number of initiatives aimed at publicizing the project through promotional products like a detailed map of the area that connects the area's geological sites and other local resources. Communities' involvement on geoconservation of the "Atlantic Geopark" territory is a challenging goal, and this implies the implementation of a territorial-based program that brings residents closer to the geopark concept.

Acknowledgements
This study was supported by Portuguese funds by FCT - Fundação para a Ciência e a Tecnologia, I.P. (Portugal) in the frame of UIDB/00073/2020 (https://doi.org/10.54499/UIDB/00073/2020) and the UIDP/00073/2020 (https://doi.org/10.54499/UIDP/00073/2020) projects of the I & D unit Geosciences Center (CGeo). S.C.S. benefits from an FCT grant with reference 2024.03829.BD.

References

ADELO, 2021. Projeto Geoparque Atlântico - ADELO. https://www.youtube.com/watch?v=NFVJGIL4PX8&t=1s&ab_channel=ADELOADLBM

AD ELO, 2024. Heritage Routes. https://rotasdopatrimonio.adelo.pt/en/ (retrieved in 17.02.2024)

Carcavilla, L., López-Martínez, J. & Durán, J.J., 2007. Patrimonio geológico y geodiversidad: investigación, conservación, gestión y relación com los espacios naturales protegidos. Instituto Geológico y Minero de España, Serie Cuadernos del Museo Geominero 7, 1-360.

CNU (2024). Geoparques Mundiais da UNESCO. https://unescoportugal.mne.gov.pt/pt/redes-unesco/geoparques-mundiais-da-unesco (retrieved in 17.02.2024).

Custódio, S.C., Henriques, M.H., Rosado-González, E.M., Vaz, N.M. & Sá, A.A., 2024. Selected Geoheritage Resources of "Atlantic Geopark" Project (Central Portugal). Geosciences, 14(3), 81.

Henriques, M.H. & Brilha, J, (2017. UNESCO Global Geoparks: a strategy towards global understanding and sustainability, Episodes 40(4), 349-355.

Henriques, M. H., Pena Dos Reis, R., Brilha, J. & Mota, T.S., 2011. Geoconservation as an emerging geoscience, Geoheritage 3(2), 117-128.

IDRME, (1991). International Declaration of the Rights of the Memory of the Earth. https://www.visitgeoparks.org/geopark-history (retrieved in 17.02.2024).

Freire-Lista, D., Figueiredo, F. & Henriques, M.H., 2024. Ançã Limestone. The stone that carved Portugal, in: Ehling, A., Kaur, G., Jackson, P. N. W., Cassar, J., Lama, E. A. & Heldal, T. (Eds.), The First 55 IUGS Heritage Stones, IUGS Subcommission on Heritage Stones, 22-23. https://iugs-geoheritage.org/publications-dl/IUGS-FIRST-55-STONES-WEB-BOOK.pdf (retrieved in 17.02.2024).

UNESCO, 2022. Application dossier for UNESCO Global Geoparks. https://unesdoc.unesco.org/ark:/48223/pf0000383890 (retrieved in 17.02.2024).

UNESCO, 2024. UNESCO Global Geoparks. https://www.unesco.org/en/iggp/geoparks/about (retrieved in 17.02.2024).

Vaz, N., Rosado-González, E., Lourenço, J.M., Custódio, S., Henriques, M.H., Fidalgo, M., Santos, A. & Sá, A.A., 2024. Rotas do Património - Heritage Routes, Bairrada, Mondego e Atlântico. AD ELO – Associação de Desenvolvimento Local da Bairrada e Mondego.

Vaz, N., Rosado-González, E., Lourenco, J., Correia, P., Custódio, S., Henriques, M.H. & Sá, A.A., 2023. Projeto Geoparque Atlântico–um compêndio com mais de 600 milhões de anos de geodiversidade, in: Font, E., Dinis, P.A., Lopes, F.C. (Eds.), Livro de Roteiros das Excursões do XI Congresso Nacional de Geologia "Geociências e Desafios Globais", Universidade de Coimbra Coimbra, 114–131.

17th INTERNATIONAL CONGRESS of the Geological Society of Greece

BULLETIN OF THE GEOLOGICAL SOCIETY OF GREECE, SP. PUBL.

EXTENDED ABSTRACT 056

The transitional deposits from carbonates to clastic in the Pindos foreland basin: an example from the Mazia village, Ioannina region, Greece

Dalgkitsi P.[1], Uchman A.[2], Botziolis Ch.[1], Zelilidis P.[3], Bourli N.[1], Zelilidis A.[1]

1 University of Patras, Department of Geology, Laboratory of Sedimentology, 26504, Patras, Greece. giotad19@gmail.com

2 Faculty of Geography and Geology, Institute of Geological Sciences, Jagiellonian University, Gronostajowa 3a, 30-387 Kraków, Poland.

3 University of Patras, Department of Geology, Laboratory of Paleontology and Stratigraphy 26504, Patras, Greece

In the NW part of the Ionian Basin (Ioannina region, Western Greece), Triassic evaporites and Jurassic to upper Eocene carbonates (interbedded with minor cherts and shales) are overlain by Eocene to Miocene siliciclastics. These deposits reflect the depositional environments that prevailed during the pre-orogenic, extensional stage and the following syn-orogenic, contractional stage, respectively. During the Middle Eocene, a transition from extension to compression and growing of the Pindos Orogen took place. This caused a change of sedimentation from slope carbonate to siliciclastic submarine fan deposits. Clastic deposits accumulated in a pre-foreland basin at the margin of the Apulian microcontinent from the Late Eocene to the early Miocene because of the uplift of Pindos Orogen and the activity of Pindos Thrust. This change is relatively rapid, so the total thickness of the transitional beds is up to 12.67 m in the Mazia village. In the lower 5 m, there are only thinly bedded mudstones, whereas in the upper 7.5 m within the thinly bedded mudstones there are sandstones and marly limestones. The mudstone is thin- to medium-bedded (0.01–0.02 m) and is either structureless or parallel-laminated. The sandstone beds display sharp bases and include sedimentary structures, such as parallel and ripple cross-laminations. Individual carbonate beds may be either structureless, parallel, or ripple-cross laminated calcarenites. Some of them show an upward transition from structureless (base of the beds), through parallel-lamination to ripple-cross-lamination (top of the bed). This facies association is interpreted as deep-water abyssal plain deposits, according to the dominant lithology and sedimentary structures. Within the marly limestone beds, the trace fossils *Chondrites intricatus, C. targionii, Planolites isp., Nereites isp.,* and *Avetoichnus* are recognized. In the underlying deposits, *Zoophycos* is present. The overlying clastic deposits in the area contain diverse trace fossils typical of the *Nereites* ichnofacies. The sedimentological and ichnological features point to the transition from the *Zoophycos* to the *Nereites* ichnofacies and slope to abyssal plain deposition.

Key words: slope facies, carbonates, Eocene, Greece.

17th INTERNATIONAL CONGRESS of the Geological Society of Greece

BULLETIN OF THE GEOLOGICAL SOCIETY OF GREECE, SP. PUBL.

EXTENDED ABSTRACT 057

Statistics on seismic moment tensors for the Aegean Sea and surrounding area: preliminary results

Dasoula M. G.[1*], Roumelioti Z.[1], Sokos E.[1], Kokkalas, S.[1]
*(1) Department of Geology, University of Patras, Patras, Greece, *up1074036@ac.upatras.gr*

Abstract
Moment tensors (MTs) are an essential tool for understanding earthquake source processes, improving seismic hazard assessment at various scales, and mitigating earthquake disaster risk. The Aegean Sea and its environs have the highest seismic activity in Europe and the Eastern Mediterranean, providing a wealth of earthquake data that can be used for moment tensor computations. In this work, we summarize moment tensor solutions published by the Global Centroid Moment Tensor Group (GCMT) and compare a subset of them with corresponding moment tensors from the Institute of Geodynamics of the National Observatory of Athens (NOA). We statistically examine the two datasets, primarily from the point of view of the style of faulting implied by the moment tensors in the study area and the associated Mw reporting. We also analyze the metrics of this comparison with respect to various factors, such as the location and magnitude of the associated earthquakes, their hypocentral depth, etc. Overall, we find a good agreement between the moment tensors of GCMT and NOA for 85% of the cases studied. Poor comparisons are mostly restricted to moderate magnitude events along the Hellenic Arc.

Moment tensors of the Global Centroid Moment Tensor Group
There are many institutions and universities around the world that study seismic data and publish MTs. The reliability of each is an issue that often concerns researchers. When conducting seismic research on a particular area, the GCMT project MTs are often used as a reference, as they are the most widely accepted by the seismological community.
For more than 40 years, the GCMT project has provided MTs for strong to moderate earthquakes around the globe using methods that involve inversion of long-period seismic waveforms based on normal mode summation and a 1D Earth model with path corrections (Dziewonski et al., 1981). In 2004, GCMT methods and processing underwent significant changes towards the incorporation of intermediate-period surface waves (Ekström et al., 2014). This led to improvements in shallow earthquake source parameters and a significant reduction in the smallest earthquake size for which GCMT publishes solutions.
In this first part of our work, we review all published GCMT solutions for the wider Aegean region (the exact study area is shown in Figure 1a), with statistics focusing on the implied style of faulting and moment magnitude, Mw, reporting. In total, we review 746 solutions, whose epicenters are shown in Figure 1a. The distribution of solutions unsurprisingly follows the distribution of seismicity in the area, with most MTs corresponding to earthquakes along the Hellenic arc, in the transition area of the Ionian islands, the Gulf of Corinth, and a zone subparallel to the western coast of Turkey. The well-known North Aegean trough zone collects a fair number of solutions, but is not as pronounced as in the seismicity maps. Figure 1b shows the distribution of solutions with Mw or Mw_GCMT to distinguish from another subset in the following. Nearly 80% of the dataset consists of solutions for earthquakes with Mw<5.5. Figure 1c shows how the Mw in GCMT MTs is distributed over time and clearly reflects the methodological change of GCMT in 2004, which resulted in a sudden appearance of much smaller earthquakes in the catalog.
The MTs were classified according to the implied fault style following the projection technique of Kaverina et al. (1996) and the classification scheme of Álvarez-Gómez (2014, 2019) implemented in the FMC software. The scheme is based on the plunges of the three eigenvectors of the moment tensors (P, B, T axes) and their relations and includes seven types of faulting: normal (N), normal with strike-slip component (N-SS), strike-slip with normal component (SS-N), strike-slip (SS), strike-slip with reverse component (SS-R), reverse with strike-slip component (R-SS) and reverse (R). The projection of the classification diagram is shown in the inset of Figure 2a. Figure 2a shows the projections of all 746 MTs, with the dimensions of the circle symbols analogous to the size of the earthquakes and their color reflecting the hypocentral depth. About 43% of the MTs are classified as N or N-SS, 23% as R or R-SS, and 34% as SS, SS-N, or SS-R. Overall, almost half of the GCMT MTs for the study area are normal or have some normal faulting component. However, Figure 2b, which shows the cumulative seismic moment release per faulting class, clearly indicates that reverse faulting is the predominant type. This is also reflected in the concentration of larger earthquakes (larger circles in the lower right part of the plot in Figure 2a). Considering that more than 82% of the total seismic moment released by the 746 earthquakes in our dataset comes from the 55 Mw_GCMT ³ 6.0 events, i.e., above the magnitude of completeness of the GCMT catalog for the Aegean area, at least since 1985 (González,

2024), the statistics in Figure 2b can be considered representative of the total seismic activity in the Aegean region for the examined time period.

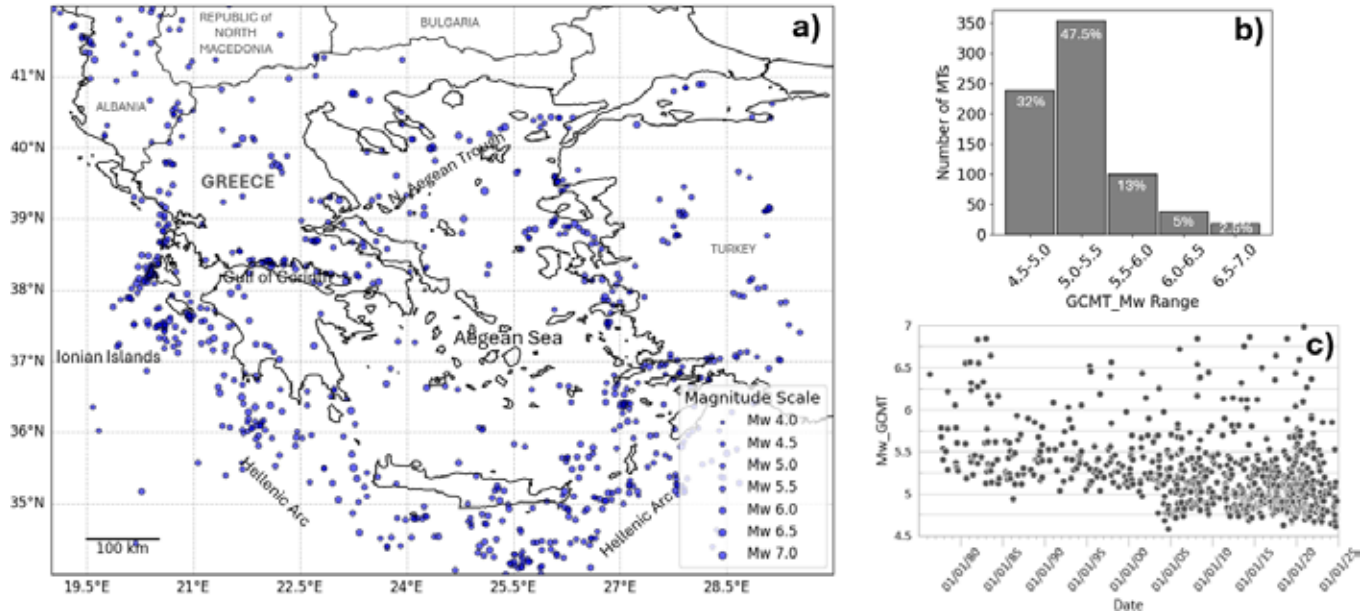

Figure 1. a) Map of the study region showing the epicenters of earthquakes with reported moment tensors in the GCMT catalog and the distributions of b) solutions in M_w bins and c) M_w with time.

Another interesting observation in Figure 2a is the concentration of most intermediate depth earthquake MTs near the center and more generally in the mixed faulting parts of the diagram. This may reflect the increased complexity of the stress field and source processes at greater depths within the subducting system of the Aegean region, the uncertainty of data processing in such depths that result in mixed mode fault-type, the complexity of data from fault branching with decollement surfaces or any combination of these.

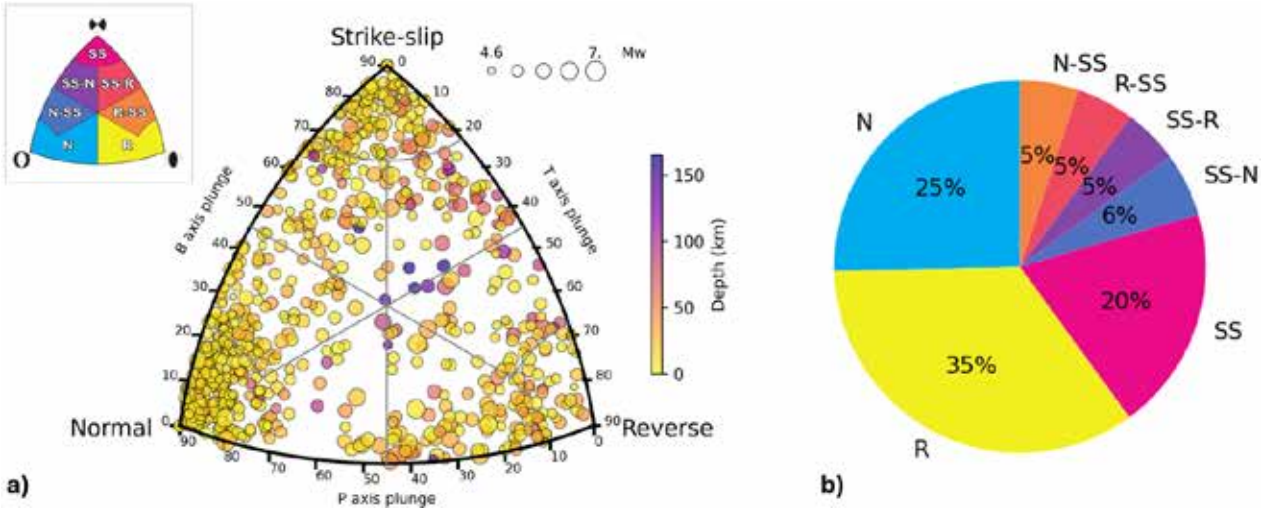

Figure 2. a) Faulting type classification diagram with seven types: N (normal), N-SS (normal with strike-slip component), SS-N (strike-slip with normal component), SS (strike-slip), SS-R (strike-slip with reverse component), R-SS (reverse with strike-slip component), R (reverse). Circle symbols are colored according to the hypocentral depth, and their dimensions are analogous to the magnitude of the earthquakes. The inset (after Álvarez-Gómez, 2014, 2019) shows the sectors of the diagram and corresponding classes b) pie chart with moment release by each class as a percentage of the total moment release from all earthquakes in the examined dataset.

Comparison of GCMT and National Observatory of Athens moment tensors: Faulting Style

The Institute of Geodynamics of the National Observatory of Athens (NOA) provides moment tensors for strong, moderate and even relatively weak earthquakes (down to ~Mw=3.5) as part of its routine services. The MTs published so far by NOA, either automatically derived or manually processed, are based on full waveform inversion of regional broadband waveforms and can be divided into two parts. The first part includes the solutions for the period 2001-2011, when NOA used the method of Hermann and Ammon (2002) (e.g., Konstantinou et al., 2010; Konstantinou, 2015). The second part includes the MTs since 2012, derived by the method of Sokos and Zahradnik (2008), more recently extended by Zahradnik and Sokos (2018) and implemented in the software packages ISOLA and GISOLA (Triantafyllis et al., 2021). This is currently the method routinely used at NOA, and relevant results from its implementation are available on the institute's website (https://bbnet.gein.noa.gr/HL/seismicity/mts).

In order to quantify how well these regional MTs compare to those of the GCMT, we collected the seismic events that occurred in the Aegean and the wider area from 2001 to 2023, for which solutions are available from both sources (i.e., GCMT and NOA). We identified 450 events and as a result we created a database of 450 pairs of MTs. The locations of these events are shown on the map in Figure 3a.

We first examined the pairs of MTs for their similarity in implied fault geometry. To quantify similarity, we adopted an angular measure of the relative orientations of the two MTs in each pair, specifically the smallest angle required to rotate the principal axes of one MT into the principal axes of its paired MT. This angle has been studied extensively by Kagan (e.g., 1991, 2007) and is therefore often referred to as the "Kagan angle". A detailed description of the Kagan angle can be found in the aforementioned publications by Kagan himself and, for example, in Tape and Tape (2012) and references therein.

To define the Kagan angles for our dataset, we used the homonymous MATLAB function (Kolar, 2025). The results are incorporated into the map in Figure 3a by coloring the epicenters based on three classes of Kagan angles: 0˚ - 30˚, indicating that the two focal mechanisms are very similar, 30˚ - 50˚ for acceptable resemblance that allows the focal mechanisms to be identified as similar, and >50˚, where the two focal mechanisms in a pair are very different. Figure 3b shows examples of MT pairs from our dataset for different levels of Kagan angle. The distribution of computed Kagan angles in Figure 3a suggests that there is good agreement between GCMT and NOA solutions, i.e. most epicenters (85%) are colored blue (63%) or yellow (22%), implying Kagan angles <50˚. Red colored epicenters represent only 15% of the cases examined and are almost exclusively located in the outer parts of the study area, where earthquake epicenters are poorly covered in azimuth by the Hellenic Unified Seismological Network, the backbone data source for NOA MT inversions. The largest concentrations of high Kagan angles occur along the southeastern part of the Hellenic Arc and the Ionian Islands.

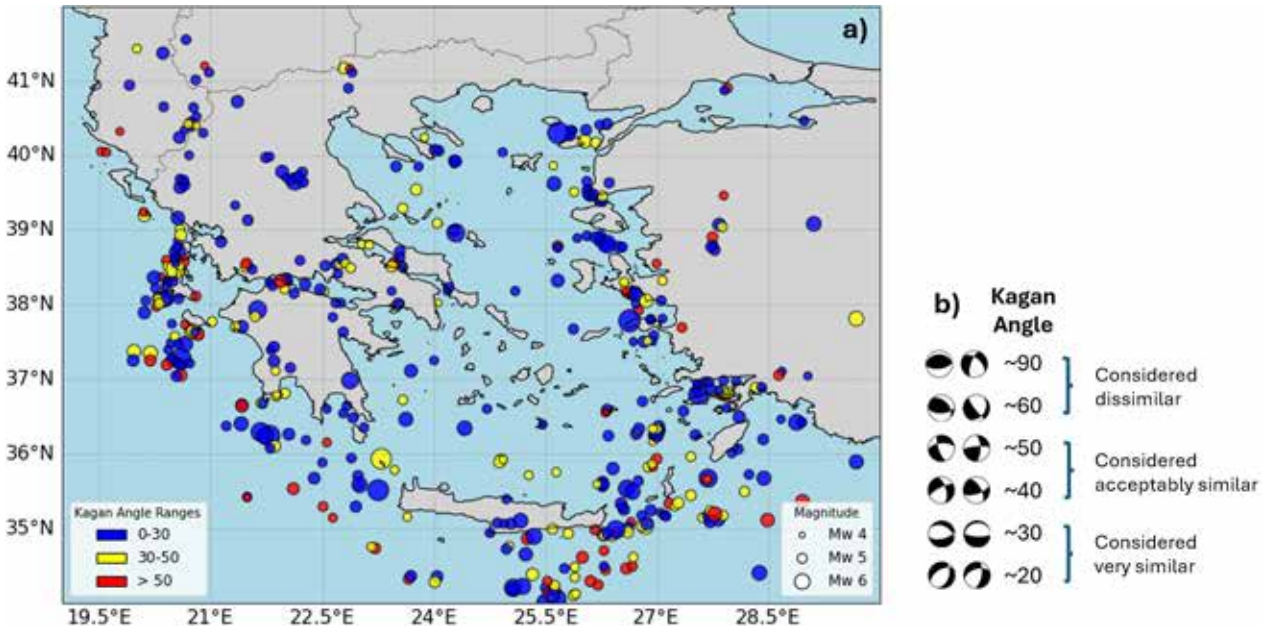

Figure 3. a) Map of the study region with epicenters of earthquakes for which both the GCMT and NOA have published MTs. Circle symbols are colored by Kagan angle ranges. b) Example pairs of MTs from the studied dataset for various levels of the Kagan angle.

Kagan angles were also examined as a function of earthquake magnitude (Mw), hypocenter depth, and time, as shown in Figure 4. Figure 4a shows the distribution of angles with the Mw_GCMT, where it is noticeable that high magnitude events (>6) have low Kagan angles. All angles >50˚ appear at lower magnitudes and especially at Mw<5.5. Combining this observation with the distribution in Figure 3a leads to the expected result that MTs of events with Mw<5.5 in the periphery of our study area are not always accurately resolved.
Figure 4b shows how the Kagan angles vary with the hypocentral depth of the events in our dataset. Most of the high Kagan angle values are concentrated at shallow depths, following the distribution of seismicity. However, several high angles appear to be distributed throughout the sampled depth interval, and the paucity of data at great depths does not allow us to draw any firm conclusions about a possible relationship between changes in the similarity of MT pairs and depth.
Finally, Figure 4c shows the Kagan angles with respect to the date of the events/MTs and gives the impression that the number of events associated with high angles has remained relatively stable over the years (2001-2023), despite the significant methodological changes by both GCMT and NOA. Moreover, since 2012, NOA has adopted GISOLA and has also allowed the release of automatic MT solutions, which has increased the number of events with MT pairs. The high Kagan angles have not followed this increase, indicating that the MT solutions provided by GCMT and NOA have become more similar in recent years.

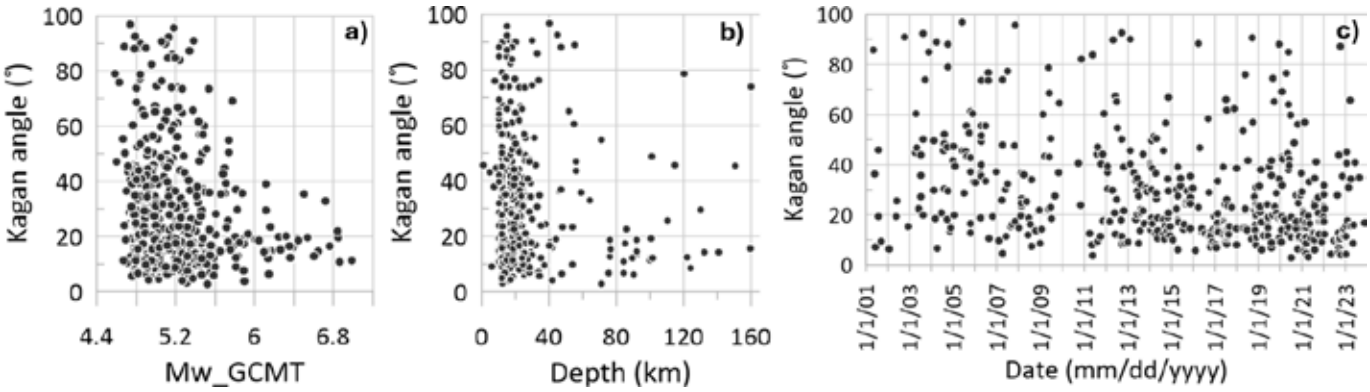

Figure 4. Distribution of computed Kagan angles with respect to a) Mw_GCMT, b) the hypocentral depth of the earthquakes in the examined dataset and c) the date of occurrence of the earthquakes considered to coincide with the date of MT solutions release.

Comparison of GCMT and National Observatory of Athens moment tensors: Mw

The moment tensor is derived by modeling the full waveform and amplitude of the seismic waves, providing the most accurate measure of earthquake energy to date. The radiated seismic energy, in turn, is directly related to the seismic moment and, through it, to the Mw. Thus, the routine computation of MTs has provided a rich dataset of Mw values that should be consistent around the globe. However, it has been shown that different Mw catalogs can show systematic discrepancies. This is, for example, the case of Mw reported by GCMT and Mw reported by NOA based on their respective MT solutions as highlighted by Konstantinou (2015). Konstantinou (2015) collected MTs from GCMT and NOA concerning the same earthquakes and the period May 2001 to October 2014, formed a dataset of 185 paired MTs and examined the differences in their respective Mw values. He concluded that NOA Mw values are smaller than GCMT Mw values by 0.15-0.25 magnitude units and attributed this rather systematic difference to the limited bandwidth in NOA inversions methods with respect to GCMT.
In this final part of our work, we use our paired GCMT-NOA MTs to perform a similar comparison to that performed by Konstantinou (2014). It should be noted that in addition to the differences that may arise from the different methods, data, and metadata of the two MT solution sources, there are also minor differences that may result from the post-processing of the moment tensor metrics. These arise, for example, from the use of a slightly different relation to calculate Mw from the seismic moment, M_0 (Kanamori, 1977; Hanks and Kanamori, 1979), the form of these relations (i.e., to be used with M_0 in N×m or in dyn×cm and rounding tactics of the relations constants), and from different rounding tactics of the reported Mw. To constrain the latter, we have recalculated the Mw of both GCMT and NOA directly from the reported values of M_0 using Kanamori's (1979) relation. The comparison of the derived sets of Mw values is shown in Figure 5a and the result of the standard regression is expressed by the blue thick line described by:

$$Mw\_NOA=1.032(\pm0.014)Mw\_GCMT-0.367(\pm0.074) \quad (1)$$

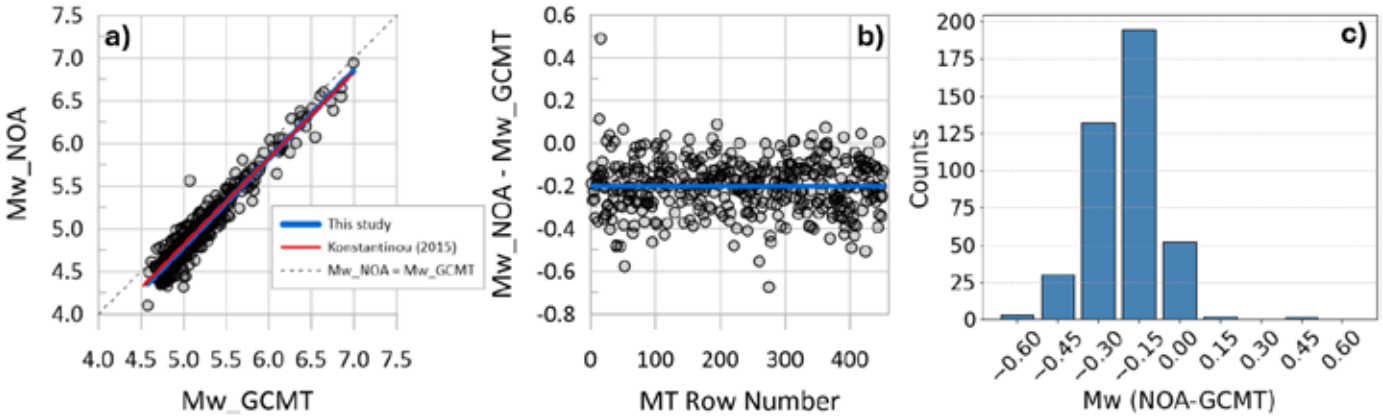

Figure 5. a) Moment magnitude of NOA (Mw_NOA) versus moment magnitude of GCMT (Mw_GCMT) from the corresponding moment tensors. The thick blue line indicates the standard regression result of this study, the red line the orthogonal regression results of Konstantinou (2015) and the dashed gray line the 1:1 relation. b) Differences of the two examined Mw sets with the blue line marking the average difference of 0.2 magnitude units. c) Distribution of Mw differences in 0.15 difference bins.

Equation (1) shows a coefficient of determination R^2=0.93, which is slightly improved (by 0.01) compared to that of the relationship of Konstantinou (2015), despite the fact that our dataset is more than twice as large. Our result is also compared graphically with that of Konstantinou (2015) in Figure 5a, where it is evident that the two lines are practically identical in the upper half and differ only slightly towards lower magnitudes. In fact, our result seems to deviate more from the 1:1 line (gray dashed line) as the magnitude decreases.

Figures 5b,c show the distribution of the differences between the two magnitudes in our dataset, and the blue line shows the practically constant mean of -0.20. Almost all differences are below zero, confirming that Mw_NOA is systematically lower than Mw_GCMT.

Conclusions/Discussion

We present preliminary results of an extensive statistical investigation and comparison of moment tensors (MTs) of earthquakes in the Aegean Sea and surrounding area, using data from the Global Centroid Moment Tensor (GCMT) project and the Institute of Geodynamics of the National Observatory of Athens (NOA). We investigate the MTs with respect to the implied faulting type during strong to moderate magnitude earthquakes in the area, the moment magnitudes (Mw), and the consistency between the two datasets.

Statistical analysis of the GCMT's 40-year archive of 746 MTs for the area showed that approximately 80% of this dataset consists of solutions for earthquakes with Mw<5.5. It also showed that although normal faulting is more frequent, reverse faulting accounts for the largest share of seismic moment release in the form of larger earthquakes. This is consistent with the mechanics involved, which are not facilitated by gravity as in normal faulting, with compressional forces often "locking" large areas and preventing movement for extended periods. This allows for the long build-up of stress that is eventually released in larger magnitude earthquakes.

We also examined the comparison of 450 pairs of MTs from GCMT and NOA for earthquakes from 2001 to 2023. To quantify the similarity/difference in the proposed fault geometry, we used the Kagan angle and concluded that the two compared sets of MTs show good agreement in 85% of the cases studied. Poor comparison of MTs provided by GCMT and NOA for the same events was found for only 15% of the pairs studied and was mostly associated with moderate magnitude events (Mw<5.5) along the Hellenic arc. Over time, despite methodological changes in both GCMT and NOA, the number of events with high Kagan angles has remained stable and the similarity between MT solutions may have increased over time, as suggested by the larger number of good comparisons in recent years.

A comparison of Mw values from GCMT and NOA MTs confirmed previous studies (e.g., Konstantinou, 2015) that NOA Mw values are systematically lower than GCMT Mw values by an average of 0.20 magnitude units. Regression analysis of Mw values showed that this difference is consistent across the magnitude range, with a slightly larger deviation from the 1:1 Mw_NOA - MwGCMT relationship as magnitude decreases.

Acknowledgements

We acknowledge the Global Centroid Moment Tensor project and the National Observatory of Athens for the invaluable moment tensor data provided for decades. The study was carried out in the framework of the research project "UNMASK", supported by the

Hellenic Foundation for Research and Innovation (H.F.R.I.) under the “2nd Call for H.F.R.I. Research Projects to support Faculty Members & Researchers” (Project Number: 2724).

References

Álvarez-Gómez, J. A., 2019. FMC—Earthquake focal mechanisms data management, cluster and classification. SoftwareX, 9, 299-307.

Álvarez-Gómez, J. A., 2014. FMC: a one-liner Python program to manage, classify and plot focal mechanisms. Geophysical Research Abstracts, Vol. 16, EGU2014-10887

Dziewonski, A. M., T.-A. Chou, J. H. Woodhouse, 1981. Determination of earthquake source parameters from waveform data for studies of global and regional seismicity. J. Geophys. Res., 86, 2825-2852, doi:10.1029/JB086iB04p02825

Ekström, G., M. Nettles, A.M. Dziewonski, 2012. The global CMT project 2004-2010: Centroid-moment tensors for 13,017 earthquakes, Phys. Earth Planet. Inter., 200-201, 1-9, doi:10.1016/j.pepi.2012.04.002

González, Á., 2024. Improvements and heterogeneities of the Global Centroid Moment Tensor catalog. Seism. Res. Lett. 95(6), 3566-3578.

Hanks, T.C., H. Kanamori, 1979. A moment magnitude scale, J. Geophys. Res. 84(B5), 2348-2350.

Herrmann, R.B., C.J. Ammon, 2002. Computer programs in seismology source inversions: User’s manual, version 3.30, report, St. Louis University, St. Louis, Missouri.

Kagan, Y. Y., 1991. 3-D rotation of double-coupleearthquake sources, Geophys. J. Int., 106(3), 709-716.

Kagan, Y.Y., 2007. Simplified algorithms for calculating double-couple rotation. Geophys. J. Int. 171, 411–418.

Kanamori, H., 1977. The energy release in great earthquakes. J. Geophys. Res. 82(20), 2981-2987.

Kaverina, A.N., A.V. Lander, A.G. Prozorov, 1996. Global creepex distribution and its relation to earthquake-source geometry and tectonic origin. Geophysical Journal International 125, 249–265.

Kolar, P., 2025. Kagan angle (https://www.mathworks.com/matlabcentral/fileexchange/70040-kagan-angle), MATLAB Central File Exchange. Retrieved January 24, 2025.

Konstantinou, K.I., 2015. Moment Magnitude Estimates for Earthquakes in the Greek Region: A Comprehensive Comparison. Bulletin of the Seismological Society of America 105(5), 2555–2562, doi: https://doi.org/10.1785/0120150088

Konstantinou, K.I., N.S. Melis, K. Boukouras, 2010. Routine Regional Moment Tensor Inversion for Earthquakes in the Greek Region: The National Observatory of Athens (NOA) Database (2001–2006). Seismological Research Letters 81(5), 750–760, doi: https://doi.org/10.1785/gssrl.81.5.750

Sokos, E. N., J. Zahradník, 2008. ISOLA a Fortran code and a Matlab GUI to perform multiple-point source inversion of seismic data. Computers and Geosciences, 34, 967-977.

Tape, W., C. Tape, 2012. Angle between principal axis triples. Geophys. J. Int., 191, 813-831.

Triantafyllis, N., I.E. Venetis, I. Fountoulakis, E.-V. Pikoulis, E. Sokos, Ch.P. Evangelidis, 2021. Gisola: A High-Performance Computing Application for Real-Time Moment Tensor Inversion. Seismological Research Letters, 93(2A), 957–966, doi: https://doi.org/10.1785/0220210153

Zahradník, J., E. Sokos, 2018. ISOLA code for multiple-point source modeling, in: S. D’Amico (ed.), Moment Tensor Solutions, Springer Natural Hazards, https://doi.org/10.1007/978-3-319-77359-9_1

17th INTERNATIONAL CONGRESS of the Geological Society of Greece

BULLETIN OF THE GEOLOGICAL SOCIETY OF GREECE, SP. PUBL.

EXTENDED ABSTRACT 058

Environmental Seismic Intensity Scale (ESI 2007)

Deligianni Stamatia
(1) University of Aegean, Mytilene, Greece, stamatia.deligianni@gmail.com

Introduction / Background

The Environmental Seismic Intensity Scale (ESI 2007), introduced by the International Union for Quaternary Research (INQUA), is an innovative tool for quantitatively assessing macroseismic intensities. The scale comprises 12 levels, based exclusively on the environmental impacts of earthquakes, such as surface ruptures, tectonic uplifts, landslides, liquefaction, and hydrological changes. Unlike traditional macroseismic intensity scales, which focus on damage to anthropogenic structures, ESI 2007 relies on physical observations, eliminating uncertainties associated with socioeconomic and cultural factors (Michetti et al., 2007).

The ESI 2007 scale offers several advantages over traditional macroseismic intensity scales. First, it relies on natural data, providing an independent assessment of earthquake intensity while reducing the influence of anthropogenic factors (Serva, 1994). Second, it enables the comparison of earthquakes from different time periods, geographical locations, and tectonic settings (Porfido et al., 2007). Third, the scale captures local variations in intensity, making it particularly useful in microzonation studies (Ota et al., 2010). Additionally, it is suitable for assessing seismic intensity in areas without anthropogenic infrastructure or population coverage (Tatevossian, 2007). Finally, the integration of paleoseismological data enhances the understanding of seismic hazards and contributes to the development of long-term risk management strategies (Serva et al., 2016).

Despite its advantages, the ESI 2007 scale has certain limitations. Its application requires specialized knowledge of geological phenomena and access to high-quality data. Moreover, it does not replace traditional macroseismic intensity scales but functions complementarily, enhancing the environmental perspective (Papathanasiou et al., 2011).

The ESI 2007 is a crucial tool for site selection in seismic hazard studies. Through the analysis of environmental parameters and the mapping of geological features, the scale identifies areas of increased seismic vulnerability. These include regions with a high probability of liquefaction, active faults, and geomorphological changes. Furthermore, the use of historical and paleoseismological data strengthens predictive capabilities and the effectiveness of risk management strategies. In remote or sparsely populated areas, ESI 2007 provides critical data that cannot be derived from traditional approaches.

In conclusion, ESI 2007 is an exceptional tool for the quantitative and objective assessment of seismic intensity. It expands our understanding of the environmental impacts of earthquakes and enhances the management of natural hazards on a global scale.

Methodology

This study employs a systematic approach involving data collection, the creation of a GIS database, and the generation of maps to analyze earthquakes in western Turkey. The analyzed events include the Gediz, Simav-Kütahya, Samos-Izmir, Marmaris, and Izmit earthquakes. Data were collected from geological observations, historical records, and seismological databases. These data were integrated into a GIS system, enabling the visualization of tectonic structures and affected areas.

The map generation process involved processing geospatial data to highlight active faults, liquefaction zones, and high seismic risk areas. The analysis utilized high-resolution data, enhancing the accuracy of the mapping.

Results

The study focused on the investigation of the environmental, geomorphological, and socioeconomic impacts of five major seismic events that affected the Eastern Mediterranean and Western Turkey. The regions analyzed were Marmaris (1957), Gediz (1970), Izmit (1999), Simav-Kütahya (2011), and Samos-Izmir (2020). The collected and analyzed data provide a comprehensive view of the severity of geodynamic phenomena and their effects on both the natural and anthropogenic environment, contributing to the understanding of the mechanisms governing these phenomena.

In Marmaris, the 1957 earthquake, with an ESI intensity of 8, caused extensive surface ruptures with vertical and horizontal ground displacements of up to 2 meters. Secondary phenomena
such as liquefaction, landslides, and local tsunamis caused severe damage to agricultural lands, infrastructure, and buildings.

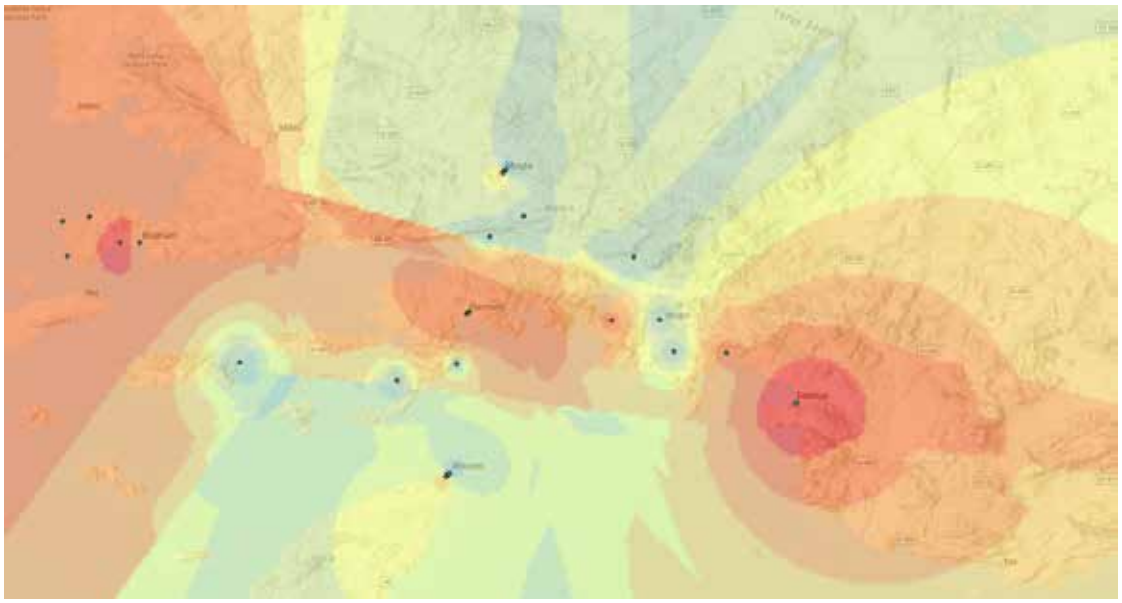

Figure 1. Map of Seismic Intensity Curves for the 1957 Marmaris Earthquake.

The Gediz earthquake of 1970, with an ESI intensity of 7, resulted in intense geomorphological phenomena such as subsidence and landslides. The impacts were catastrophic for the local economy and population, leading to building collapses and disruptions to critical infrastructure, necessitating extensive restoration efforts.

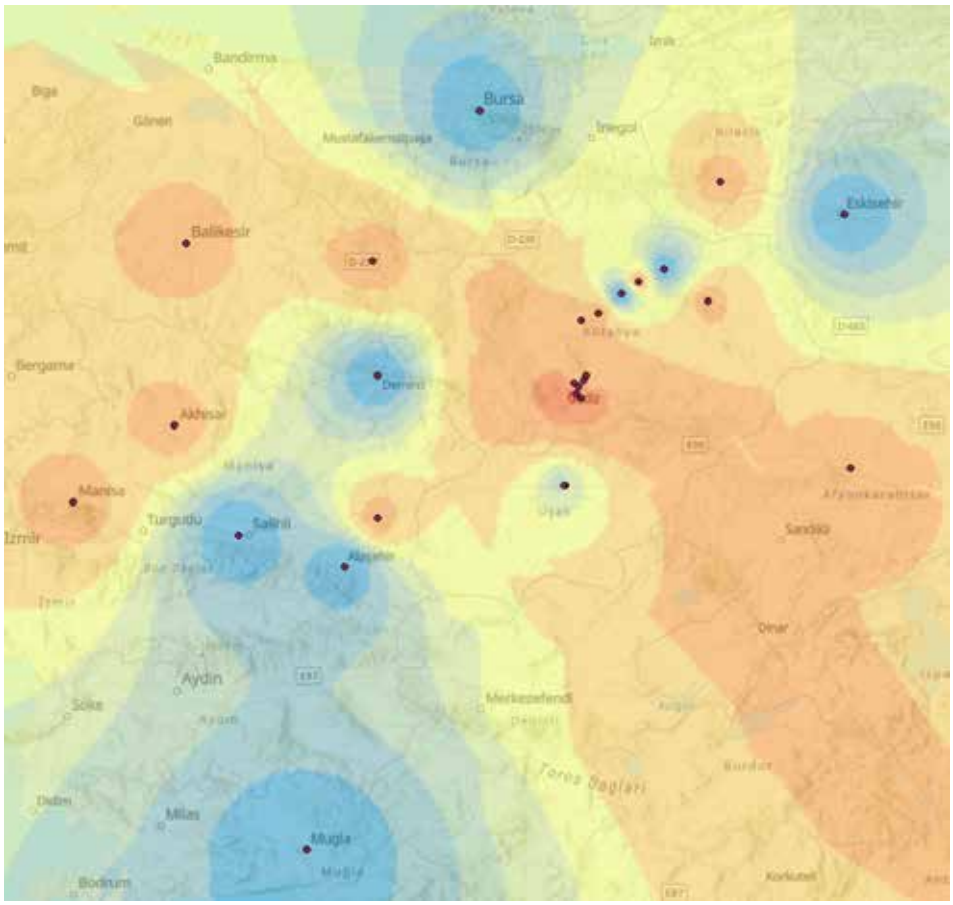

Figure 2. Map of Seismic Intensity Curves for the 1970 Gediz Earthquake

The 1999 Izmit earthquake, with an ESI intensity of 8, was one of the most destructive events, with extensive ruptures exceeding 150 kilometers in length and ground displacements surpassing 5 meters. The geomorphological and anthropogenic impacts were dramatic, as industrial zones and residential areas were destroyed, resulting in numerous fatalities and injuries.

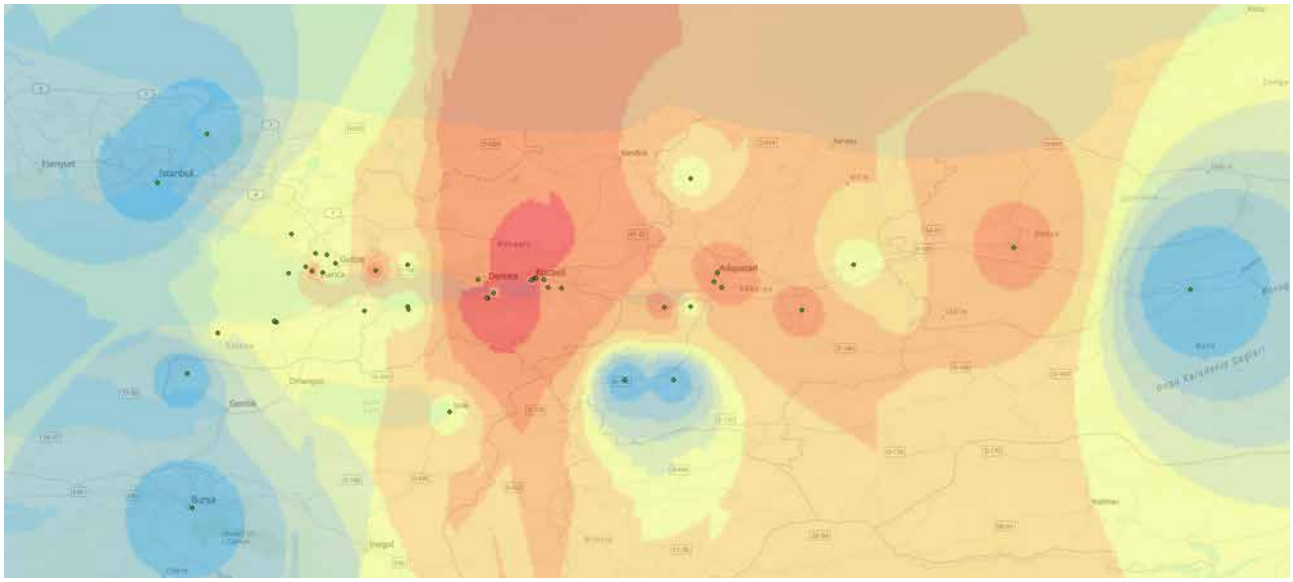

Figure 3. Map of Seismic Intensity Curves for the 1999 Izmit Earthquake.

The 2011 Simav-Kütahya earthquake, with a lower intensity (ESI 6), caused significant geomorphological changes, including widespread subsidence and new landslides. These alterations affected local ecosystems, infrastructure, and the daily lives of residents, requiring substantial restoration efforts.

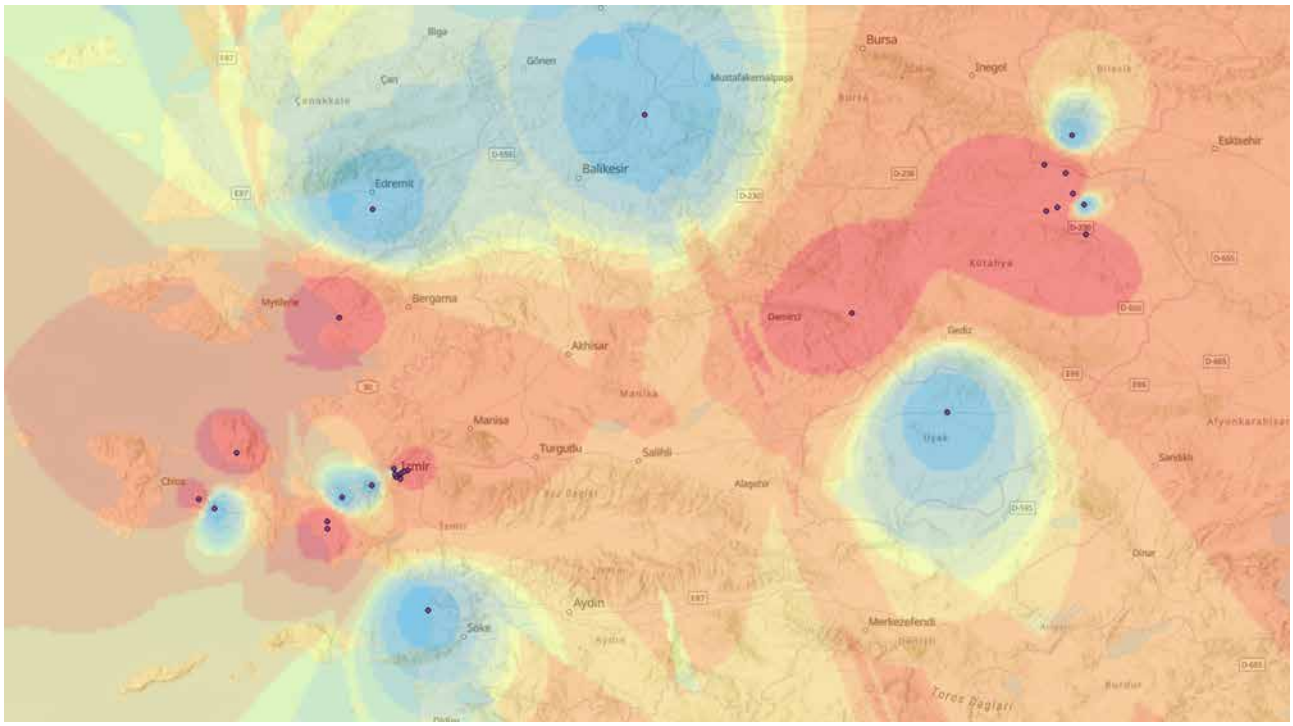

Figure 4. Map of Seismic Intensity Curves for the 2011 Simav - Kutahya Earthquake.

Finally, the 2020 Samos-Izmir earthquake, with an ESI intensity of 8, caused a combination of geodynamic phenomena. Extensive ruptures with displacements of up to 5 meters, as well as secondary impacts such as

liquefaction, landslides, and tsunamis, had devastating consequences for coastal zones and urban centers, with severe socioeconomic impacts.

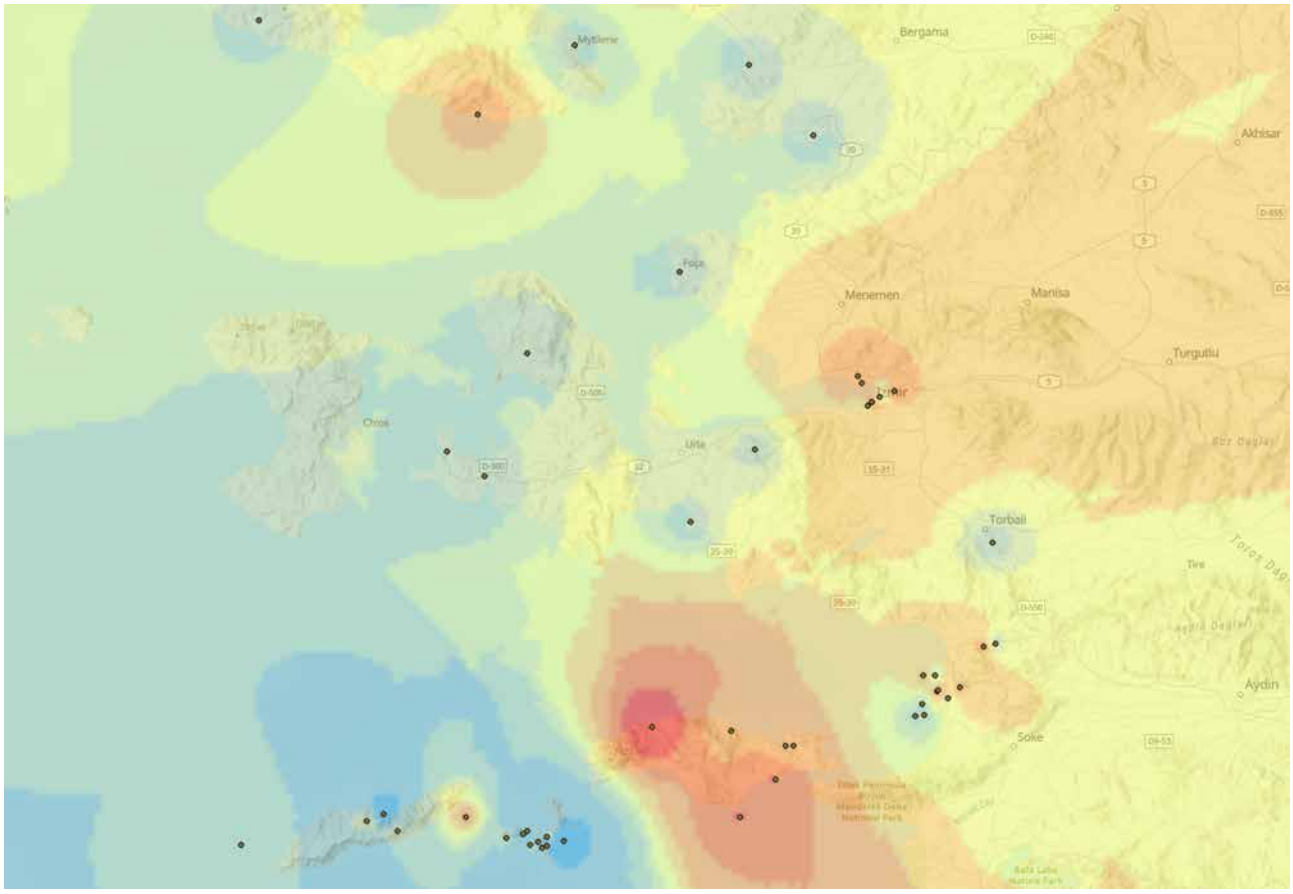

Figure 5. Map of Seismic Intensity Curves for the 2020 Samos - Izmir Earthquake.

Comparison with the Mercalli Scale

This study emphasizes the comparison of earthquakes in five significant regions of the Eastern Mediterranean using the Mercalli and ESI 2007 scales to assess their impacts. The earthquakes of Gediz (1970), Izmit (1999), Simav-Kütahya (2011), Marmaris (1957), and Samos-Izmir (2020) are evaluated based on their primary and secondary consequences on the anthropogenic and natural environments. The Mercalli scale focuses on damage to infrastructure, human casualties, and perceived impacts by human populations, while the ESI 2007 scale records geological and environmental changes, such as ruptures, ground liquefaction, landslides, and morphological alterations.

Specifically, the Izmit and Samos-Izmir earthquakes exhibited intense ruptures and extensive geomorphological changes, demonstrating the utility of the ESI 2007 scale for understanding impacts at a natural level. On the other hand, the Gediz and Simav-Kütahya earthquakes showed more pronounced social impacts, such as residential destruction, effectively captured by the Mercalli scale. The Marmaris earthquake, with its significant effects on both the anthropogenic and natural environment, underscores the need for a combined use of both scales for a more comprehensive understanding of impacts.

The comparison of these scales reveals that their integration provides valuable complementary data for better understanding and managing seismic risks and their impacts. The findings highlight the importance of a multidimensional approach to seismic analysis for improved preparedness and recovery.

Discussion

To visualize the above results, contour maps were created in GIS, capturing the deformation of the Earth's surface. The geometry of the contour lines was examined to determine whether the ellipsoidal shape formed by the contours aligns with the orientation and geometry of the fault responsible for each earthquake. The findings revealed that, in most cases, the shape of the contour lines matches the location and mechanism of the main fault, highlighting the

dynamics of the geodynamic phenomena.
For instance, in the case of the Gediz earthquake (1970), the contour maps depicted deformation aligned with the fault in the area, with the intensity of deformation being stronger near the fault and gradually diminishing with distance. In the case of the Samos-Izmir earthquake (2020), the contour maps captured the deformation caused by the offshore fault between Samos and Izmir in great detail. The ellipsoidal shape of the contours was consistent with the orientation of the fault, highlighting zones of intense deformation concentrated in the coastal areas and urban centers of the region. The contour lines revealed higher deformation values close to the fault, gradually decreasing towards the interior of Izmir and Samos. Moreover, significant secondary impacts such as landslides and liquefaction were recorded in areas of greater deformation. This analysis provided a clear depiction of the dynamics of the seismic event and its geomorphological impacts.
While the comparison between the Mercalli and ESI 2007 scales, presented in the Results section, highlights their complementary nature in evaluating seismic impacts, the Discussion focuses on the limitations and broader implications of these tools. The Mercalli scale, despite its widespread use in capturing human-centric impacts, is limited in its ability to detail geomorphological and environmental changes. Conversely, the ESI 2007 scale excels in documenting geological alterations but may face challenges in highly urbanized regions or in areas where secondary phenomena like tsunamis obscure field evidence.
One critical finding of this study is the role of ESI 2007 in enhancing the spatial and environmental understanding of seismic phenomena. By focusing on physical deformation, such as ruptures and landform changes, ESI 2007 provides insights that are often overlooked by traditional scales like Mercalli. However, its reliance on field observations introduces practical limitations in remote or inaccessible terrains. To address these challenges, future research could incorporate remote sensing technologies, such as LiDAR, InSAR, and satellite imagery, to supplement and expand ESI 2007 analyses.
The integration of both scales offers a multidimensional approach to seismic risk assessment. While the Mercalli scale effectively captures social and structural impacts, ESI 2007 adds a layer of detail about environmental consequences. This dual perspective is particularly valuable for regions like Samos and Izmir, where both anthropogenic and natural environments were significantly affected by the 2020 earthquake.
Furthermore, previous studies, such as Michetti et al. (2007), emphasize the utility of ESI 2007 in regions with significant environmental changes. Our findings build on this by demonstrating how integrating ESI 2007 with Mercalli can provide a more comprehensive framework for seismic preparedness and recovery strategies. This approach could be further refined by applying machine learning algorithms to analyze patterns of seismic impact across multiple datasets, enhancing predictive models for future events.
In conclusion, this study underscores the necessity of a multidimensional framework for analyzing seismic phenomena. The integration of the Mercalli and ESI 2007 scales not only broadens the understanding of seismic impacts but also contributes to more effective disaster risk reduction strategies, emphasizing the value of combining geological, environmental, and social perspectives.

Acknowledgments

I would like to express my heartfelt gratitude to Professors Alexandros Chatzipetros, Spyridon Pavlidis, and Georgios Drakatos for their invaluable guidance and unwavering support during the completion of this dissertation. Their expertise and insightful scientific observations significantly contributed to the shaping of this study and the enhancement of my scientific approach.
Their contribution was pivotal, and I extend my sincere appreciation for their continuous support throughout my academic journey.

References

Ambraseys, N.N., 1988. Engineering seismology. Earthquake Engineering & Structural Dynamics 17, 1-30.]
Caputo, R., Pavlides, S., Chatzipetros, A., 2000. Earthquake surface faulting: Earthquake fault mechanics and implications for seismic hazard assessment. Annals of Geophysics 43, 831-847.
Chatzipetros, A., Pavlides, S., 2003. Active faults in the Aegean region. Tectonophysics 367, 123-136.
Chatzipetros, A., Pavlides, S., 2005. Geological and paleoseismological investigations of active faults in northern Greece. Geological Society of Greece Bulletin 37, 230-245.
Jackson, J., McKenzie, D., 1988. The relationship between plate motions and seismic moment tensors, and the rates of active deformation in the Mediterranean and Middle East. Geophysical Journal International 93, 45-73.
Jenkins, D.G., 1988. Recent developments in seismic hazard assessment in Greece. Tectonophysics 159, 323-339.
McKenzie, D., 1972. Active tectonics of the Mediterranean region. Geophysical Journal International 30, 109-185.
Papazachos, B., Papazachou, C., 2003. The earthquakes of Greece. Ziti Editions.

Papazachos, C., Papazachou, K., Pavlides, S., 1997. Seismicity and neotectonics of the Hellenic arc. Geophysical Journal International 131, 687-699.

Papanikolaou, D., Vassilakis, E., 2008. The neotectonic structure of the Aegean volcanic arc. Journal of the Geological Society 165, 501-512.

Pavlides, S., 1993. Paleoseismicity in the Eastern Mediterranean region. Annals of Geophysics 36, 221-228. [Journal Article]

Pavlides, S.B., Caputo, R., 2004. Magnitude versus faults' surface parameters: quantitative relationships for earthquake geodynamics. Bulletin of the Seismological Society of America 94, 2082-2099.

Scholz, C.H., 2002. The mechanics of earthquakes and faulting. Cambridge University Press.

Stiros, S.C., Pirazzoli, P.A., 1995. Paleoseismicity in the Aegean region. Tectonophysics 249, 195-209.

Taymaz, T., Yolsal-Çevikbilen, S., Ulutaş, E., 2007. Earthquake mechanisms in the Eastern Mediterranean. Bulletin of the Seismological Society of America 97, 273-290.

17th INTERNATIONAL CONGRESS of the Geological Society of Greece

BULLETIN OF THE GEOLOGICAL SOCIETY OF GREECE, SP. PUBL.

EXTENDED ABSTRACT 059

The Triassic post-collisional high-K alkali-calcic granites in the Vertiskos Unit, Serbo-Macedonian Massif: insights from Miriofito granite, Kerkini complex, Greece

Dimitri K.[1], Stouraiti C.[1], Amanatidou D.[1], Soukis K.[1]
(1) Faculty of Geology and Geoenvironment, National and Kapodistrian University of Athens, Athens, Greece; sge1900022@uoa.gr

Introduction

This paper presents new geochemical and mineral chemistry data of the Early Triassic granitic rocks of Miriofito intrusion, which comprises part of the Kerkini Granite Complex (KGC), in northern Greece (Poli *et al*., 2009). We revisit the issue of petrogenesis of Miriofito granite (MIR) which, according to available literature data, illustrates, together with the main Kerkini intrusion, variable behaviour combining A- and I-type characteristics (Christofides *et al*., 1999; 2007; Poli *et al*., 2009; Himmerkus *et al*., 2009). The main objective of the study is to examine the geochemical characteristics of MIR, as well as to contribute to the existing knowledge regarding the granite's tectonic setting.

Regional Geology

The Serbo-Macedonian massif (SMM) is a NW–SE-trending crystalline complex consisting of amphibolite- to granulite-facies gneisses and schists, and together with the Rhodope massif to the east, constitutes the crystalline core of the internal Hellenides. The SMM comprises two major basement units, the Vertiskos and Kerdilion (Kockel *et al*., 1978; Kilias *et al*., 1999; Himmerkus *et al*., 2007). The Vertiskos unit occupies the central part of the SMM and is mainly composed of felsic augen and mica gneisses which attained amphibolite-facies conditions. U-P zircon dating on the crystalline rocks of this unit revealed three major magmatic episodes: i) 458.8 ± 11 M and 460 Ma (Himmerkus *et al*., 2007; Papapavlou, 2021), ii) 300 ± 1 Ma from the central part of the Arnea Pluton (Abbo *et al*., 2020), and iii) 243.6 ± 1.5 Ma for the Arnea A-type granitoid and 247 Ma for Kerkini granite complex (Poli *et al*., 2009).
The Kerkini granite complex (KGC) comprises a large intrusion, the Muries granite (MUR), and two smaller bodies, the Miriofito granite (MIR) and the Kastanousa granodiorite (KAS) (Christofides *et al*., 1999).

Methods

Seven (7) granite samples were collected from two areas, five (5) from Miriofito and two (2) from Kerkini (Fig. 1). The mineralogical composition of the samples was determined using optical microscopy, Scanning Electron Microscopy accompanied by Energy Dispersive System (SEM/EDS) and X-ray Diffraction analysis (XRD). Geochemical analyses included X-ray Fluorescence Spectroscopy (XRF) and Inductively Coupled Plasma Mass Spectrometry (ICP-MS).

Results and Discussion

The typical MIR rock type is a biotite-bearing (±muscovite) granite which ranges to (±muscovite) leucogranite (Fig.1). It consists of a high content of quartz, K-feldspar, albite and Fe-biotite (annite). The characteristic micrographic texture of quartz in K-feldspar, the perthitic K-feldspar and the occurrence of anorthoclase in the studied rocks indicate that this granite represents the last stage of crystallisation, at shallow intrusion depth and high PH2O (subsolvus granite). Mineral relationships show that biotite is a late magmatic phase after feldspar crystallisation. The mineral chemistry of biotite reveals that the primary ferroan magmatic biotite has been re-equilibrated by a hydrothermal fluid. Muscovite is entirely phengitic in composition and represents a secondary phase forming at the expense of the primary magmatic minerals. In the profoundly altered parts (veins, cracks) minerals such as grossular, fluorite, epidote, monazite, Fe-Ti oxides and sulfides occur.
Geochemically it is a high-K to ultrapotassic granite, variably peraluminous i.e. low- to high-peraluminousity as indicated by the ASI (= mol. $Al_2O_3/CaO + Na_2O + K_2O$) values i.e. 1 to 1.25. The trace element systematics indicate the dominant role of K-feldspar and minor plagioclase fractionation in the differentiation of Miriofito

intrusion. Advanced fractional crystallisation is supported by large depletions of Sr-Ba-Eu, P and Ti associated with feldspars, apatite/monazite and Fe-Ti-oxides (rutile, ilmenite) respectively.
In the discrimination diagrams for I-S- and A-type granites the Miriofito and Kerkini granite both straddle the field of A-type (Whalen et al. 1987). Our new geochemical data illustrates a strong enrichment of K, Cs, Rb, Th and U relative to the average continental crust, for the Miriofito granite and even more so for Kerkini granite. This enrichment is considered a source characteristic for the high-K calc-alkaline (HKCA), either juvenile crust or K- enriched lithospheric mantle. Further use of tectonic discrimination diagrams for granites (Pearce *et al*., 1984) delineates a trans-discriminant affinity for the MIR samples, between volcanic arc and within-plate environments, while other discrimination diagrams show explicitly a volcanic arc setting, or active continental margin settings. In general, rocks belonging to the high-K calc-alkaline magmatism occurs in a post-collisional setting, commonly after 30 to 50 Ma after the cessation of subduction (Bonin et al. 1990; Liégeois *et al*., 1998).

Figure 1. Field occurrence of Miriofito (left) and Kerkini (right) granites.

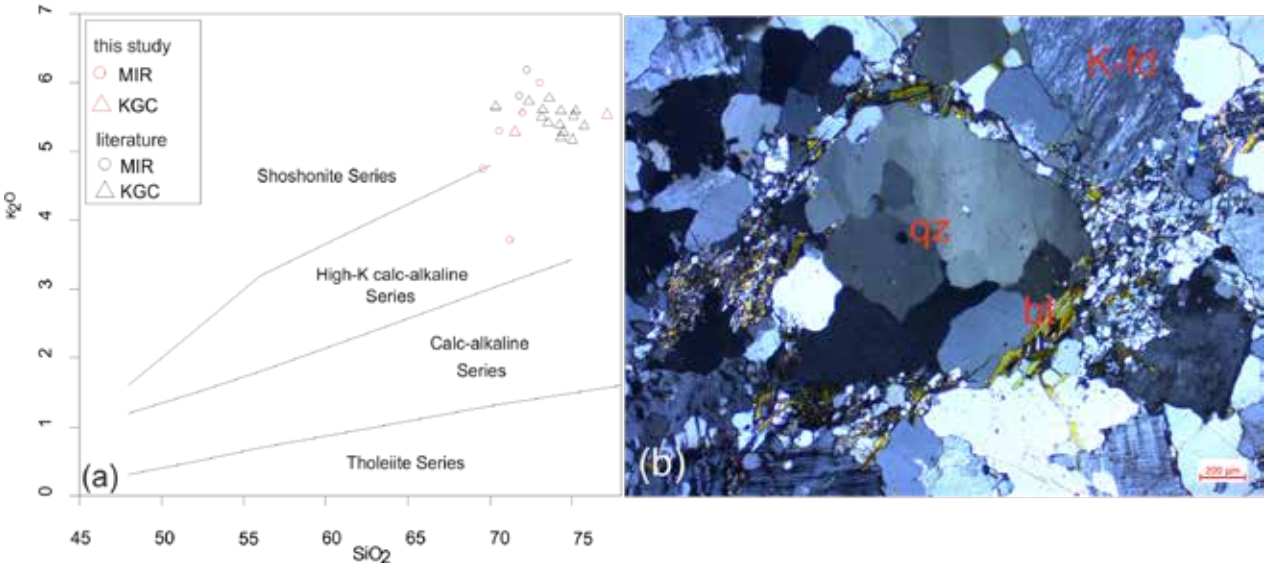

Figure 2(a) Miriofito and Kerkini samples (red symbols) plotted on the SiO_2 *vs.* K_2O classification diagram of Peccerillo and Taylor (1976). Literature data after Christofides *et al*. (1999). (b) Photomicrograph of Miriofito biotite granite (crossed pollars).

Conclusions

- Our new geochemical data agrees with published data for a common origin of Miriofito and Kerkini granite. The Miriofito granite has high SiO_2 (69.5–72.3 wt.%), K_2O (3.7–6.7 wt.%) and Na_2O (3–4 wt.%) and low MgO (0.02–0.4 wt.%) and is ferroan alkali-calcic in composition. It belongs to the high-K magma series and is a highly fractionated and peraluminous A-type granite.
- Petrographic evidence indicates that the granite rose to shallow crustal levels and underwent advanced fractional crystallisation of K-feldspar, minor plagioclase, apatite, and Ti-bearing phases (rutile, ilmenite, titanite).
- Tectonic discrimination diagrams indicate that the whole complex Kerkini-Miriofito-Kastanousa intrusion was likely formed in a post-collisional setting, linked to a transition in the geodynamic setting from an arc-related to a post-collisional extensional setting in the Vertiskos realm.
- The main point is that the generation of the HKCA magma needs the former existence of an important subduction phase to generate this type of source. The K-enrichment event is considered to reflect a subcontinental mantle enrichment /or K-rich mafic crust from the preceding subduction period.

Acknowledgements

The authors are grateful to the Hellenic Survey of Geology and Mineral Exploration (H.S.G.M.E.) for preparing the thin section and providing access to the Scanning Electron Microscope facility.

References

Abbo, A., Avigad, D., Gerdes, A., 2020. Crustal evolution of peri-Gondwana crust into present day Europe: the Serbo-Macedonian and Rhodope massifs as a case study. Lithos 356–357, 105295. http://doi.org/10.1016/j.lithos.2019.105295

Bonin, B., 1990. From orogenic to anorogenic settings: evolution of granitoid suites after a major orogenesis. Geological Journal 25, 261–270. http://doi.org/10.1002/gj.3350250309

Christofides G., Koroneos A., Pe-Piper G., Katirtzoglou K., Chatzikirkou A., 1999. Pre-Tertiary A-Type magmatism in the Serbomacedonian massif (N. Greece): Kerkini granitic complex. Bull. Geol. Soc. Greece, xxxiii, 131-148.

Christofides G., Koroneos A., Liati A., Kral J., 2007. The A-Type Kerkini granitic complex in North Greece: geochronology and geodynamic implications. Bull. Geol. Soc. Greece, xl, 700-711.

Himmerkus, F., Anders, B., Reischmann, T., Kostopoulos, D., 2007. Gondwana-derived terranes in the northern Hellenides. In 4-D Framework of Continental Crust (eds RD Hatcher, MP Carlson, JH McBride and JR Martinez Catalán), pp. 379–90. Geological Society of America, Memoirs no. 200.

Himmerkus, F., Reischmann, T., Kostopoulos, D., 2009. Serbo-Macedonian revisited: a Silurian basement terrane from northern Gondwana in the Internal Hellenides, Greece. Tectonophysics 473, 20–35. doi: 10.1016/j.tecto.2008.10.016.

Kilias, A., Falalakis, G., Mountrakis, D., 1999. Cretaceous–Tertiary structures and kinematics of the Serbomacedonian metamorphic rocks and their relation to the exhumation of the Hellenic hinterland (Macedonia, Greece). International Journal of Earth Sciences 88, 513–31. doi: 10.1007/ s005310050282.

Kockel, F., Mollat, H., Walther, H. W., 1977. *Erlauterungen zur geologicschen karte der Chalkidiki und angrenzender Gebiete 1/100.000 (Nord Griechenland)*. Hanover: Bundesanstalt für Geowissenschaften und Rohstoffe, 119 pp.

Liégeois, J-P., Navez, J., Hertogen, J., Black, R., 1998. Contrasting origin of post-collisional high-K calc-alkaline and shoshonitic versus alkaline and peralkaline granitoids. The use of sliding normalization. Lithos, 45, 1-28.

Papapavlou, K., 2021. Zircon U– Pb–Hf snapshots on the crustal evolution of the Serbo-Macedonian massif: new insights from Ammouliani island (Northern Greece). Geological Magazine 158: 2079–2086. https:// doi.org/10.1017/S0016756821000698.

Pearce, J.A., Harris, N.B.W., Tindle, A.G., 1984. Trace element discrimination diagrams for the tectonic interpretation of granitic rocks. J. Petrol. 25, 956–983.

Peccerillo, A., Taylor, S. R., 1976. Geochemistry of Eocene calc-alkaline volcanic rocks from the Kastamonu area, Northern Turkey. Mineralogy and Petrology, 58, 63–81.

Poli, G., Christofides, G., Koroneos, A., Soldatos, T., Perugini, D., Langone, A., 2009. An Early Triassic granitic magmatism—Arnea Kerkini granitic complexes—In the Vertiskos unit (Serbo-macedonian massif, north-

eastern Greece) and its significance in the geodynamic evolution of the area. *Acta Vulcanologica*, *21*, 47–70.
Whalen, J. B., Currie, K. L., Chappell, B. W., 1987. A-type granites: geochemical characteristics, discrimination and petrogenesis. Contributions to Mineralogy and Petrology, 95, 407-419.

17th INTERNATIONAL CONGRESS of the Geological Society of Greece

BULLETIN OF THE GEOLOGICAL SOCIETY OF GREECE, SP. PUBL.

EXTENDED ABSTRACT 060

Biogenicity of Arsenic Sulfide Biomorphous Structures in Deep-Sea Hydrothermal Vents, Kolumbo Arc Volcano: Morphological, Mineralogical and Geochemical Evidence

Dimou E.[1], Papoutsa A.[1], Pletsas V[1], Zegkinoglou N.[1], Kilias S.[1,] Nomikou P.[1], Polymenakou P.[2]
(1) National and Kapodistrian University of Athens, Athens, Greece, evidim25@gmail.com
(2) Hellenic Centre for Marine Research, Heraklion Crete, Greece

Research Highlights
In this study we argue about the biogenicity of biomorphous structures related with As-mineralization from the Kolumbo diffuser chimneys based on their syngenicity and indigenousness, geological context, morphology and composition.

Introduction
Modern seafloor hydrothermal vents present a hostile environment for life which consists of high acidity, discharge of high-temperature magmatic gases and potentially toxic metal(loids) such as As, Sb, Pb, Tl. Arsenic is widely recognized as a major pollutant for marine ecosystems and a potentially toxic element harmful to most living organisms (Hu *et al*., 2020). It is established that hydrothermal vent fields are a vast microbial habitat, hosting a significant population of microorganisms (Runge *et al*., 2023, Kilias *et al*., 2013) Furthermore, this kind of environment is regarded as analogue for the emergence of primordial life while As-enriched oceans are considered a potential cradle for the origin of life (Russel *et al*., 2005, Hu *et al*., 2020). To endure direct exposure to such extreme environments, various microbial species have evolved resistance mechanisms involving detoxification, biotransformation and even generating energy by oxidizing arsenite. (Hu *et al*., 2020). It is well known that microorganisms in the hydrothermal vents can contribute significantly to the formation of mineral deposits rich in metal(loid)s (Southam and Saunders, 2005, Kilias *et al*., 2013). However, little is known about the microbial processes associated with the precipitation of arsenic sulfides. (Hu *et al*., 2020). Here we present morphological, mineralogical and geochemical evidence for the biogenicity of arsenic sulfides on the active hydrothermal diffusers at Kolumbo arc volcano.

Geological Background
The submarine volcano of Kolumbo located in the Anhydros Basin, Aegean Sea as part of the Christiana-Santorini-Kolumbo volcanic field that lies in the center of the Hellenic Volcanic Arc (HVA). Kolumbo crater has a basal diameter of 3 km with NE-SW orientation. (Hector *et al*., 2024). On top of the crater lies an active hydrothermal vent field with diffuser chimneys emitting shimmering water to ~265°C pure gaseous CO2 fluid forming, a polymetallic Au-rich Seafloor Massive Sulfides (SMS) deposit. The studied samples present four distinct mineralogical zones. The thick porous Inner Sulfide-Sulfate Core (ISSC) is composed of barite, pyrite, marcasite, sphalerite, galena, Pb-Sb sulfosalts, minor anglesite, and minor chalcopyrite. Surrounding the ISSC is the Outer Arsenic Layer (OAsL), which contains barite, pyrite, sphalerite, Pb-Sb sulfosalts, stibnite, As-Pb-Sb sulfosalts, and amorphous arsenic-rich sulfides resembling realgar and orpiment. Encasing the OAsL is a gelatinous orange to brown Surface of Fe-rich Microbial Crust (SFeMC), primarily composed of amorphous Fe-(hydrated)-oxyhydroxides. In this study we focus on the OAsL where the As-related biomorphous structures are observed on that layer (Kilias *et al*., 2013).

Materials and methods
Sampling
The samples studied were collected during two oceanographic expeditions collected from the northern part of the Kolumbo crater floor using the Remotely Operated Vehicles (ROV) Hercules and Max Rover.
Optical microscopy and Scanning electron microscopy
All samples were petrographically examined via transmitted and reflected light microscopy at the Department of Geology and Geoenvironment, National and Kapodistrian University of Athens (NKUA). The biomorphous structures were further observed under a Scanning Electron Microscope (SEM) in order to a) examine the morphologies and textural relationships under high magnification, b) obtain semi-quantitative X-ray elemental maps. For that purpose, a Nova NanoSEM Field Emission-SEM (FE-SEM) was utilized, equipped with, a BacksSattered Electron (BSE) detector, a Secondary Electron (SE) detector, and a Bruker X Flash EDS detector. Samples were carbon-coated with an average thickness of 15 nm, to achieve surface conductivity, and the instrument was operated at a 30-kV accelerating voltage, while electron beam stability was calibrated using a copper standard.

Raman spectroscopy

Raman spectroscopy analyses were performed using a Renishaw inVia Raman confocal microscope, equipped with two lasers, emitting at 532 (green) and 785 nm (red). The green and red lasers are coupled with gratings of 1800 and 1200 groves per mm^2, respectively. Spectra were obtained using the 785 nm laser with a power range between 0.5 and 0.05 mW, due to the varying stability and fluorescence of the analysis spots. Samples were exposed to the laser through a long-focal distance, 50X objective lens with 0.55 numerical aperture, and with the measured spectral range extended from 100 to 3200 cm^{-1}. The obtained spectra were then processed by the WiRE software for Windows. Background noise was reduced by the subtraction of a polynomial baseline, and cosmic ray removal corrections were performed for all spectra.

Results

Optical Microscopy

To provide a detailed description, the biomorphous structures are classified in three types based on morphology as well as differences in chemistry. Type 1 structures are identified as diatoms species. Type 2 are filamentous biomorphs. Type 3 are globular biomorphs. Diatom morphology is very evident in Fig. 1. After thorough observation and due to morphology and spectroscopic data (see below) we conclude that it belongs to Chaetoseros sp., one of the most diverse planktonic diatom species (De Luca *et al*., 2019). The main characteristic of the family is the existence of setae that appear to come out from the valve of the cells. Setae help diatoms create chains of cells that a expand for tens of micrometers. To prevent the chains from extending too far, terminal setae are produced from several cells. Each cell exhibits an outer layer known as frustule. It is crucial to mention that diatoms in this study demonstrate different levels of As-mineralization. Diatoms are mostly observed in open spaces and in close association with barite.

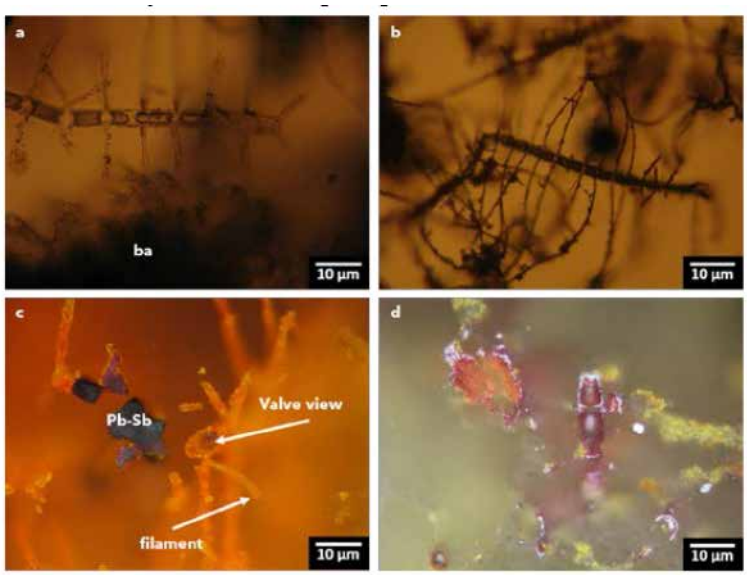

Figure 1. a) Two non-As-mineralized diatom chains with visible intercalary and terminal setae, also the frustule and aperure are very clear b) Partially mineralized diatom with longer setae c) Valve view of a diatom, partially mineralized frustule and setae, also a filamentous type 2 biomorph can be observed d) Fully mineralized diatom, only the cells remain

The type 2 biomorphous structures are filamentous and extend up to several tens of micrometers. Depending on their width, a stibnite core is visible which appears black or gray depending on parallel or crossed polaroids under reflected light, while arsenic is mostly in the form of orpiment. The filaments exhibit a plethora of different characteristics. (Fig. 2). Some of them appear more lineal and demonstrate terminal swelling while others exhibit twisting and branching or even septated structures (Qu *et al*., 2023). Sometimes those can co-exist. The thinner filaments tend to form net-like structures and exhibit pinching (Hu *et al*., 2020). Furthermore, in some cases filaments appear to grow on diatoms (Fig 2. c). It is important to note that even the thinner filaments exhibit a stibnite core, but it is not always visible due to scale. The filaments are usually found as intergrowths with stibnite and Pb-Sb sulphosalts on a barite substrate as they also develop in open space. Type 3 biomorphous orpiment like structures are quite different in morphology

(Fig. 3). They appear as globules either observed on diatoms (mostly on setae) or forming grape-like structures in open spaces. Their diameter is not bigger than 3 micrometers. They can be found in association with filaments as well. (Fig. 4). It is interesting that when a lineal substrate appears (like a diatom seta or a needle-like stibnite) these globular biomorphs can display a string of beads (Qu *et al*., 2023).

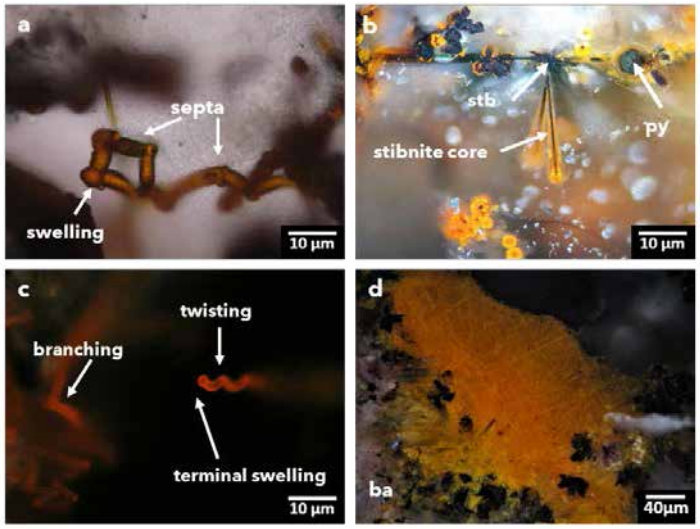

Figure 2. a) Thick filament with swelling and septated structures b) Linear filament with visible stibnite core c) Filaments that exhibit branching as well as twisting and terminal swelling on the same time d) Thinner filaments with net-like structures on a barite substrate.

Mineral Chemistry-SEM EDS

Further detailed geochemical analyses on biomorphous structures were performed by SEM-EDS to evaluate their chemical composition. The results showed the presence of As-sulfide in all the examined biomorphs. Regarding type 1 biomorphs, SEM-EDS confirmed the presence of silica which further proves they are diatoms. As it has been established, diatoms are known to form silica cell walls (Hildebrand, 2008). It is evident (Fig. 5) that silica is distributed on the frustule as well as on setae. When it comes to filamentous biomorphs, SEM-EDS confirms the stibnite core as well as the As-sulfide shell and absence of silica. As for the globular biomorphs, arsenic, antimony and sulfur seem to be equally dispersed.

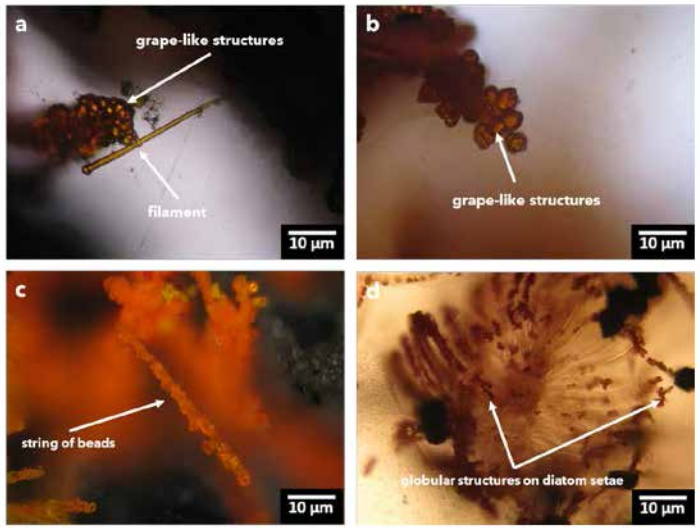

Figure 3. a) Globular structures in asociation with filaments b) Grape-like structures in open space c) Globular biomorphs forming a string of beads d) Globules on diatom setae

Spectral characterization of biomorphous structures

The contribution of Raman spectroscopy for this study was crucial. Point analyses revealed the presence of carbonaceous matter (CM) in all the biomorphs under investigation. Raman mapping was used to better understand the pattern of mineral phases on the studied biomorphs. Spectroscopic data showed the presence of amorphous hydrated silica and orpiment (As_2S_3) and realgar (As_4S_4) mineralization on biomorphous structures (Papoutsa *et al*., 2024). The occurrence of CM as a structural component was verified by the occurrence of first order (1000-1650cm^{-1}) and second-order (2500-3200 cm^{-1}) bands (Papoutsa *et al*., 2024). The notable features consist of a prominent G-band at 1583 cm^{-1}, distinct from the D2 band at approximately 1608 cm^{-1}, along with clearly defined D1 and D4 peaks at 1347 cm^{-1} and 1245 cm^{-1}, respectively. G/D2 band ratio was used to better interpret the distribution of CM. For the type 1 biomorphs, Raman peaks at ~490, 602, 812, 980 and 1000 cm^{-1} are indicative of Si-OH (hydrated silica) that compose the diatomaceous cell wall (Papoutsa *et al*.,2024). The hydrated silica seems to be concentrated mainly on the frustule. Regarding the filamentous biomoprhs, Raman spectroscopy confirmed the presence of stibnite core and orpiment-realgar shell. CM was also identified within the structure.

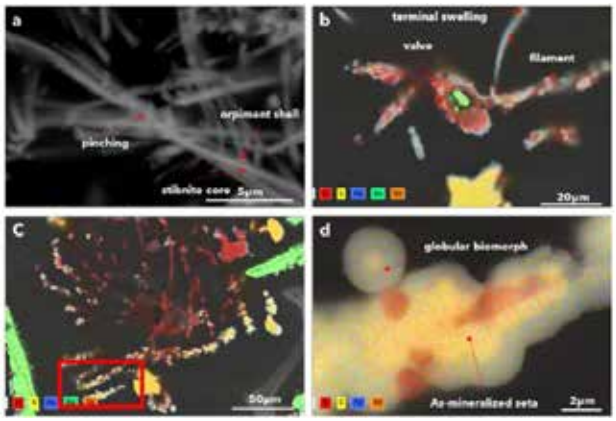

Figure 4:FE-SEM microphotographs and elemental maps of biomorphs. a) Open space filamentous cluster exhibiting pinching features. Note the differentiation in brightness, indicating the presence of a denser stibnite core. b) Microphotograph of As-filament and valve view of a diatom. Note the characteristic presence of Si on the diatom frustule and the absence of Si in the filament. c) Partially mineralized diatom. d) Zoomed area of C (red box) showing the replacement of Si by As and Sb sulfides. Globular biomorphs can be observed growing on the surface of mineralized diatoms. Also displaying a distinct Sb-rich core and an As-rich shell.

As for the globular structures, CM and orpiment were identified as well. However, it is important to note that their small diameter approaches the limit of spatial resolution of Raman mapping with the available objective lens. Regardless that, Raman maps of CM distribution in the type 3 structures, were successfully constructed.

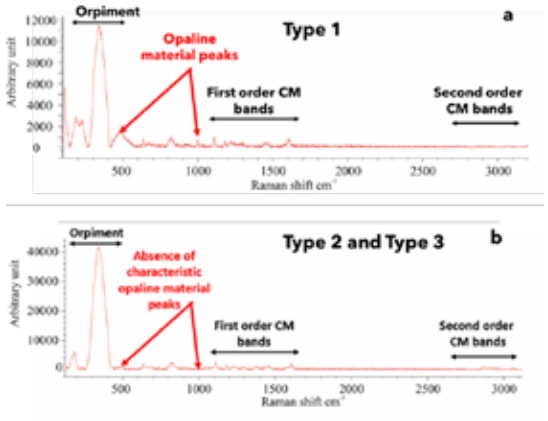

Figure 5. a) Point analysis of a diatom frustule with visible CM peaks, orpiment peaks and opaline material peaks b) Point analysis of filamentous and globular structures with CM and orpiment peaks, also absence of opaline material peaks as it is characteristic for diatoms.

Criteria for biogenicity

To examine the biogenic origin of the aforementioned biomorphs, 4 criteria were tested. (Ivarsson *et al*., 2015)

Geological context

Modern hydrothermal vent fields associated with Seafloor Massive Sulfides (SMS) deposition are widely regarded as significant microbial habitats (Hu *et al*., 2020). They sustain extraordinary biological communities, featuring rare and endemic species uniquely adapted to the conditions of hydrothermal vents (Georgieva *et al*., 2021). SMS being the closest modern analogue of ancient Volcanogenic Massive Sulfides (VMS) deposits, which are proven to be one the earliest known habitats for microbial life (Hu *et al*., 2020). Therefore, these types of environments are closely associated with the history of life and its origination (Hu *et al*., 2020, Georgieva *et al*., 2021). The fossil record of hydrothermal vents possibly represents the earliest direct evidence of life on Earth, highlighting their significance as biological habitats throughout Earth's history. Hydrothermal vent microbial communities consist of relatively high concentrations of a few species that rely on chemosynthesis for survival such as Proteobacteria and Campylobacterota (Georgieva *et al*., 2021).

Syngenicity and indigenousness

All the observed biomorphs, and especially the filaments and the globules, originate from the surface of the minerals present (As-Pyrite, Pb-Sb-sulfosalts, orpiment) at the chimneys and/or the surface of diatoms. The transition from the mineral surface to the filaments are smooth and undisturbed (Fig. 6) indicating that the filaments grow out of the surface of minerals. In cases, the open pore space has been colonized from a biofilm which filamentous net-like and globular grape-like structures grow (Fig. 3). The existence of the biomorphs on the outer layer of the chimneys and their close association with the primary sulfide minerals indicates that microbial activity was synchronous with the arsenic mineralization. These observations coupled with high counts of genes associated with arsenic oxidation (Papoutsa *et al*., 2024) suggest that the filamentous and globular biomorphs are indigenous of the chimneys and syngenetic with the As-sulfide deposition. Diatoms are not usually inhabiting hydrothermal vents, rather they accidentally sink from the upper levels of the water column onto the diffuser chimneys.

Morphology

The occurrence of filaments and globules as whole clusters resemble the culture media precipitates of As-respiring bacterial strain (Hu *et al*., 2020). The growth of clusters over diatoms, orpiment and other As-rich phases, achieved by penetrating and dissolving the mineral surface, mirrors microbial strategies for colonizing mineral surfaces to extract nutrients.

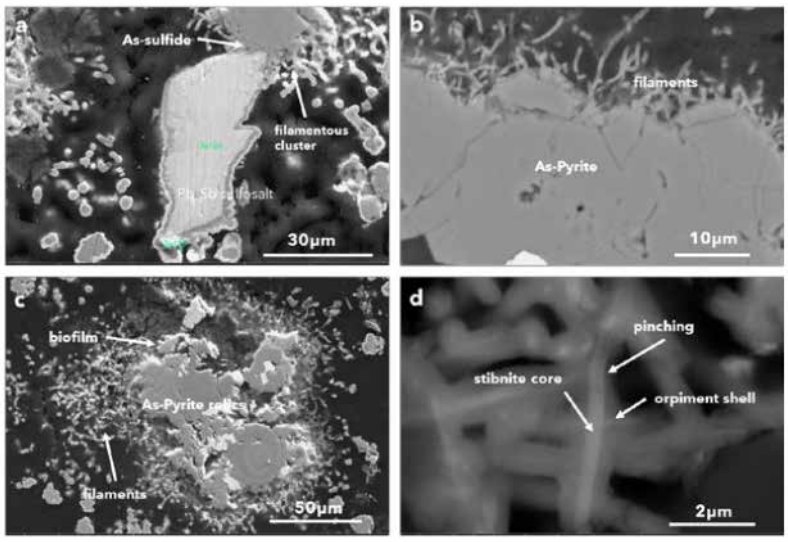

Figure 6. FEG-SEM photomicrographs of filamentous structures. a) Filaments growing on primary As-sulfides showcasing a smooth and undisturbed transition. b) Filaments growing on the surface of As-pyrite. c) Filaments colonization initiated by a biofilm formation around dissolved pyrite crystals. d) Microphotograph of thin filaments exhibiting pinching with a distinct stibnite (brighter color) core and an orpiment shell.

Composition

Despite the filamentous and globular biomorphs being embedded in epoxy resin, Raman spectroscopy revealed distinct CM within their structures. Comparisons with the spectra of the epoxy rule out contamination and confirm

that the carbonaceous matter is indigenous to the structures. Raman mapping (Fig. 7) revealed that CM is localized in specific areas such as the As-rich shell of the filaments rather than the stibnite core (Fig. 8). This suggests that indigenous CM is preserved in the late stages of the mineral paragenesis. The presence of CM in the shell of the structures agrees with other studies arguing about biogenic origin of As-sulfides (Hu *et al*., 2020) and it suggests that microbial activity was synchronous to As-sulfide deposition. Synchrotron X-ray absorption near edge structure analysis has shown that the As-

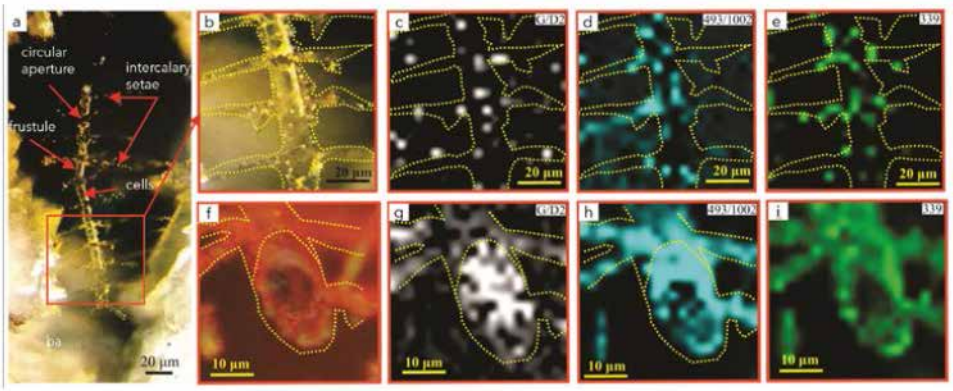

Figure 7. a) site of study b) zoomed area of Raman mapping c) distribution of CM on diatom frustule d) distribution of silica on diatom frustule e) As-Sulfide mineralization f) valve view of a diatom, another site of Raman mapping g) distribution of CM h) distribution of silica on diatom frustule i) As-Sulfide mineralization on diatom frustule and setae, it is also visible that the site in f) is more mineralized than diatom in a) (Papoutsa *et al*., 2024)

sulfides in the diffusers contain a mixture of As (II) and As (III). These heterogeneities in the valence of As can be credited to microbial activity. Metagenomic libraries constructed from the Kolumbo vents, which revealed high counts of functional genes involved in microbial oxidation of As (II) to As (III) (Papoutsa *et al*., 2024) further prove this point.

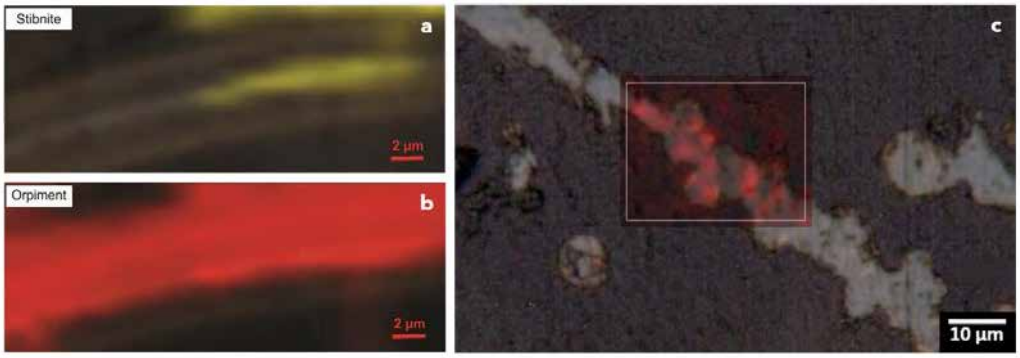

Figure 8. a) Raman map showing the distribution of stibnite in the visible core of a filament b) distribution of orpiment in the outer shell of filament (Papoutsa *et al*., 2024) c) distribution of CM on a string of beads.

Conclusions

In this study we report observations of different biomorphous structures associated with As-sulfides mineralization. Three types of biomorphs have been identified; Type 1) Diatoms, Type 2) Filaments and Type 3) Globules. The morphological features of the studied biomorphs, combined with their distinct spectroscopic characteristics and their geochemical composition along with the metagenomic data suggest that As mineralization was contemporaneous with microbial activity. The lack of diatom related gene counts in the metagenomic libraries shows that diatoms are not directly involved in the mineralization of As, rather they exist as the substrate for microorganisms to develop, providing CM and nutrient from the shallow waters to the deep sea. This theory is further supported by the fact that filamentous and globular structures seem to grow over the diatoms resembling microbial strategies for colonizing mineral surfaces.

Acknowledgments

We are thankful to NKUA for granting us access to Raman Spectroscopy at Core Facility of the School of Science. We are grateful to the Electron Microscopy Facility of the Materials Treatment Centre in VITO (Mol, Belgium) for the use of FE-SEM and the citizen

science Horizon funded project nexus-monARC for fully supporting the analyses that took place in VITO. Also, to Maria-Despoina Chrysafeni for her FE-SEM images.

References

De Luca, D., Sarno, D., Piredda, R., and Kooistra, W.H.C.F., 2019. A multigene phylogeny to infer the evolutionary history of Chaetocerotaceae (Bacillariophyta). Molecular Phylogenetics and Evolution 140, 106575.

Georgieva, M.N., Little C.T., Maslennikov, V.V., Glover, A.G., Ayupova, N.R., & Herrington, R.J. (2021). The history of life at hydrothermal vents. Earth-Science Reviews 217, 103602.

Hector, S., Patten, C.G.C., Beranoaguirre, A., Lanari, P., Kilias, S., Nomikou, P., Peillod, A., Eiche, E., and Kolb, J., 2024. Magmatic evolution of the Kolumbo submarine volcano and its implication to seafloor massive sulfide formation. Mineralium Deposita 59, 1229–1248.

Hildebrand, M., 2008. Diatoms, biomineralization processes, and genomics. Chemical Reviews 108, 4855–4874.

Hu, S.Y., Barnes, S.J., Pagès, A., Parr, J., Binns, R., Verrall, M., Quadir, Z., Rickard, W.D.A., Liu, W., Fougerouse, D., Grice, K., Schoneveld, L., Ryan, C., and Paterson, D., 2020. Life on the edge: Microbial biomineralization in an arsenic- and lead-rich deep-sea hydrothermal vent. Chemical Geology 533, 119438.

Ivarsson, M., Peckmann, J., Tehler, A., Broman, C., Bach, W., Behrens, K., Reitner, J., Böttcher, M.E., and Ivarsson, L.N., 2015. Zygomycetes in vesicular basanites from vesteris seamount, Greenland Basin - A new type of cryptoendolithic fungi. PLoS ONE 10, e0133368.

Kilias, S.P., Nomikou, P., Papanikolaou, D., Polymenakou, P.N., Godelitsas, A., Argyraki, A., Carey, S., Gamaletsos, P., Mertzimekis, T.J., Stathopoulou, E., Goettlicher, J., Steininger, R., Betzelou, K., Livanos, I., Christakis, C., Bell, K.C., Skoullos, M., 2013. New insights into hydrothermal vent processes in the unique shallow-submarine arc-volcano, Kolumbo (Santorini), Greece. Scientific Reports 3, 2421.

Papoutsa, A., Pletsas, V., Kilias, S., Dimou, E., Polymenakou, P., Nomikou, P., Papadimitriou, V., Maak, J., Ivarsson, M., Kyrpides, N.C., 2024. Raman spectroscopy evidence for arsenic-sulfide mineralized diatom-like structures in deep-sea hydrothermal vents at Kolumbo: contribution to arsenic biomineralization. 16th International GeoRAMAN Conference, Rhodes, Greece, p.49-50.

Qu, Y., Yin, Z., Kustatscher, E., Nützel, A., Peckmann, J., Vajda, V., and Ivarsson, M., 2023. Traces of Ancient Life in Oceanic Basalt Preserved as Iron-Mineralized Ultrastructures: Implications for Detecting Extraterrestrial Biosignatures. Astrobiology 23, 769–785.

Runge, E.A., Mansor, M., Kappler, A., and Duda, J.P., 2023. Microbial biosignatures in ancient deep-sea hydrothermal sulfides. Geobiology 21, 355–377.

Russell, M.J., Hall, A.J., Boyce A.J., Fallick A.E., 2005. On hydrothermal convection systems and the emergence of life. 100th anniversary special paper, Economic Geology 100, 259–270.

Southam, G., and Saunders, J.A., 2005. The Geomicrobiology of Ore Deposits. Economic Geology 100, 1067–1084.